UNCLASSIFIED

AD 408 997

DEFENSE DOCUMENTATION CENTER

FOR

SCIENTIFIC AND TECHNICAL INFORMATION

CAMERON STATION, ALEXANDRIA, VIRGINIA

UNCLASSIFIED

NOTICE: When government or other drawings, specifications or other data are used for any purpose other than in connection with a definitely related government procurement operation, the U. S. Government thereby incurs no responsibility, nor any obligation whatsoever; and the fact that the Government may have formulated, furnished, or in any way supplied the said drawings, specifications, or other data is not to be regarded by implication or otherwise as in any manner licensing the holder or any other person or corporation, or conveying any rights or permission to manufacture, use or sell any patented invention that may in any way be related thereto.

CATALOGED BY DDC
AS AD No. 408997

408 997

UNIVERSITY of PENNSYLVANIA
ELECTROMEDICAL LABORATORY
The Moore School of Electrical Engineering
PHILADELPHIA 4, PENNSYLVANIA

DDC
RECEIVED
JUL 17 1963
TISIA D

Best
Available
Copy

ONR

TECHNICAL REPORT NO. 36*

SCATTERING AND ABSORPTION OF MICROWAVES BY DISSIPATIVE DIELECTRIC OBJECTS: THE BIOLOGICAL SIGNIFICANCE AND HAZARDS TO MANKIND

A. Anne

Principal Investigator: H. P. Schwan

Electromedical Division
The Moore School of Electrical Engineering
University of Pennsylvania
Philadelphia 4, Pennsylvania

* This report was submitted by A. Anne as a thesis in partial fulfillment of the requirements for a Ph. D.

ACKNOWLEDGEMENT

Initial support for this work was provided by the Air Force Contract AF 30(602).

Since 1961 this work has been solely supported by the Office of Naval Research, Contract Nonr 551 (05).

INDEX

INDEX

TABLE OF CONTENTS

LIST OF TABLES

LIST OF ILLUSTRATIONS

BIBLIOGRAPHY

1. Aden, A. L. and Kerker, M.: Scattering of electromagnetic Waves from two concentric spheres, J. Appl. Phys., Vol. 22, No. 10, pp 1242-1246, October 1951.

2. Anne, A., Saito, M., Salati, O. M. and Schwan, H. P.: Penetration and Thermal Dissipation of Microwaves in Tissues, Report No. 62-13, Contract AF 30(602)-2344, Electromedical Division, The Moore School of Electrical Engineering, University of Pennsylvania, Philadelphia, 14 June 1962.

3. Ely, T. S. and Goldman, D. E. : Heat exchange characteristics of animals exposed to 10 cm microwaves, I.R.E. Trans. PGME-4, pp 38-43, February 1956.

4. Hiat, R. E. et al : "Forward scattering by coated objects illuminated by short wavelength radar", "The ineffectiveness of absorbing coatings on conducting objects illuminated by wavelength radar", Proc. I.R.E., Vol. 48, No. 9, pp 1630-1635, 1636-1642, September 1960.

5. Hines, H. M. and Randall, J. E. : Possible industrial hazards in the use of microwave radiation, Ele. Eng., Vol. 71, p 879, 1952.

6. Jacobs, E. : Fresnel region patterns and gain corrections of large rectangular antennas, Proc. Fifth Conference on Radio Frequency Interference Reduction, Armour Research Foundation, Chicago, October 1959.

7. Mie, G. : Beitrage zur Optik triiber Median, Ann der Physik, vol. 25, pp 377-445 (1908).

8. Penndorf, R. B. : New tables of Mie Scattering Functions for Spherical particles, AFCRC-TR-204(6), AD-98772, Air Force Cambridge Research Center, March 1956.

9. Scharfman, H. : Scattering from dielectric coated spheres in the region of the first resonance, J. Appl. Phys., Vol. 25, No. 11, pp 1352-1356, November 1954.

10. Schelkunoff, S. A. and Friis, H. P. : "Antennas: Theory and Practice", Chapter 1, John Wiely, 1952.

11. Schwan, H. P. and Li, K. : Hazards due to total body irradiation by radar, Proc. I. R. E., Vol. 44, No. 11, pp 1572-1581, November 1956.

12. Schwan, H. P. and Li, K. : The mechanism of absorption of ultrahigh frequency electromagnetic energy as related to the problem of tolerance dosage, I. R. E. Trans. PGME, Vol. 4, pp 45-49, February 1956.

13. Schwan, H. P., Carstensen, E. L. and Li, K. : Heating of Fat-Muscle Layers by Electromagnetic and Ultrasonic Diathermy, Paper 52-206, AIEE Summer General Meeting, Atlantic City, 15-19 January 1953.

14. Schwan, H. P. and Li, K. : Capacity and Conductivity of body tissues at ultrahigh frequencies, Proc. I. R. E., Vol. 41, No. 12, pp 1735-1740, December 1953.

15. Schwan, H. P. et al : Effectslof microwaves on mankind, 2nd Annual Progress Report, Contract AF 41(657)129, Electromedical Division, The Moore School of Electrical Engineering, University of Pennsylvania, Philadelphia, March 1, 1959.

16. Schwan, H. P. : Alternating current spectroscopy of biological substances, Proc. I. R. E., Vol. 47, No. 11, pp 1841-1855, November 1959.

17. Silver, S. : Microwave Antenna Theory and Design, Chapter 15, Vol. 12, Radiation Laboratory Series, McGraw-Hill, New York 1949.

18. Stratton, J. A. : Electromagnetic Theory, Chapter IX, Sections 9. 25, 9. 26, 9. 27, McGraw-Hill, New York, 1941.

19. Tables of Scattering Functions for Spherical Particles: National Bureau of Standards, Applied Mathematics Series-4, 25 January 1949.

20. Williams, D. B., Monahan, J. P., Nicholson, W. J. and Aldrich, J. J. : Biologic effects studies on microwave radiation: time and power threshholds for the production of lens opacities by 12. 3 cm microwaves, I. R. E. Trans. PGME-4, pp 17-22, February 1956.

I. DEFINITION OF PROBLEM AND APPROACH

1.0 Introduction

Health hazards, resulting from the exposure of mankind to strong sources of non-ionizing electromagnetic radiation, have been discussed by several investigators.[3, 5, 11, 12, 13, 14, 20] The harmful effects of excessive amounts of radiation either result from a general rise in total body temperature or are limited to selective temperature rises of sensitive parts of the body such as the eye. Present indications are that the effects of such radiation are caused solely by the heat resulting from the absorbed energy. It has been assumed, in the case of total body irradiation, that a fever corresponding to a temperature rise greater than $1^{\circ}C$ is intolerable. Eye cataracts are produced when the eye temperature elevation is of the order of 10° C.[20] It thus appears that significant body temperature rise is the serious hazard whenever substantial parts of the body are exposed so that conditions of total body irradiation are approximated. Based on this concept Schwan recommended a tolerance dosage of 10 milliwatts per square centimeter of total body absorption for the frequency range of interest to mankind. If one wishes to interpret this tolerance dosage in terms of the free field values of power density, which is easily measured, the absorption properties of mankind should be known.

Schwan and Li[11] have calculated the percentage of airborne radiation that is absorbed by the human body, on the assumption that the

body extremities could be ignored and the trunk of the body could be approximated by a three layer infinite plane slab made up of skin, subcutaneous fat and deep tissue such as muscle. They found that percentage of absorbed energy may vary from 20 to 100 percent depending on frequency, fat thickness and skin thickness.

The object of this paper is to study theoretically and experimentally the effects of body curvature and size and its extremities on the percentage of airborne energy that is absorbed by mankind.

2.0 Theoretical and Experimental Approach

Phantoms which simulate the shape and the electrical properties of mankind, rather than animals are chosen to study the absorption properties of mankind to electromagnetic radiation. This is because of the fact that phantoms are stable, reproducible and often subject to theoretical analysis. The behavior of animals involves many unknown factors and is presently not subject to theoretical analysis. In phantom studies one can make as exact a facsimile of the human body from an electrical point of view as is necessary to explore satisfactor-

be compared. Even for plane wave fields, theoretical problems are severe unless very simple objects such as spheres are chosen for the phantom. For experimental work, any shape may be used. If then experimental and theoretical results show good agreement for simple shapes, there will be considerable confidence in experimental results for complex shapes such as the human body. Electrolyte mixtures of KCl-Dioxane-water having the dielectric properties of human tissue, have been developed by H. P. Schwan and H. Pauly.[15] These solutions can be used to fill the phantoms for experimental work.

Scattering and absorption properties of any object can be studied in terms of the quantities defined as follows.

The Mie scattering coefficient is defined as the ratio of the total scattered power to the power that would be incident on the object's geometric cross section prior to its insertion into the field.

The relative absorption cross section is defined as the ratio of the power absorbed from the incident field to the power that would be incident on the object's geometric cross section prior to its insertion into the field.

It is apparent that this relative absorption cross section determines the power absorbed by mankind from free field measurements.

The Mie scattering coefficient and the relative absorption cross section were calculated theoretically for a homogeneous sphere having the dielectric properties of muscle tissue and a concentric

sphere where the inner sphere simulates the muscle tissue and the outer shell represents the subcutaneous fat. The calculations were based on the theory of scattering of electromagnetic radiation by spheres exposed to plane waves.[7,18] Actually a sphere with two concentric shells, made of subcutaneous fat and skin, would be a better approximation of biological subjects. Preliminary estimates, however, have shown that the computational time could not be justified. Comparison of the results for one concentric shell with those for the layered infinite slab shows that because of the close similarity, present data can be extended to the two shell case. The relative absorption cross section was determined experimentally for homogeneous spheres and dolls of human shape of different sizes. The experimental results of homogeneous spheres compared well with the theoretical results.

3.0 Electrical Substitutes for Body Tissues

All body tissues fall within the following range of electrical values throughout the total microwave frequency range.

dielectric constant	ϵ = 5 to 70
conductivity	κ = 0.1 to 200 millimho/cm
relative permeability	μ = 1

Depending on frequency and type of tissue, a variety of probable combinations of dielectric constants and conductivities within these ranges are possible. As previously stated, electrolyte mixtures of water, Dioxane and KCl having suitable combinations of properties in

the above range are available. These electrolyte mixtures are easy to use in experimental work with phantoms and allow adjustment of dielectric constant and conductivity throughout the range of interest.

The dielectric properties of these electrolytes depend on frequency. The frequency dependence is given by the following expressions.[15]

$$\epsilon = \epsilon_\infty + \frac{\epsilon_o - \epsilon_\infty}{1 + \left(\frac{f}{f_o}\right)^2} \tag{1}$$

$$\kappa = \kappa_o + 2\pi f_o \epsilon_v (\epsilon_o - \epsilon_\infty) \frac{(f/f_o)^2}{1 + (f/f_o)^2} \tag{2}$$

where ϵ = dielectric constant at any frequency

ϵ_o = dielectric constant at low frequencies, i.e., $f << f_o$

ϵ_∞ = dielectric constant at high frequencies, i.e., $f >> f_o$

ϵ_v = permittivity of air

κ = conductivity at any frequency

κ_o = conductivity at low frequencies

f = operating frequency in cycles/sec

f_o = characteristic frequency of electrolyte

= 20,000 Mc/s for KCl-dioxane-water mixture

Table 1

Dielectric data of muscle and fatty tissues for various frequencies.

Frequency Mc/s	Muscle		Fat	
	Dielectric Constant	Conductivity mMho/cm	Dielectric Constant	Conductivity mMho/cm
400	60	10	6.8	0.78
2880	60	26.3	4.5	1.1
10000	49	170	3.3	2.63

Muscle tissue has a low frequency dielectric constant of 60 and a low frequency conductivity of about 10 millimho per cm. Since the muscle tissue has high water content, its dielectric properties undergo the same frequency dependence as given by the above equations.[16] The fatty tissue on the other hand has dielectric constants and conductivities which are about tenfold smaller than the dielectric data of the muscle tissue. A summary of the dielectric data to be used for the two types of tissues is given in table 1.

II. THEORETICAL STUDIES

1.0 Theory of Scattering

The solution of the problem of the scattering of a plane electromagnetic wave by a sphere of arbitrary size and electrical properties was first given by Mie[7] in 1908. Stratton[18], solved the same problem by the use of orthogonal spherical vector wave functions. Tabulated values for both scattering and absorption of a plane electromagnetic wave by a lossy dielectric sphere are given in reference 19 for a limited range of parameters which are not of interest in the present study. Pendorf[8] has tabulated Mie scattering functions for spherical particles having real refractive indices, i.e., no electrical losses.

The solution of the problem of the scattering of a plane electromagnetic wave by two concentric spheres of arbitrary size and electrical properties was given by Aden and Kerker[1]. These formulas were used by Scharfman[9] and Hiat[4] to calculate the scattering cross section of a perfectly conducting sphere with a pure or lossy dielectric coating. Presently no data are available on the absorption of electromagnetic waves by two concentric spheres made up of lossy dielectrics.

The following discussion outlines the complete treatment of scattering and absorption of a plane wave by a homogeneous sphere with a concentric shell when the sphere and the shell are lossy dielectrics and are imersed in a medium of air. Also, it includes the reduction of theseresults when the thickness of the shell is zero and the limiting

case where the radius of the sphere is small compared to the wavelength of the electromagnetic radiation.

Let us assume that a homogeneous isotropic sphere of radius a_1 and propagation constant k_1 is surrounded by a concentric shell of radius a_2 and propagation constant k_2 and the whole is embedded in an infinite medium of air with propagation constant k_3. The inner sphere, the shell and the surrounding medium are called regions 1, 2, and 3. A uniform plane wave linearly polarized in the x-direction, is propagated through the medium in the positive z-direction (figure 1).

Assuming a time dependence of exp ($j\omega t$) for the electric and magnetic field vectors and further assuming that the permeabilities of the three regions are equal to the permeability of free space (μ_v) then the propagation constants are:

$$k_1 = \sqrt{\omega^2 \mu_v \epsilon_1 \epsilon_v - j\omega \mu_v \chi_1} \qquad (3)$$

$$k_2 = \sqrt{\omega^2 \mu_v \epsilon_2 \epsilon_v - j\omega \mu_v \chi_2} \qquad (4)$$

$$k_3 = \sqrt{\omega^2 \mu_v \epsilon_v} = \frac{2\pi}{\lambda} \qquad (5)$$

where

ω = angular frequency in radians

λ = wavelength in meters

ϵ_v = 8.854×10^{-12} farads/meter (permittivity of air).

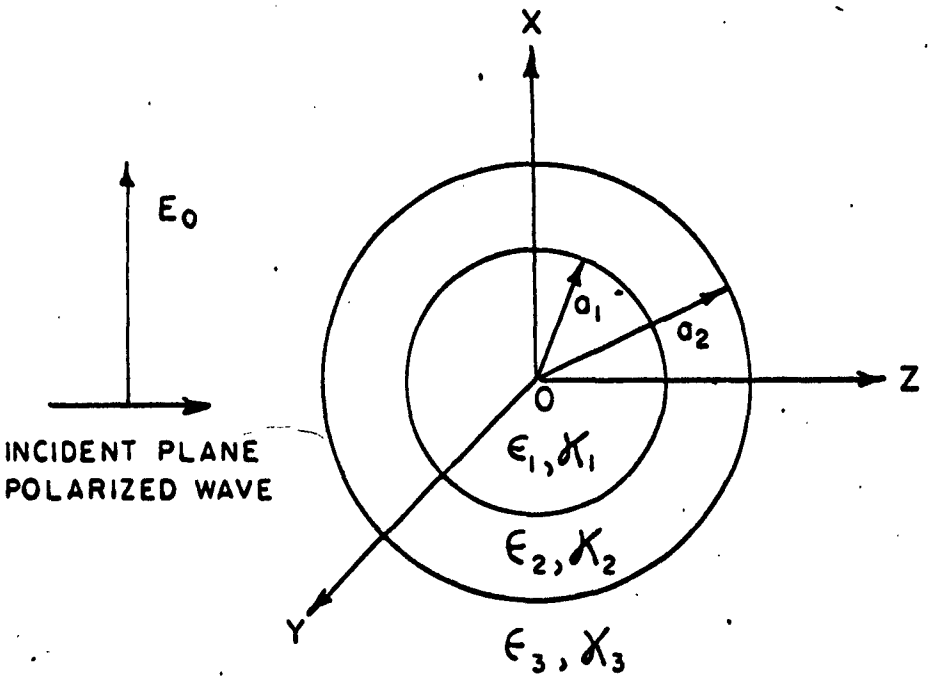

A PLANE WAVE, POLARIZED IN THE X DIRECTION AND TRAVELING IN THE Z DIRECTION IS SHOWN INCIDENT ON THE CONCENTRIC SPHERE PHANTOM.

FIGURE 1

GEOMETRY OF CONCENTRIC SPHERE PHANTOM.

$\mu_v = 4\pi \times 10^{-7}$ henries/meter (permeability of air)

ϵ_1, ϵ_2 = dielectric constants of regions 1 and 2

κ_1, κ_2 = conductivity in mho/meter of regions 1 and 2

Following Stratton[18], the scattered energy can be written as:

$$W_s = \pi \frac{E_0^2}{K_3^2} \sqrt{\frac{\epsilon_v}{\mu_v}} \sum_{n=1}^{\infty} (2n+1) \left(|a_n^r|^2 + |b_n^r|^2 \right) \qquad (6)$$

The total energy received by the sphere from the incident wave and then in part scattered and in part absorbed is given by:

$$W_t = -\pi \frac{E_0^2}{K_3^2} \sqrt{\frac{\epsilon_v}{\mu_v}} \, Re \sum_{n=1}^{\infty} (2n+1) \left(a_n^r + b_n^r \right) \qquad (7)$$

where E_0 = the amplitude of the incident electric field in volts/meter.

The coefficients a_n^r and b_n^r are respectively, the amplitudes of oscillations of magnetic and electric type of the external field and are given by equations (8) and (9). (See Appendix I for derivation of the coefficients).

$$\left[N_2 a_1 h_n^{(2)}(N_2 a_2) \left\{ N_1 \sigma_n(N_1 a_1) - N_2 \sigma_n(N_2 a_1) \right\} \left\{ \sigma_n(a_2) - N_2 \rho_n(N_2 a_2) \right\} \right.$$

$$\left. + j_n(N_2 a_2) H_n^{(2)}(N_2 a_1) \left\{ N_2 \rho_n(N_2 a_1) - N_1 \sigma_n(N_1 a_1) \right\} \left\{ \sigma_n(a_2) - N_2 \sigma_n(N_2 a_2) \right\} \right]$$

$$a_n^r = -\frac{j_n(a_2)}{h_n^{(2)}(a_2)} \qquad (8)$$

$$\left[j_n(N_2 a_1) h_n^{(2)}(N_2 a_2) \left\{ N_1 \sigma_n(N_1 a_1) - N_2 \sigma_n(N_2 a_1) \right\} \left\{ \rho_n(a_2) - N_2 \rho_n(N_2 a_2) \right\} \right.$$

$$\left. + j_n(N_2 a_2) h_n^{(2)}(N_2 a_1) \left\{ N_2 \rho_n(N_2 a_1) - N_1 \sigma_n(N_1 a_1) \right\} \left\{ \rho_n(a_2) - N_2 \sigma_n(N_2 a_2) \right\} \right]$$

$$\frac{}{}$$

$$\left[j_n(N_2 a_1) h_n^{(2)}(N_2 a_2) \left\{ N_2 \sigma_n(N_1 a_1) - N_1 \sigma_n(N_2 a_1) \right\} \left\{ N_2 \sigma_n(a_2) - \rho_n(N_2 a_2) \right\} \right.$$

$$\left. + j_n(N_2 a_2) h_n^{(2)}(N_2 a_1) \left\{ N_1 \rho_n(N_2 a_1) - N_2 \sigma_n(N_1 a_1) \right\} \left\{ N_2 \sigma_n(a_2) - \sigma_n(N_2 a_2) \right\} \right]$$

$$b_n^r = -\frac{j_n(a_2)}{h_n^{(2)}(a_2)} \qquad (9)$$

$$\left[j_n(N_2 a_1) h_n^{(2)}(N_2 a_2) \left\{ N_2 \sigma_n(N_1 a_1) - N_1 \sigma_n(N_2 a_1) \right\} \left\{ N_2 \rho_n(a_2) - \rho_n(N_2 a_2) \right\} \right.$$

$$\left. + j_n(N_2 a_2) h_n^{(2)}(N_2 a_1) \left\{ N_1 \rho_n(N_2 a_1) - N_2 \sigma_n(N_1 a_1) \right\} \left\{ N_2 \rho_n(a_2) - \sigma_n(N_2 a_2) \right\} \right]$$

where

$$\rho_n(x) = \frac{h_{n-1}^{(2)}(x)}{h_n^{(2)}(x)} - \frac{n}{x} \tag{10}$$

$$\sigma_n(x) = \frac{j_{n-1}(x)}{j_n(x)} - \frac{n}{x} \tag{11}$$

$$N_1 = \frac{k_1}{k_3} = \sqrt{\epsilon_1 - j\frac{\sigma_1}{\omega \epsilon_v}} \tag{12}$$

$$N_2 = \frac{k_2}{k_3} = \sqrt{\epsilon_2 - j\frac{\sigma_2}{\omega \epsilon_v}} \tag{13}$$

$$a_1 = a_1 k_3 = \frac{2\pi}{\lambda} a_1 \tag{14}$$

$$a_2 = a_2 k_3 = \frac{2\pi}{\lambda} a_2 \tag{15}$$

The functions $j_n(x)$ and $h_n^{(2)}(x)$ are the spherical Bessel and Henkel functions:

$$j_n(x) = \sqrt{\frac{\pi}{2x}} \; J_{n+\frac{1}{2}}(x) \tag{16}$$

$$h_n^{(2)}(x) = \sqrt{\frac{\pi}{2x}} \; H_{n+\frac{1}{2}}^{(2)}(x) \tag{17}$$

Mie Scattering Coefficient

The power that would be incident on the geometric cross section of the sphere prior to its insertion into the field is given by the product of the power density of the plane wave in free space and its geometric cross sectional area, $A = \pi a_2^2$. In free space, the power density P_d of a uniform plane wave is given by:

$$P_d = \frac{E_o^2}{2}\sqrt{\frac{\epsilon_v}{\mu_v}} = \frac{E_o^2}{754} \text{ watt/sq-meter} \tag{18}$$

The Mie scattering coefficient K_s, as previously defined on page 3 is then:

$$K_s = \frac{W_s}{\pi a_2^2 P_d} = \frac{2}{\alpha_2^2}\sum_{n=1}^{\infty}(2n+1)\left(|a_n|^2 + |b_n|^2\right) \tag{19}$$

Relative Absorption Cross Section

The power, W_a, absorbed by the non-homogeneous sphere from a

uniform plane wave field is:

$$W_a = W_t - W_s \tag{20}$$

The relative absorption cross section S, as previously defined on page 3 is

$$S = \frac{W_a}{\pi a_2^2 P_d} = -\frac{2}{\alpha^2}\sum_{n=1}^{\infty}(2n+1)\left\{Re\,(a_n^{\sim}+b_n^{\sim})+\left(|a_n^{\sim}|^2+|b_n^{\sim}|^2\right)\right\} \tag{21}$$

Reduction to a Homogeneous Sphere

For the special case of $a_1 = a_2$ and $k_2 = k_3$ our model becomes a homogeneous sphere of radius a_1 embedded in air and equations (8) and (9) become:

$$a_n^{\sim} = -\frac{j_n(\alpha_1)}{h_n^{(2)}(\alpha_1)}\;\frac{\sigma_n(\alpha_1) - N_1\,\sigma_n'(N_1\alpha_1)}{\rho_n(\alpha_1) - N_1\,\sigma_n'(N_1\alpha_1)}$$

$$b_n^{\sim} = -\frac{j_n(\alpha_1)}{h_n^{(2)}(\alpha_1)}\;\frac{\sigma_n(N_1\alpha_1) - N_1\,\sigma_n(\alpha_1)}{\sigma_n(N_1\alpha_1) - N_1\,\rho_n(\alpha_1)}$$

which are identical with those given by Stratton[18].

Limiting Case: $a_1 \ll 1$

If the wavelength of the incident plane wave is very large compared to the radius of the sphere so that $a_1 \ll 1$ (eq. 14), the magnitude of the electric and magnetic oscillations of second and higher order are small compared with the magnitude of the first order electric oscillations.[18] Under these conditions, the Mie scattering coefficient and the relative absorption cross section become:

$$K_s = \frac{8}{3} \frac{(1-\epsilon_1)^2 + \left(\frac{\kappa_1}{\omega \epsilon_v}\right)^2}{(2+\epsilon_1)^2 + \left(\frac{\kappa_1}{\omega \epsilon_v}\right)^2} a_1^4 \qquad (24)$$

$$S = \frac{4524\, a_1 \kappa_1}{(2+\epsilon_1)^2 + \left(\frac{\kappa_1}{\omega \epsilon_v}\right)^2} \qquad (25)$$

If $\epsilon_1 \gg 1$, it can be seen from eq. (24) that the Mie scattering coefficient is independent of the dielectric constant and conductivity of the sphere. It is always proportional to a_1^4. Hence the scattered energy is proportional to λ^{-4} or the fourth power of the frequency provided dielectric constant and conductivity do not change with frequency. This is the well known Rayleigh law of scattering.

Equation (25) for the relative absorption cross section was previously derived under the assumption that the wavelength of the incident radiation was large compared to the radius of the sphere.[15] This is the same as assuming the electrostatic case. From this equation it can also be seen that the relative absorption cross section is proportional to the radius of the sphere and if $\epsilon_1 \gg \frac{\kappa_1}{\omega \epsilon_v}$, it is proportional to the conductivity of the sphere,

2.0 Computations and Results

2.1 Homogeneous Sphere:

The homogeneous sphere model having the dielectric properties of muscle was used to provide a basis for the analysis of experimental work and to give an insight into the problem. The Mie scattering coefficient

and the relative absorption cross section were calculated as a function of a_1. Both quantities are functions of the parameters dielectric constant, conductivity and frequency. Hence calculations were made to investigate the effect of changes in one parameter when the other two were kept constant. The following combinations of parameters were investigated:

a.) $\epsilon_1 = 60$ $\quad \kappa_1 = 1, 2, 10, 26.3, 72$ $\quad$ at $f = 2880$

b.) $\epsilon_1 = 74.5$ $\quad \kappa_1 = 26.3$ $\quad$ at $f = 2880$

c.) $\epsilon_o = 60$ $\quad \kappa_o = 10$ $\quad$ at $f = 400, 2880, 10000$

where κ is in millimho/cm and f is in Mc/s.

A low frequency conductivity, κ_o, of 10 millimho/cm was used for the muscle tissue in the calculations. In cases (a) and (b) the conductivity, κ_1, of 26.3 millimho/cm corresponds to the above low frequency conductivity at $f = 2880$ Mc/s. In case (b) the dielectric constant 74.5 is that of the saline solution at $f = 2880$ Mc/s. In case (a) the conductivity values were varied around the conductivity of muscle tissue (26.3 millimho/cm) to study the effect of changes in conductivity when the dielectric constant and the frequency were kept constant. In case (b) Mie scattering coefficient and relative absorption cross section were calculated for saline solution. This in combination with (a) determines the effect of variation in dielectric constant for constant values of conductivity and frequency so that saline solution could be used in the doll experiments to be described later instead of KCl-dioxane-water solution which decomposes the plastic of the dolls. In case (c) the effects of

changes in frequency were investigated for constant values of low frequency conductivity and dielectric constant. A frequency of 2880 Mc/s was chosen so that theoretical and experimental results obtained with an available microwave generator could be compared. The other two frequencies were chosen to represent the lower and upper ends of the frequency range of biological interest. (11)

The equations for relative absorption cross section and Mie scattering coefficient were programmed for solution on a Univac I Computer. The results of the machine computations are shown in figures 2 through 11 as a function of a_1. The calculations were performed for values of a_1 in the following ranges:

a_1 = 0.01 to 2 in steps of 0.01
2.2 to 6 in steps of 0.2
7 to 24 in steps of 1
} Figures 2, 3, 5, 6

a_1 = 0.01 to 2 in steps of 0.01
2.2 to 5 in steps of 0.2
6 to 10 in steps of 1
15 to 30 in steps of 5
50, 100
} Figures 4, 7, 8, 9, 10, 11

Looking over the data, several features of importance can be enumerated.

a) For $a_1 \ll 1$

For small values of a_1 up to about 0.3, the Mie scattering coefficient K_s is independent of conductivity and dielectric constant within the range of parameters investigated and increases according to Rayleigh's law as given by equation (24). The deviation becomes quite distinct for values of a_1, larger than about 0.3 as shown in great detail in figure 12 for one case.

The relative absorption cross section S increases linearly with a_1 up to $a_1 \approx 0.03$ for all parameter values investigated. This is shown by equation (25) and figure 13. Thus, for the range of parameters investigated, "electrostatic" field interaction is only realised if the particle diameter is smaller than $\frac{1}{100}$ of the wavelength.

b.) For $0.3 < a_1 < 6$

This is the resonance region in which both S and K_s oscillate. It can be seen from equations (19) and (21) that both S and K_s depends on the coefficients a_n^r and b_n^r. The coefficients a_n^r and b_n^r are respectively the amplitudes of oscillations of magnetic and electric type. These oscillations are excited by the incident field in the sphere. These are not the natural modes of the sphere, for all are synchronous with the applied field. Whenever the impressed frequency approaches a characteristic frequency of the free oscillations of the sphere, resonance phenomena will occur. The characteristic frequencies of magnetic oscillations of the sphere satisfy the condition which makes the denominator

of a_n^r (eq. 22) vanish.[18] Likewise the natural frequencies of the electric oscillations of the sphere satisfy the condition that the denominator of b_n^r (eq. 23) shall vanish. However, the characteristic frequencies of the sphere are always complex whereas the frequency of the applied field is real. Consequently the denominators of a_n^r and b_n^r can be reduced to minimum values, but never quite to zero, so that the catastrophe of infinite amplitudes is safely avoided. It can be seen from figures 2 through 7 that the amplitudes of the oscillations of both S and K_s depend primarily on conductivity and decreases considerably with increas- in a_1. It is most pronounced near $a_1 \sim 1$.

c.) For $a_1 \gg 1$

Both the relative absorption cross section and the Mie scattering coefficient tend to be independent of frequency for specified values of low frequency dielectric constant ϵ_o and conductivity κ_o. At a given frequency, both are independent of conductivity values throughout the range of 1 to 26 millimho/cm. As the conductivity increases beyond 26 millimho/cm, however, K_s increases while S decreases.

d.) Changes in conductivity

As the conductivity is increased, the major effect on both the relative absorption cross section (S) and the Mie scattering coefficient (K_s),

figures 2 to 7, is a reduction of the amplitude of resonances for $0.3 < a_1 < 6$.

e.) Changes in dielectric constant ϵ

For constant frequency and conductivity, the effect of an increase in dielectric constant from 60 to 74.5 is to shift the resonant peaks towards lower values of a_1 (figures 8 and 9). For $a_1 \geq 6$, as the dielectric constant increases, K_s increases while S decreases. However, the changes in K_s and S are less than 5 percent.

f.) Changes in frequency

For constant values of low frequency conductivity κ_o and dielectric constant ϵ_o, the effects of changes in frequency are somewhat greater for the relative absorption cross section (figure 10) than for Mie scattering coefficient (figure 11) in the region $0.3 < a_1 < 1$. The effects of frequency on S and K_s outside of this region are less than 10 percent.

Returning to equation (21), it can be seen that the relative absorption cross section is of the form:

$$S = F\left(\frac{a}{\lambda}, \epsilon - j\frac{\kappa}{\omega \epsilon_v}\right) \qquad (26)$$

This equation states that S is a function of the ratio $\frac{a}{\lambda}$ i.e., of the curvature and wavelength and of the complex dielectric constant. Thus it is possible to increase the wavelength and radius by the same factor for constant S provided that the complex dielectric constant is also kept constant. Thus the results obtained at a frequency f_1, conductivity κ_1, and radius a_1 can be applied at a different frequency f_2 and radius

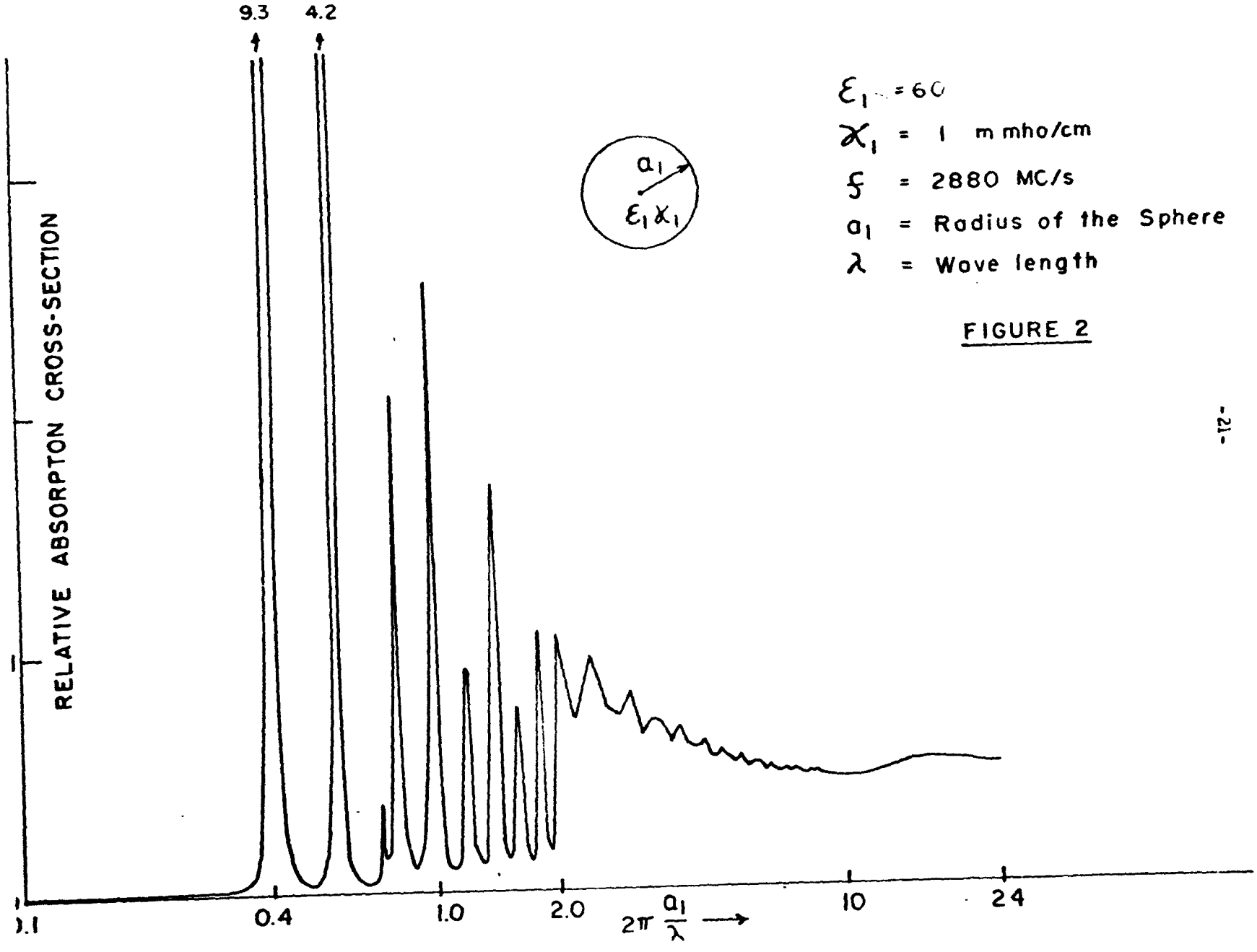
9.3
4.2
RELATIVE ABSORPTON CROSS-SECTION
a_1
$\varepsilon_1 \chi_1$
ε_1 = 60
χ_1 = 1 m mho/cm
f = 2880 MC/s
a_1 = Radius of the Sphere
λ = Wave length
0.1
0.4
1.0
2.0
$2\pi \frac{a_1}{\lambda} \rightarrow$
10
24

FIGURE 2

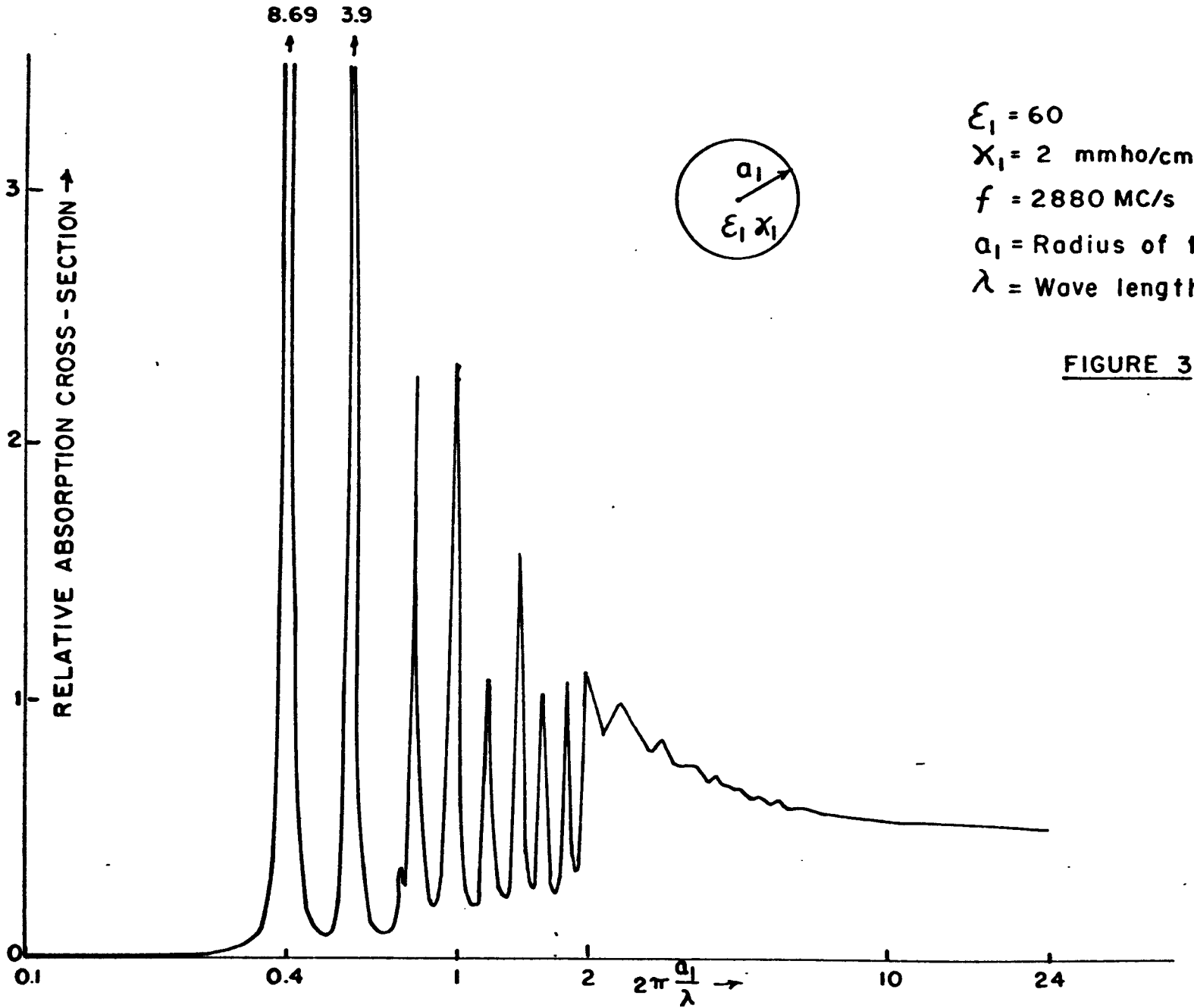
8.69
3.9
RELATIVE ABSORPTION CROSS-SECTION →
0
1
2
3
0.1
0.4
1
2
$2\pi\frac{a_1}{\lambda}$ →
10
24
a_1
$\varepsilon_1 \chi_1$
$\varepsilon_1 = 60$
$\chi_1 = 2$ mmho/cm
$f = 2880$ MC/s
a_1 = Radius of the Sphere
λ = Wave length

FIGURE 3

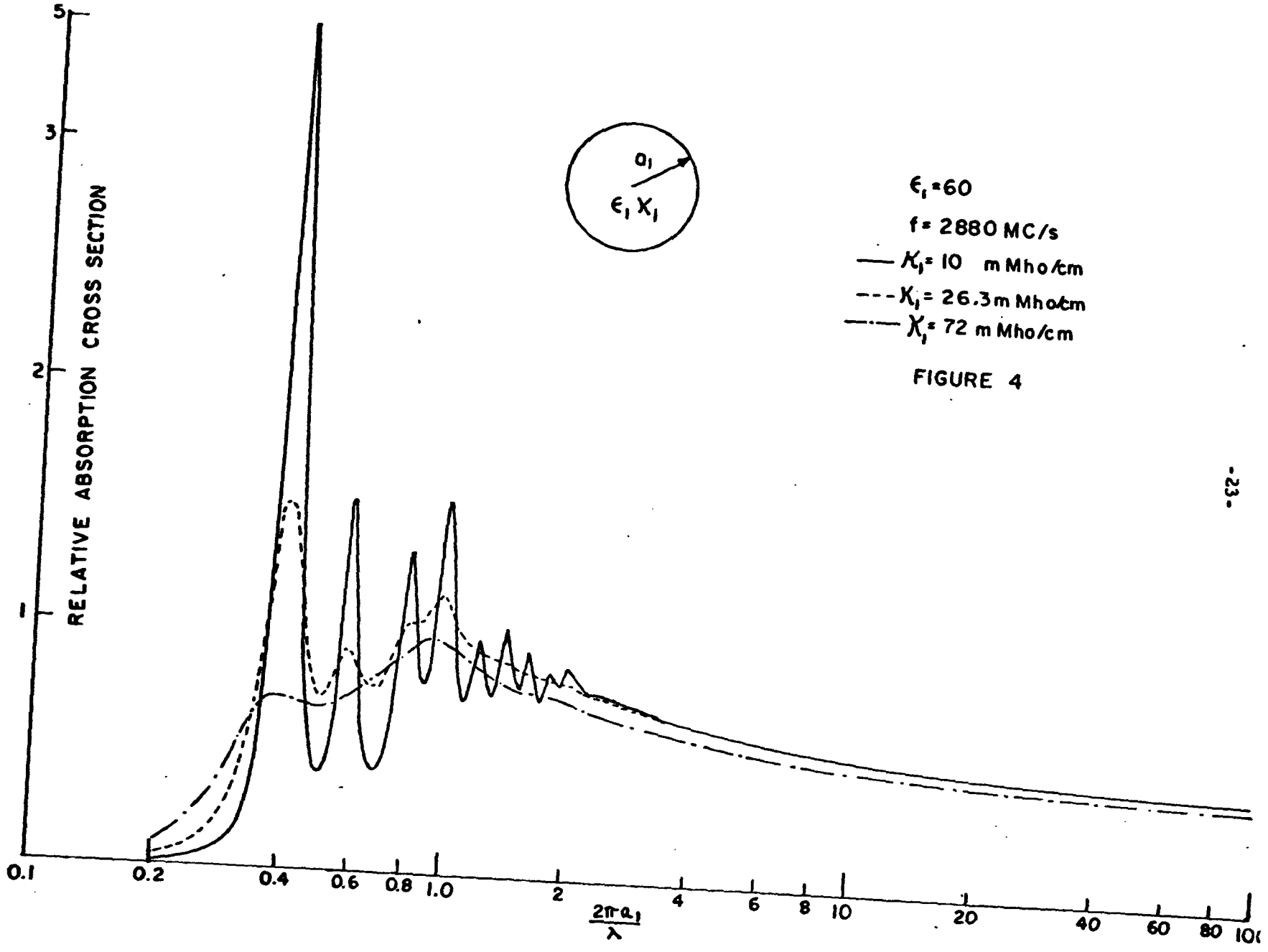
RELATIVE ABSORPTION CROSS SECTION
5
3
2
1
0.1
0.2
0.4
0.6
0.8
1.0
2
4
6
8
10
20
40
60
80
100
$\frac{2\pi a_1}{\lambda}$
a_1
ϵ_1, χ_1
$\epsilon_1 = 60$
f = 2880 MC/s
χ_1 = 10 m Mho/cm
χ_1 = 26.3 m Mho/cm
χ_1 = 72 m Mho/cm

FIGURE 4

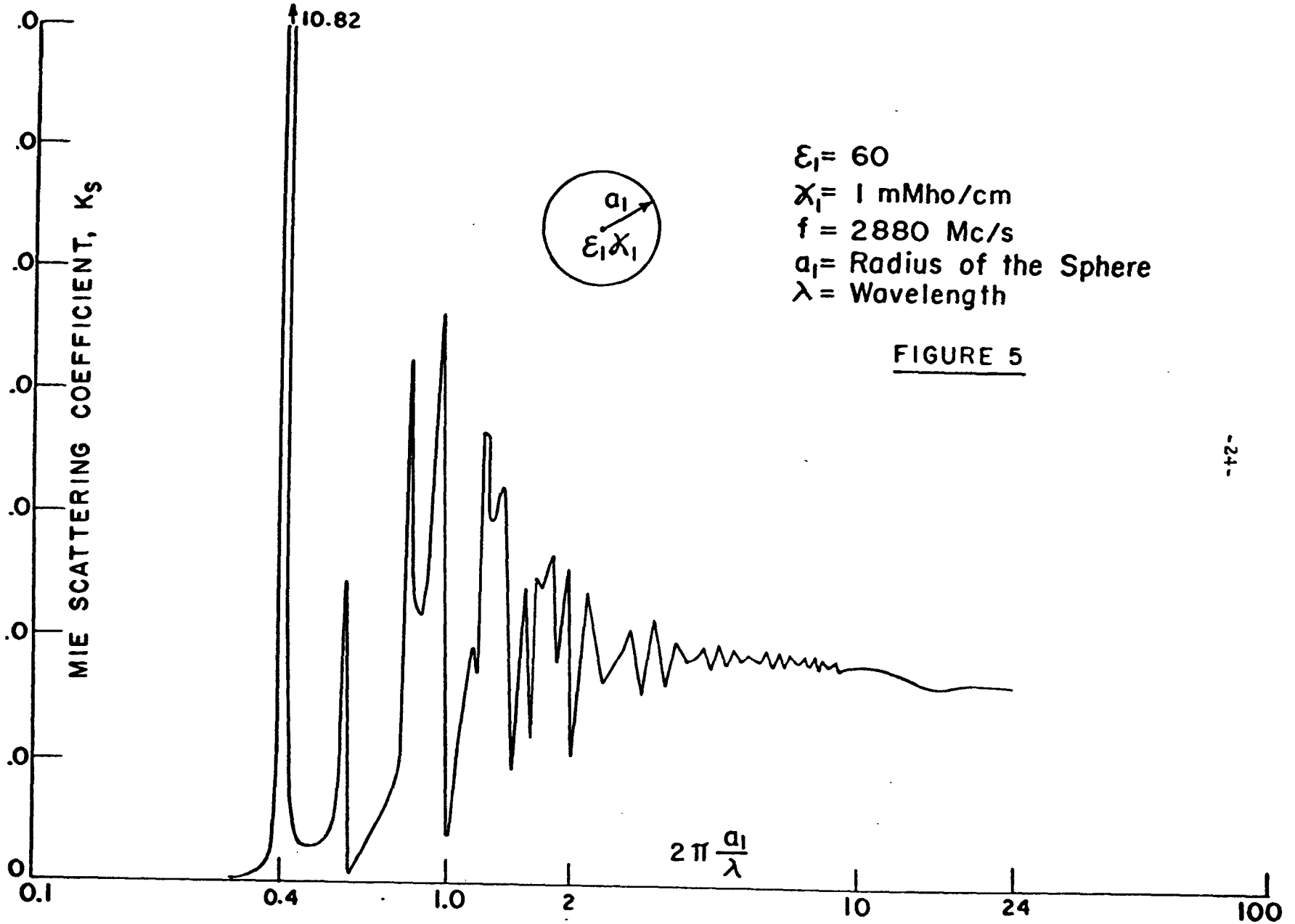
10.82
.0
.0
.0
.0
.0
.0
0
MIE SCATTERING COEFFICIENT, K_S
a_1
$\varepsilon_1 \gamma_1$
ε_1= 60
γ_1= 1 mMho/cm
f = 2880 Mc/s
a_1= Radius of the Sphere
λ = Wavelength
$2\pi \frac{a_1}{\lambda}$
0.1
0.4
1.0
2
10
24
100

FIGURE 5

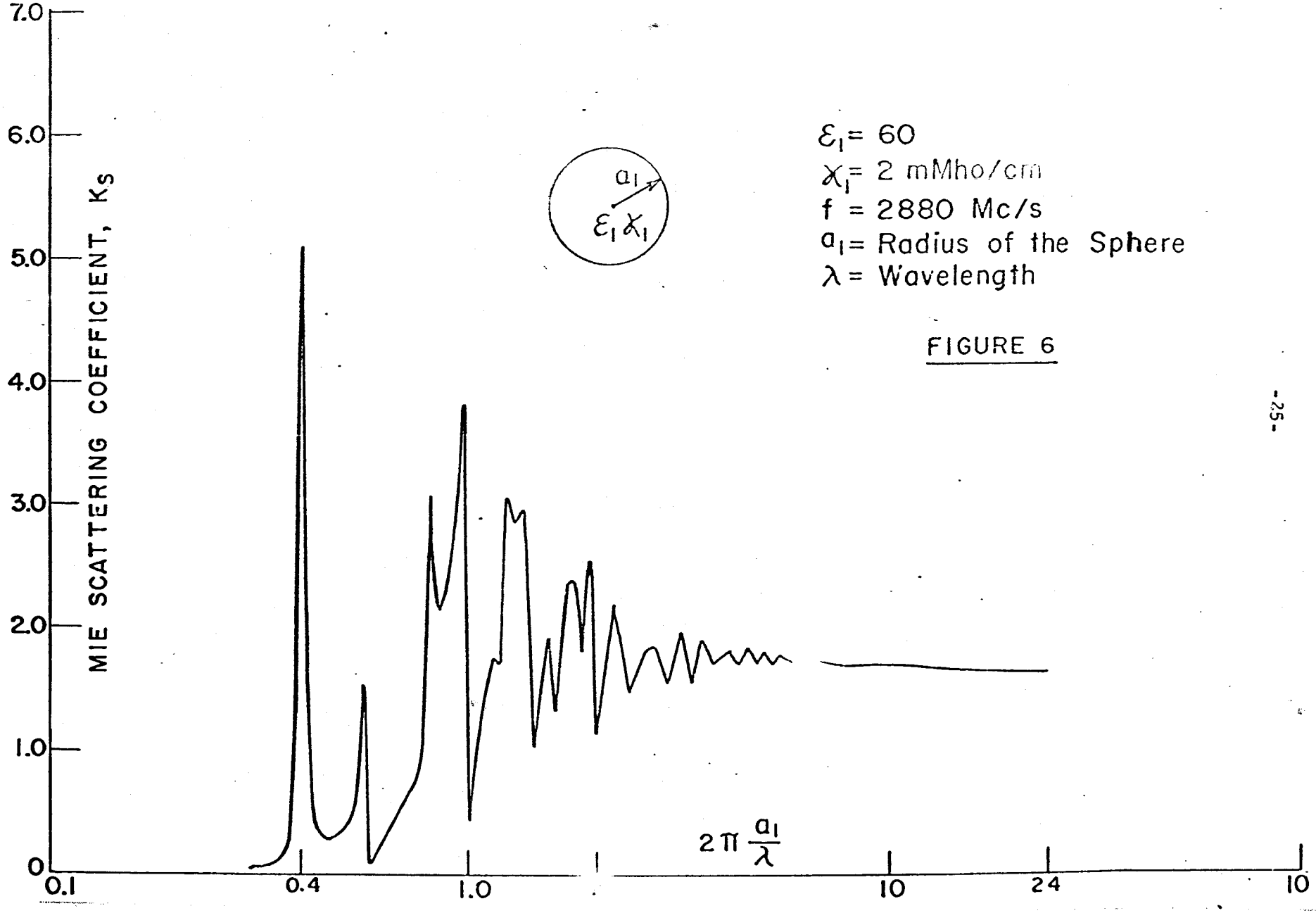
7.0
6.0
5.0
4.0
3.0
2.0
1.0
0
MIE SCATTERING COEFFICIENT, K_S
a_1
$\varepsilon_1 \chi_1$
$\varepsilon_1 = 60$
$\chi_1 = 2$ mMho/cm
$f = 2880$ Mc/s
a_1 = Radius of the Sphere
λ = Wavelength
0.1
0.4
1.0
$2\pi \frac{a_1}{\lambda}$
10
24
10

FIGURE 6

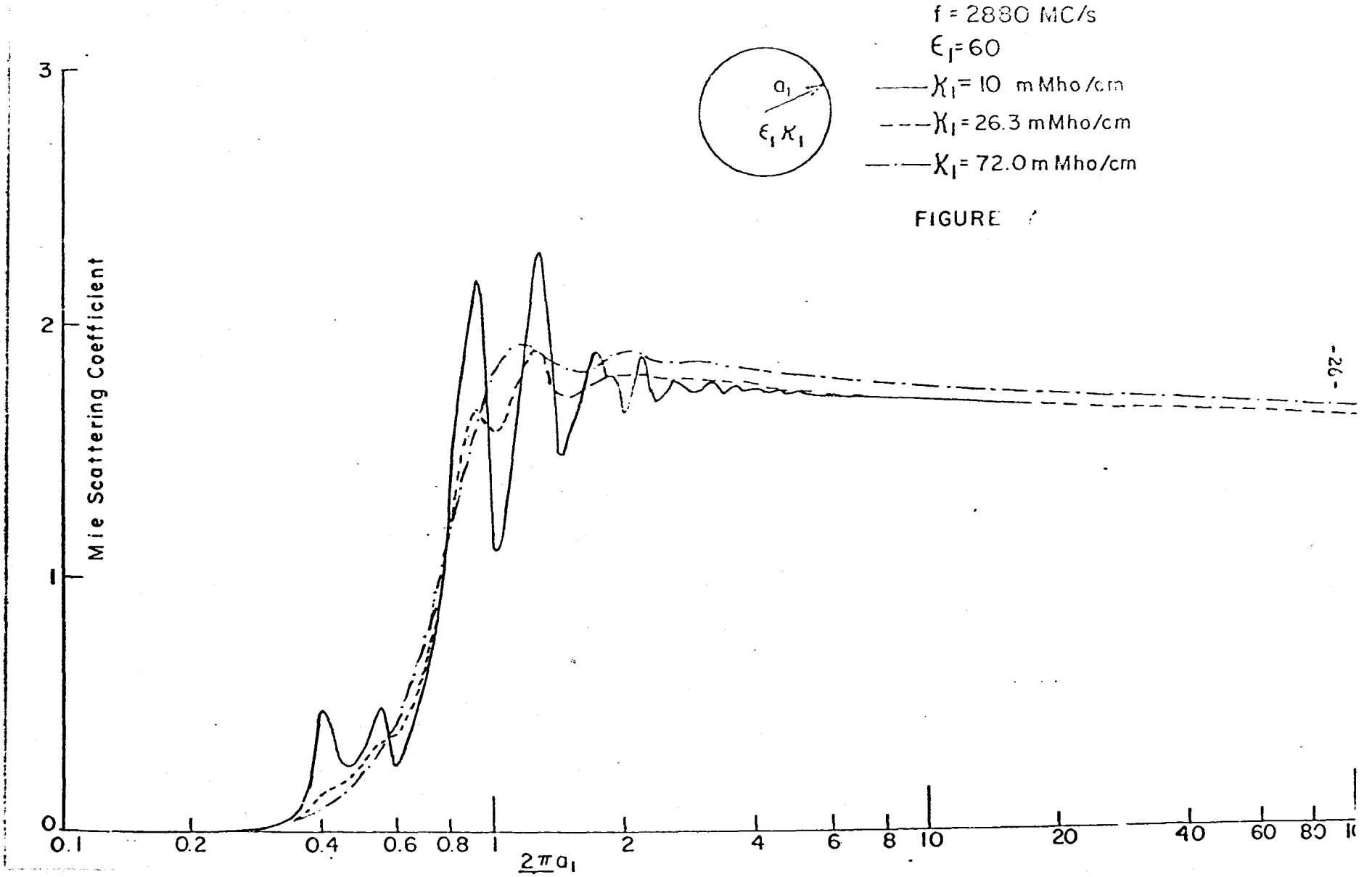
f = 2880 MC/s
$\epsilon_1 = 60$
$\chi_1 = 10$ m Mho/cm
$\chi_1 = 26.3$ m Mho/cm
$\chi_1 = 72.0$ m Mho/cm
a_1
$\epsilon_1 \chi_1$
Mie Scattering Coefficient
0
1
2
3
0.1
0.2
0.4
0.6
0.8
1
2
4
6
8
10
20
40
60
80
$2\pi a_1$

FIGURE

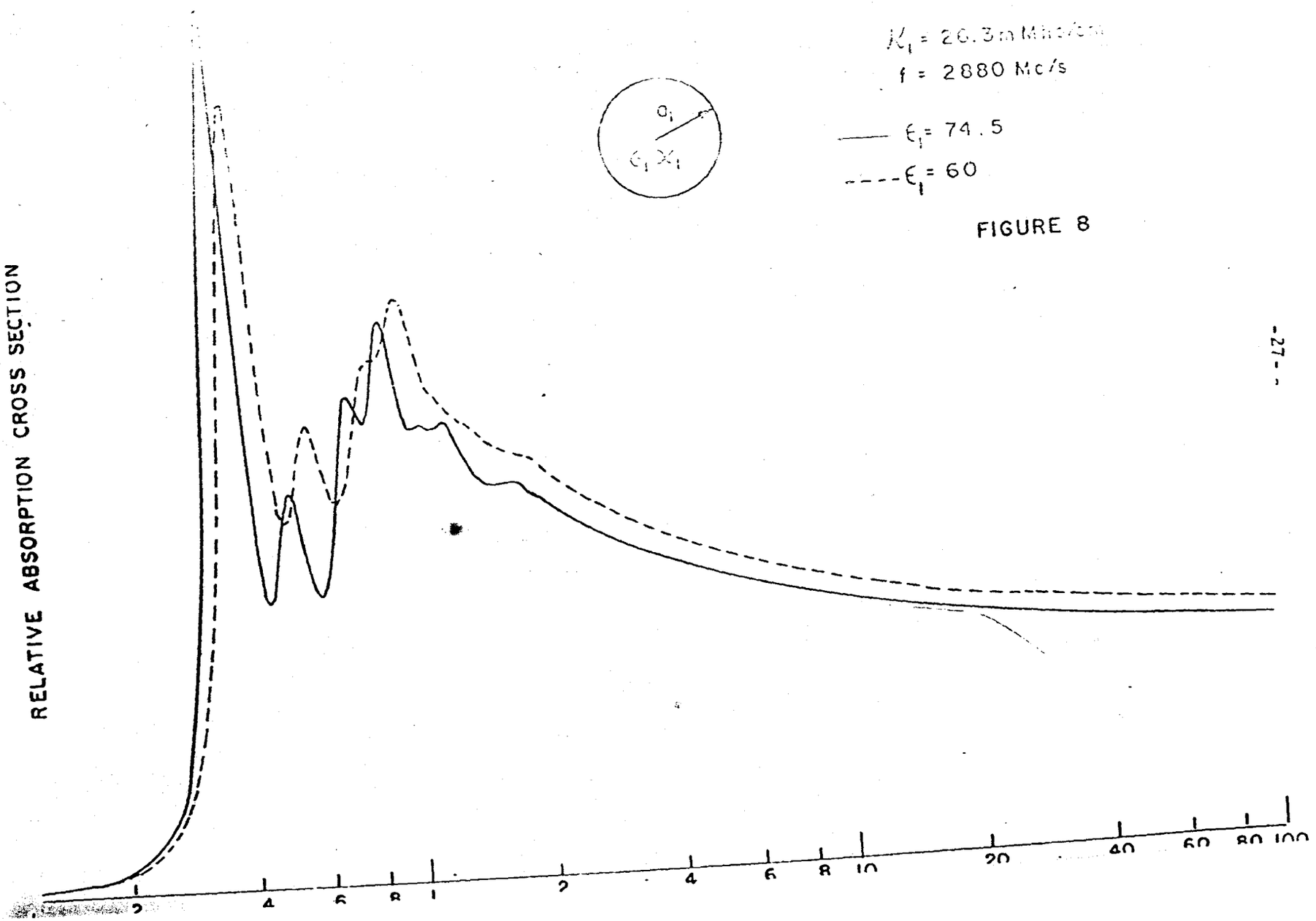
RELATIVE ABSORPTION CROSS SECTION
K_1 = 20.3 m Mc/s
f = 2880 Mc/s
a_1
$\epsilon_1 \mu_1$
—— ϵ_1 = 74.5
----ϵ_1 = 60
2
4
6
8
1
2
4
6
8
10
20
40
60
80
100

FIGURE 8

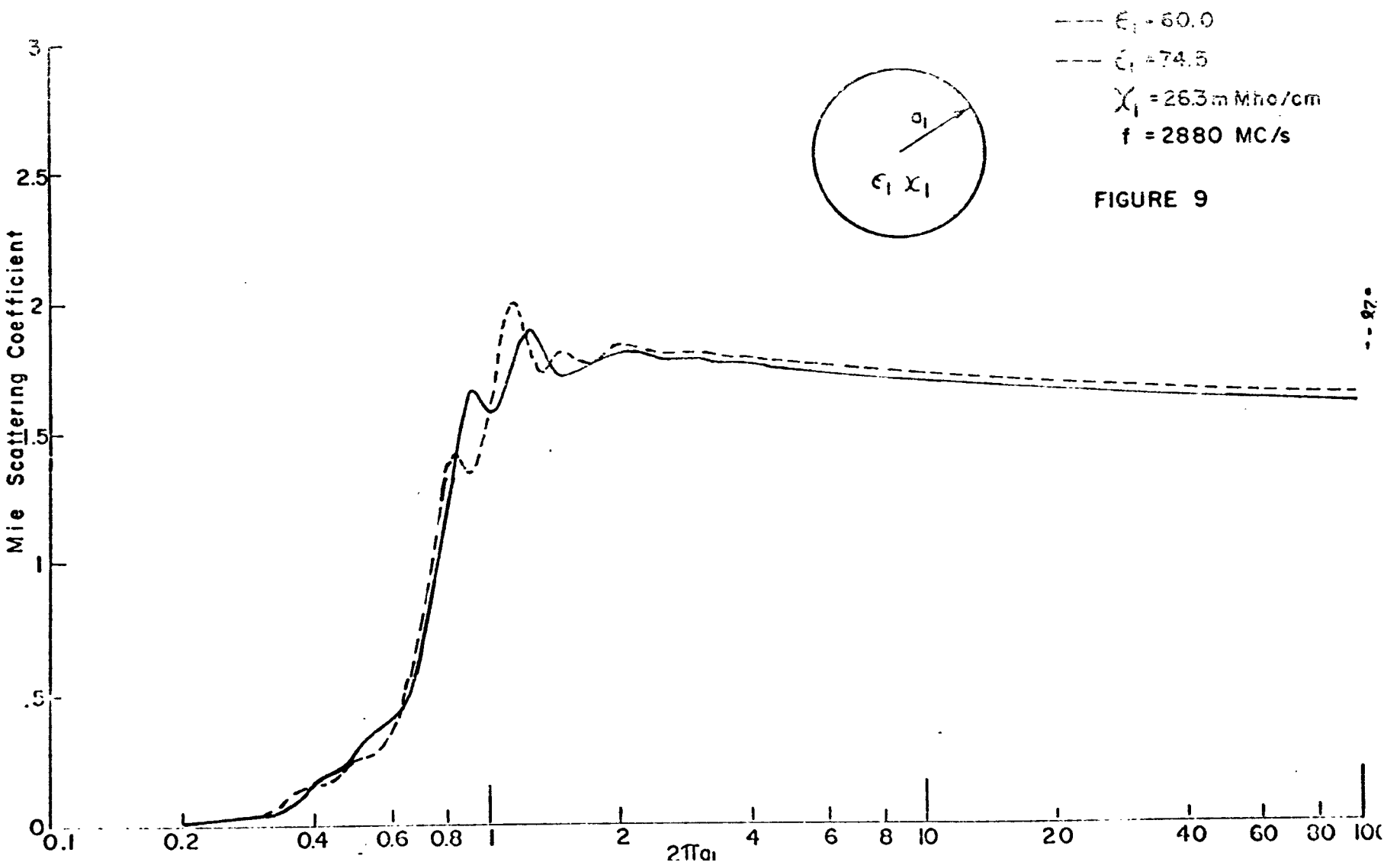
ϵ_1 = 60.0
ϵ_1 = 74.5
χ_1 = 26.3 m Mho/cm
f = 2880 MC/s
a_1
ϵ_1 χ_1
Mie Scattering Coefficient
0
.5
1
1.5
2
2.5
3
0.1
0.2
0.4
0.6
0.8
1
2
4
6
8
10
20
40
60
80
100
$2\pi a_1$

FIGURE 9

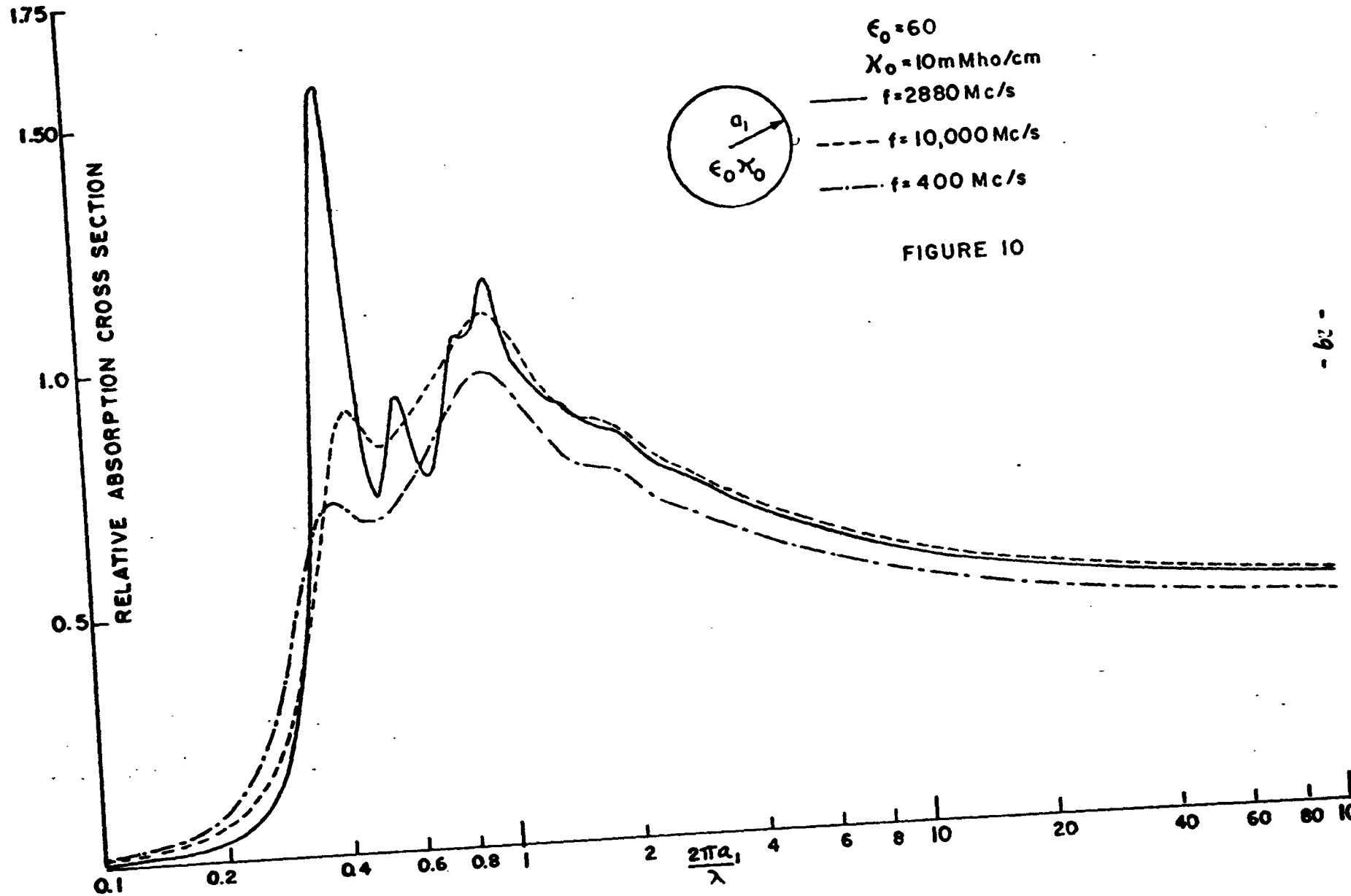
$\epsilon_0 = 60$
$\chi_0 = 10$ m Mho/cm
f = 2880 Mc/s
f = 10,000 Mc/s
f = 400 Mc/s
a_1
$\epsilon_0 \chi_0$
RELATIVE ABSORPTION CROSS SECTION
1.75
1.50
1.0
0.5
0.1
0.2
0.4
0.6
0.8
1
2
4
6
8
10
20
40
60
80
100
$\frac{2\pi a_1}{\lambda}$

FIGURE 10

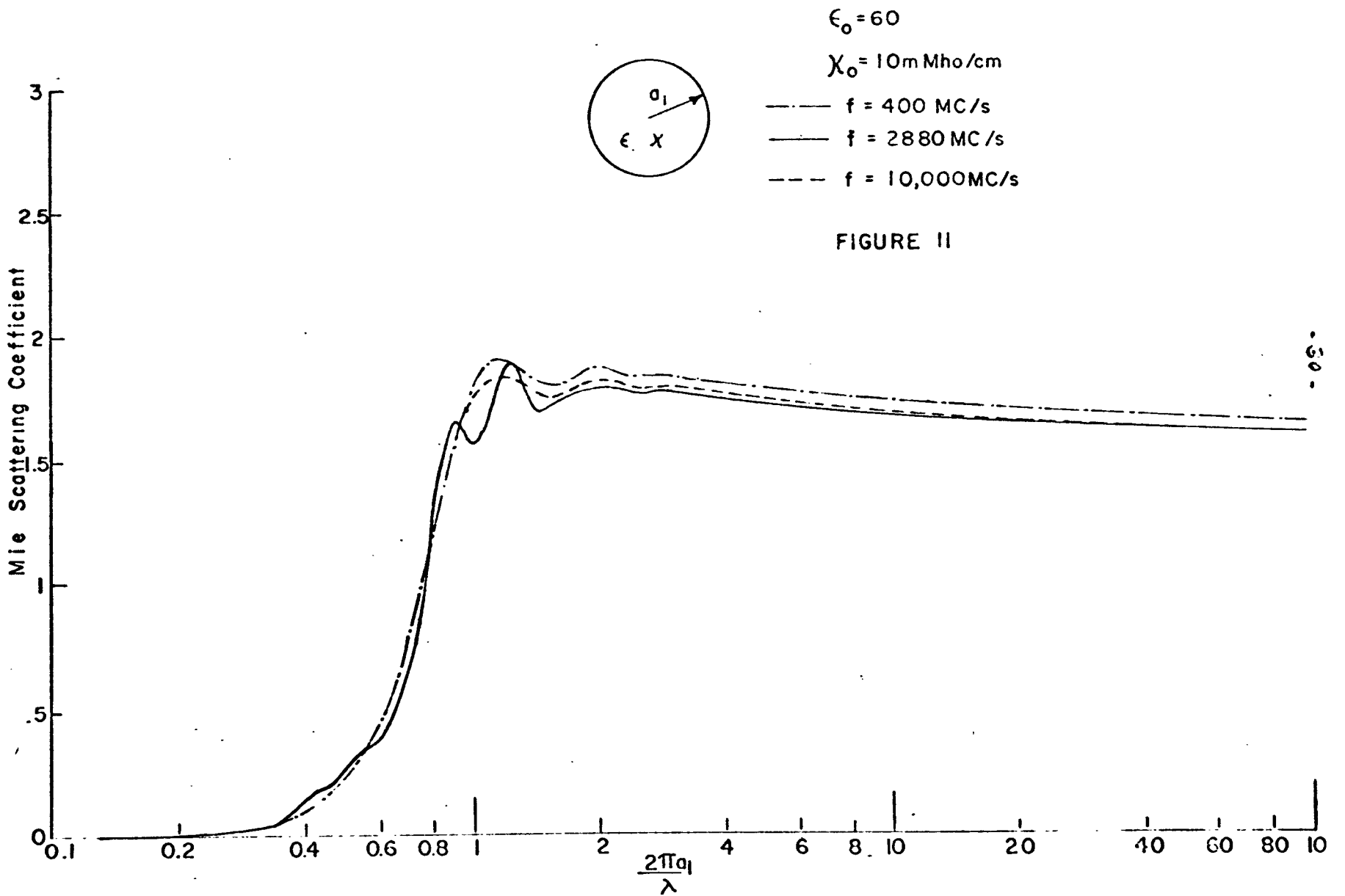
$\epsilon_0 = 60$
$\chi_0 = 10$ m Mho/cm
a_1
ϵ χ
f = 400 MC/s
f = 2880 MC/s
f = 10,000MC/s
Mie Scattering Coefficient
3
2.5
2
1.5
1
.5
0
0.1
0.2
0.4
0.6
0.8
1
2
4
6
8
10
20
40
60
80
10
$\frac{2\pi a_1}{\lambda}$

FIGURE 11

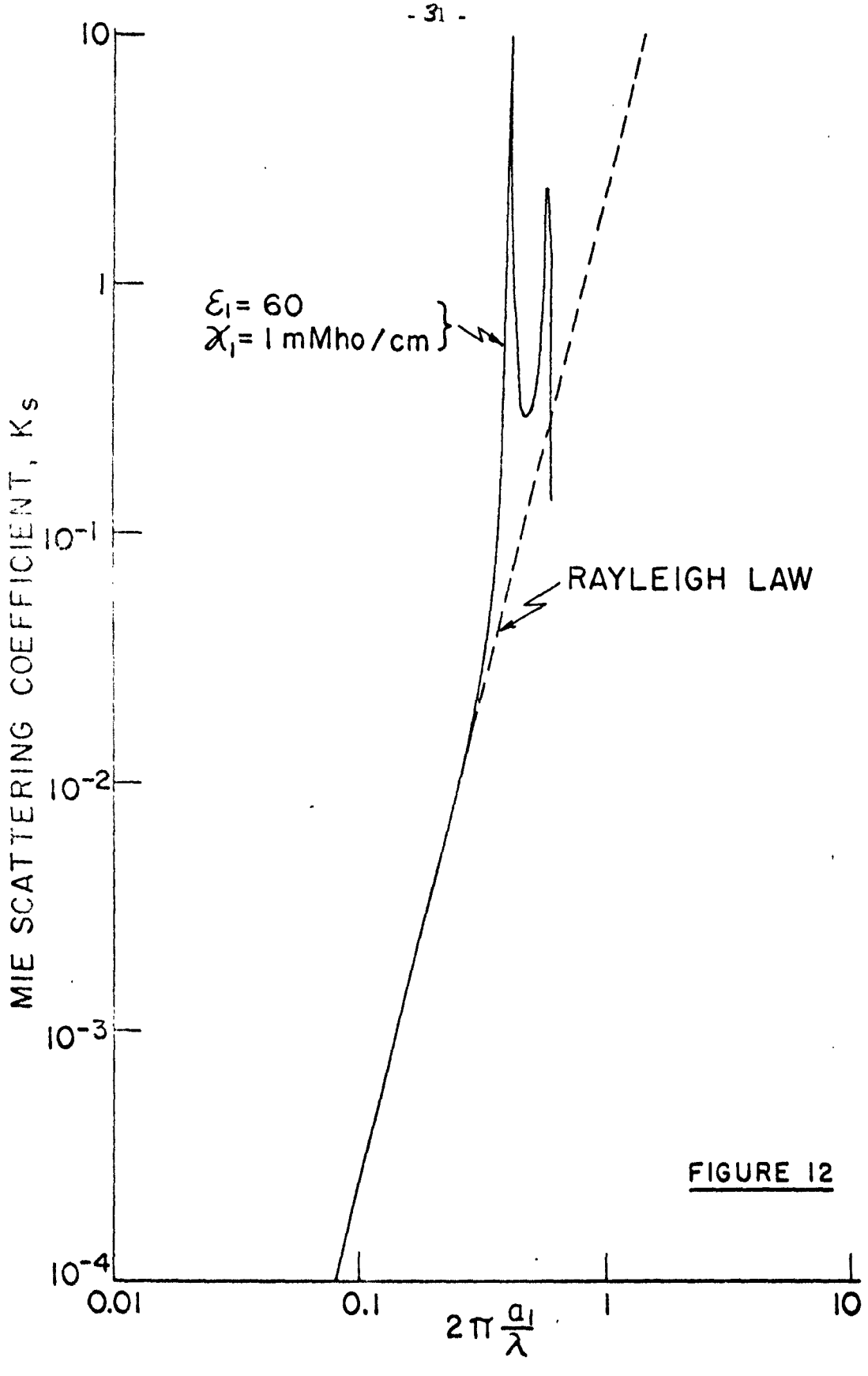
10
1
10^{-1}
10^{-2}
10^{-3}
10^{-4}
MIE SCATTERING COEFFICIENT, K_s
$\varepsilon_1 = 60$
$\sigma_1 = 1$ mMho/cm
RAYLEIGH LAW
0.01
0.1
1
10
$2\pi \frac{a_1}{\lambda}$

FIGURE 12

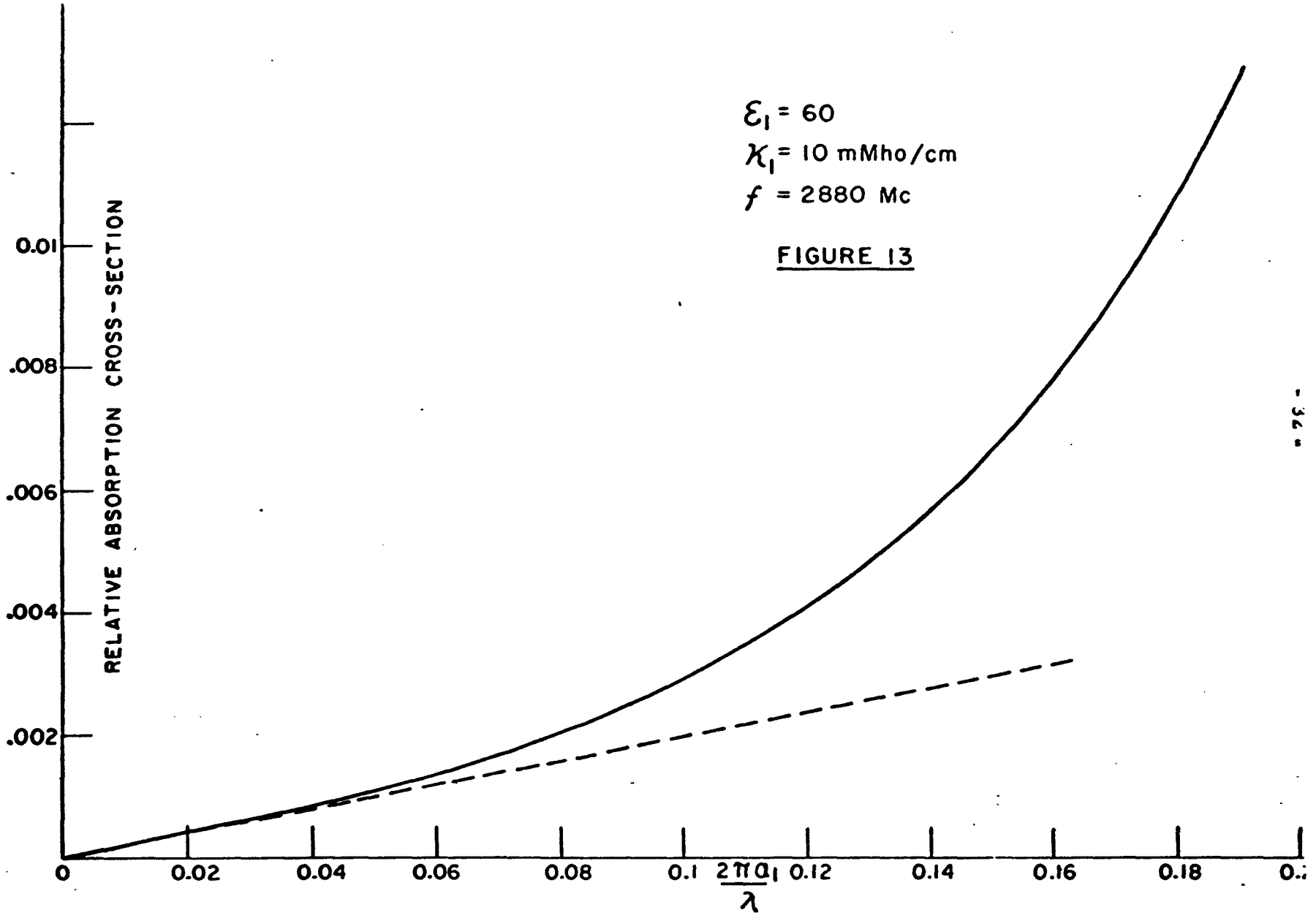
$\varepsilon_1 = 60$
$\kappa_1 = 10$ mMho/cm
$f = 2880$ Mc
RELATIVE ABSORPTION CROSS-SECTION
0.01
.008
.006
.004
.002
0
0.02
0.04
0.06
0.08
0.1
0.12
0.14
0.16
0.18
$\frac{2\pi a_1}{\lambda}$

FIGURE 13

$a_2 = a_1(f_1/f_2)$ provided that the dielectric constant remains the same and the new conductivity is given by:

$$\kappa_2 = \left(\frac{a_1}{a_2}\right) \kappa_1 \qquad (27)$$

2.2 Concentric Sphere

The concentric sphere model where the inner sphere simulates muscular tissues and the outer shell represents the subcutaneous fat was used to investigate the effect of a fat layer. The Mie scattering coefficient and the relative absorption cross section were calculated as a function of a_1. The results were obtained for frequencies of 400, 2880 and 10000 Mc/s for different values of fat layer thickness (d).

The results of the machine computation for relative absorption cross section and Mie scattering coefficient are shown in figures 14 through 19 as a function of a_1. The calculations were performed for values of a_1 in the following ranges:

a_1 =	0.1 to 2	in steps of 0.02
	2.2 to 3	in steps of 0.1
	4 to 10	in steps of 1
	10 to 50	in steps of 10

A curve for d = 0, corresponding to single or homogeneous sphere is included with every figure for reference purposes. The dielectric data used for the muscular and fatty tissues are given in Table II on page 6. The range of fat thickness (d) was restricted to three centimeters since it is not often that thicker fat layers will be encountered.

It can be seen from these figures, that the thickness of the shell has great influence on both relative absorption cross section and Mie scattering coefficient. For values of a_1 up to about 0.3, both S and K_s of the concentric sphere are greater than corresponding values for the single sphere. This occurs because the overall radius of the concentric sphere is greater than that of the single sphere and the thickness of the concentric shell is comparable to or greater than the radius of the single sphere.

For large values of a_1, the concentric shell appears to behave like an impedance matching transformer between inner sphere and air. As the shell thickness increases, S increases and K_s decreases with the maximum effect occurring near a thickness of $\frac{\lambda}{4}$ in the material. At this point the matching is greatest thus causing maximum absorption and minimum scattering. This is a well known phenomenon for plane waves incident on infinite plane layers of pure dielectric materials, provided that the dielectric constant of the quarter-wave layer is equal to the geometric mean of the dielectric constants of the other two layers. It has also been demonstrated by Schwan and Li[11] for multiple plane layers of lossy dielectric materials.

The influence of the concentric layer thickness is more easily discernible in figures 20 through 22 where the relative absorption cross section is plotted as a function of shell thickness (d) for frequencies of 400, 2880 and 10,000 Mc/s. The curves are given for an inner sphere radius of 16 cm which makes a_1 greater than 6 at frequencies of 2880 and 10,000

Mc/s where the impedance matching property of the concentric shell is more easily recognized than for values of a_1 less than 6. A curve for the case of infinite plane slabs ($a_1 = \infty$) is included in each figure for comparison. It can be seen that the relative absorption cross section of the sphere is always greater than that for the plane slabs but its general behavior as function of d is quite similar.

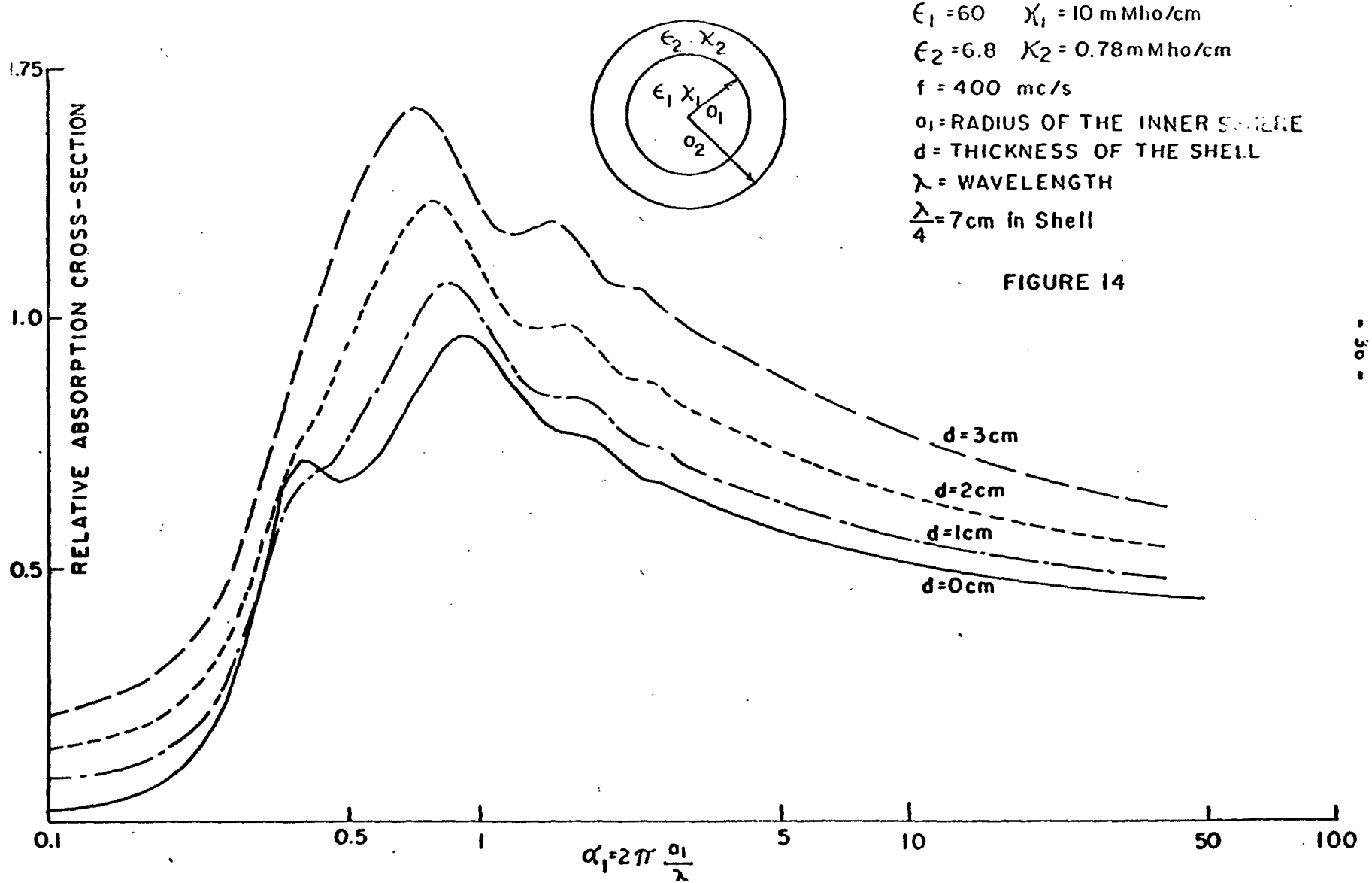
ϵ_1 =60 χ_1 = 10 m Mho/cm
ϵ_2 =6.8 χ_2 = 0.78 m Mho/cm
f = 400 mc/s
o_1 = RADIUS OF THE INNER SPHERE
d = THICKNESS OF THE SHELL
λ = WAVELENGTH
$\frac{\lambda}{4}$ = 7cm in Shell
ϵ_2 χ_2
ϵ_1 χ_1
o_1
o_2
RELATIVE ABSORPTION CROSS-SECTION
1.75
1.0
0.5
d=3cm
d=2cm
d=1cm
d=0cm
0.1
0.5
1
5
10
50
100
$\alpha_1 = 2\pi \frac{o_1}{\lambda}$

FIGURE 14

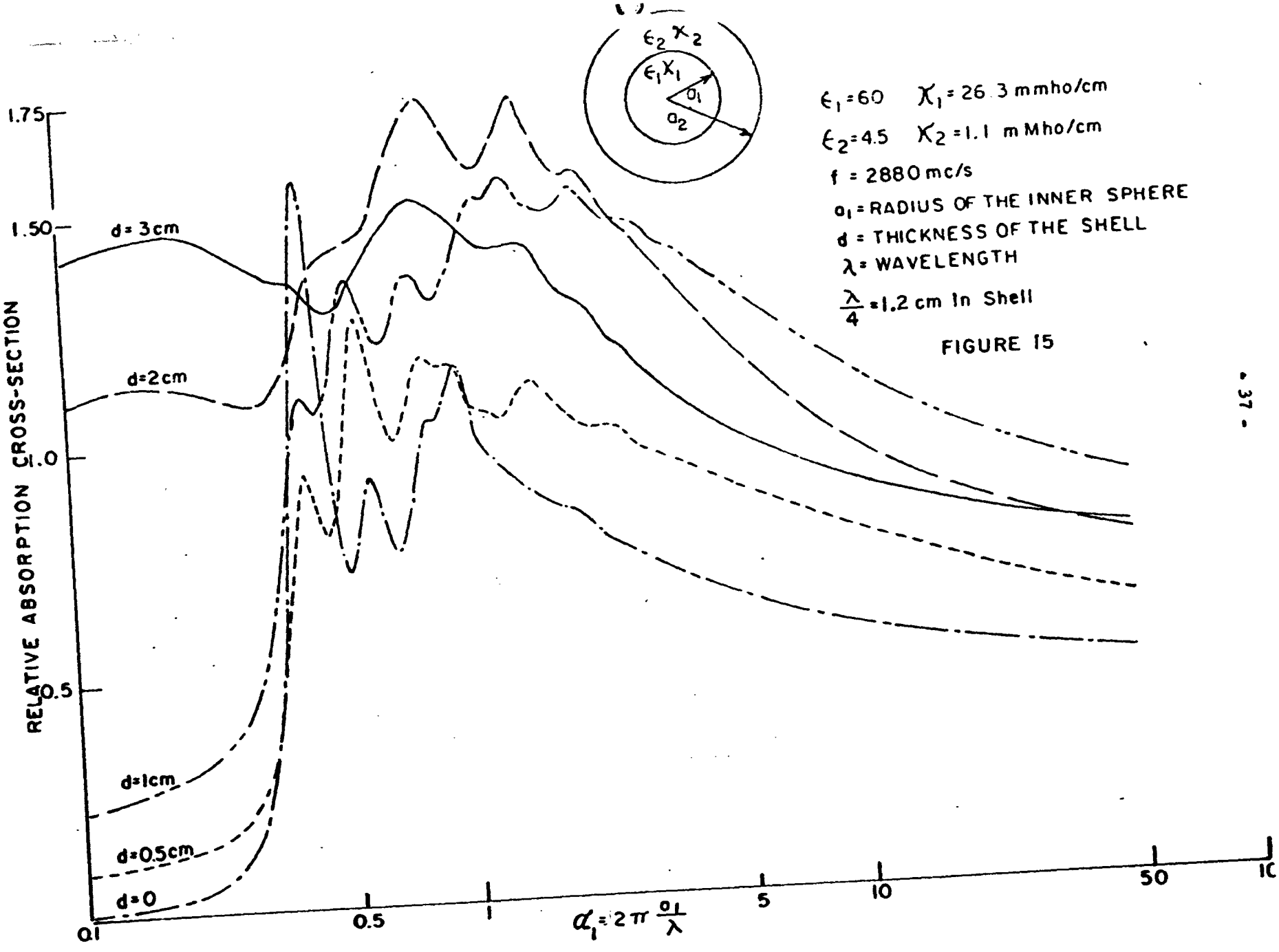
ϵ_2 χ_2
ϵ_1 χ_1
a_1
a_2
$\epsilon_1 = 60$ $\chi_1 = 26.3$ mmho/cm
$\epsilon_2 = 4.5$ $\chi_2 = 1.1$ m Mho/cm
f = 2880 mc/s
a_1 = RADIUS OF THE INNER SPHERE
d = THICKNESS OF THE SHELL
λ = WAVELENGTH
$\frac{\lambda}{4}$ = 1.2 cm In Shell
RELATIVE ABSORPTION CROSS-SECTION
1.75
1.50
1.0
0.5
d = 3cm
d=2cm
d=1cm
d=0.5cm
d=0
0.1
0.5
1
5
10
50
$\alpha_1 = 2\pi \frac{a_1}{\lambda}$

FIGURE 15

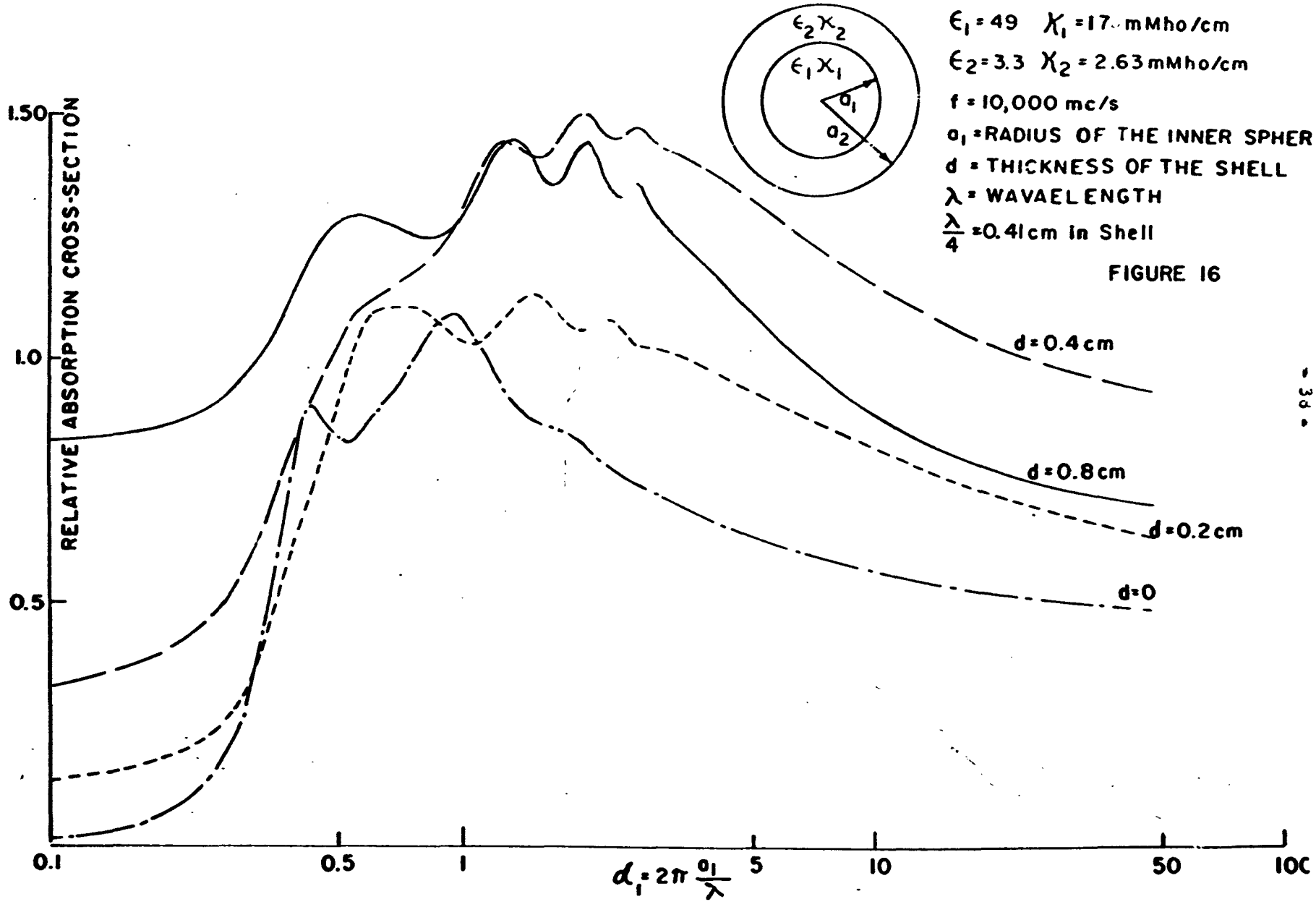
$\epsilon_2 \chi_2$
$\epsilon_1 \chi_1$
a_1
a_2
$\epsilon_1 = 49$ $\chi_1 = 17$ mMho/cm
$\epsilon_2 = 3.3$ $\chi_2 = 2.63$ mMho/cm
f = 10,000 mc/s
a_1 = RADIUS OF THE INNER SPHER
d = THICKNESS OF THE SHELL
λ = WAVAELENGTH
$\frac{\lambda}{4}$ = 0.41cm in Shell
FIGURE 16
RELATIVE ABSORPTION CROSS-SECTION
1.50
1.0
0.5
d = 0.4 cm
d = 0.8 cm
d = 0.2 cm
d = 0
0.1
0.5
1
5
10
50
100
$\alpha_1 = 2\pi \frac{a_1}{\lambda}$

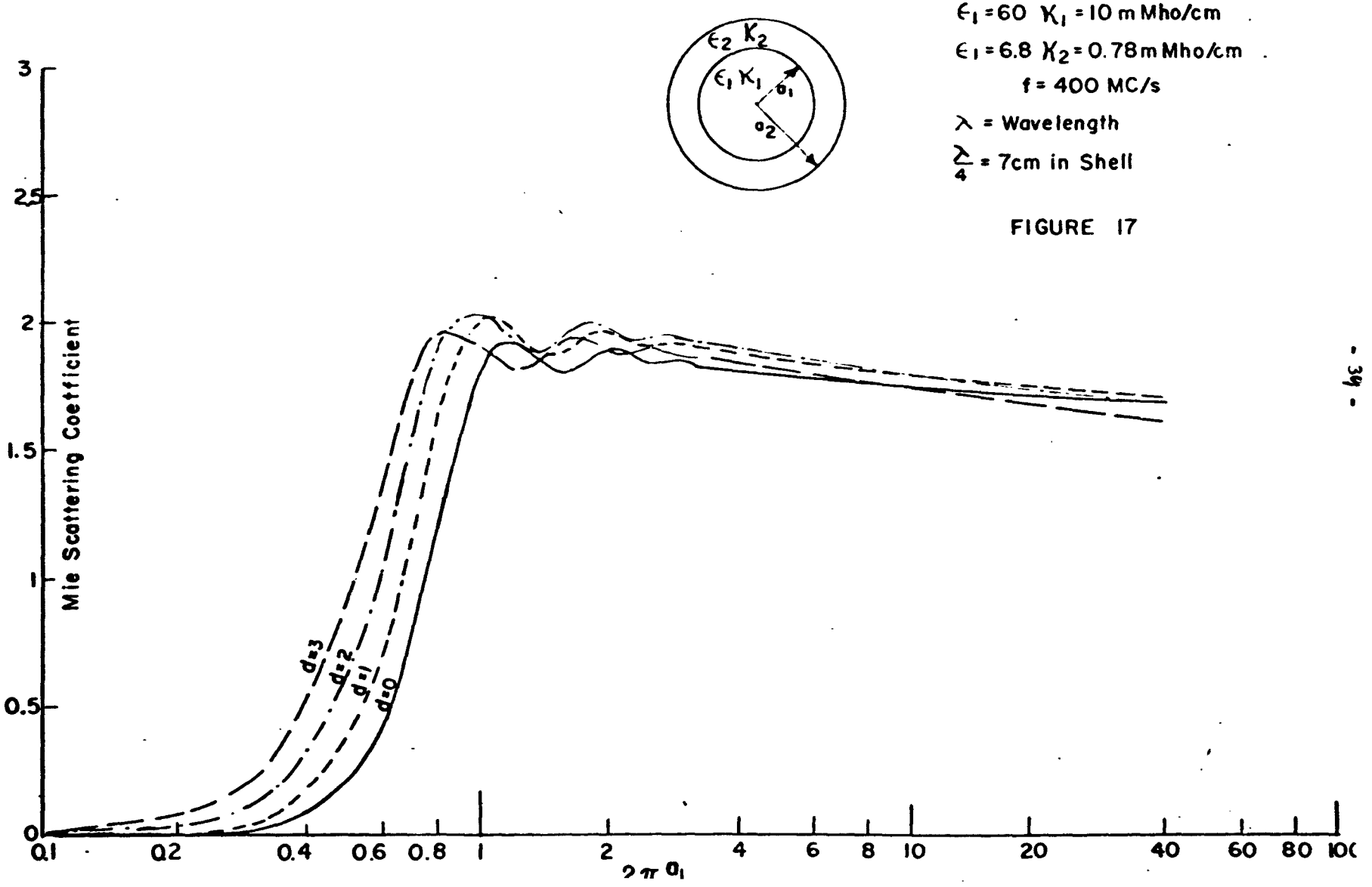
$\epsilon_1 = 60$ $\gamma_1 = 10$ m Mho/cm
$\epsilon_1 = 6.8$ $\gamma_2 = 0.78$ m Mho/cm
f = 400 MC/s
λ = Wavelength
$\frac{\lambda}{4}$ = 7cm in Shell
ϵ_2 γ_2
ϵ_1 γ_1
a_1
a_2
FIGURE 17
Mie Scattering Coefficient
3
2.5
2
1.5
1
0.5
0
d=3
d=2
d=1
d=0
0.1
0.2
0.4
0.6
0.8
1
2
4
6
8
10
20
40
60
80
100
$2\pi a_1$

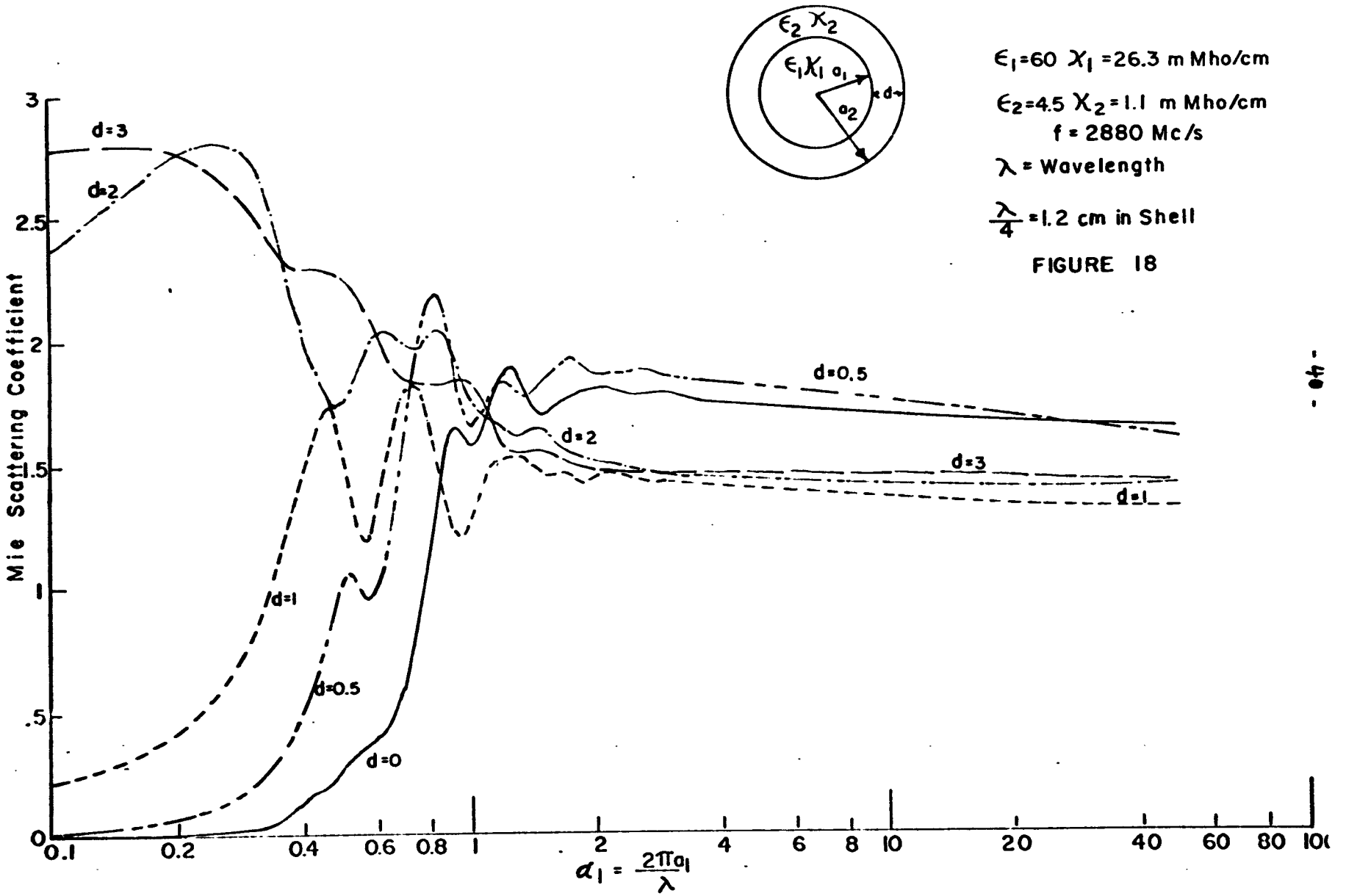
ϵ_2 χ_2
$\epsilon_1\chi_1$ a_1
a_2
d
ϵ_1=60 χ_1 =26.3 m Mho/cm
ϵ_2=4.5 χ_2 = 1.1 m Mho/cm
f = 2880 Mc/s
λ = Wavelength
λ/4 = 1.2 cm in Shell
FIGURE 18
Mie Scattering Coefficient
d=3
d=2
d=1
d=0.5
d=0
$\alpha_1 = \frac{2\pi a_1}{\lambda}$
0
.5
1
1.5
2
2.5
3
0.1
0.2
0.4
0.6
0.8
1
2
4
6
8
10
20
40
60
80
100

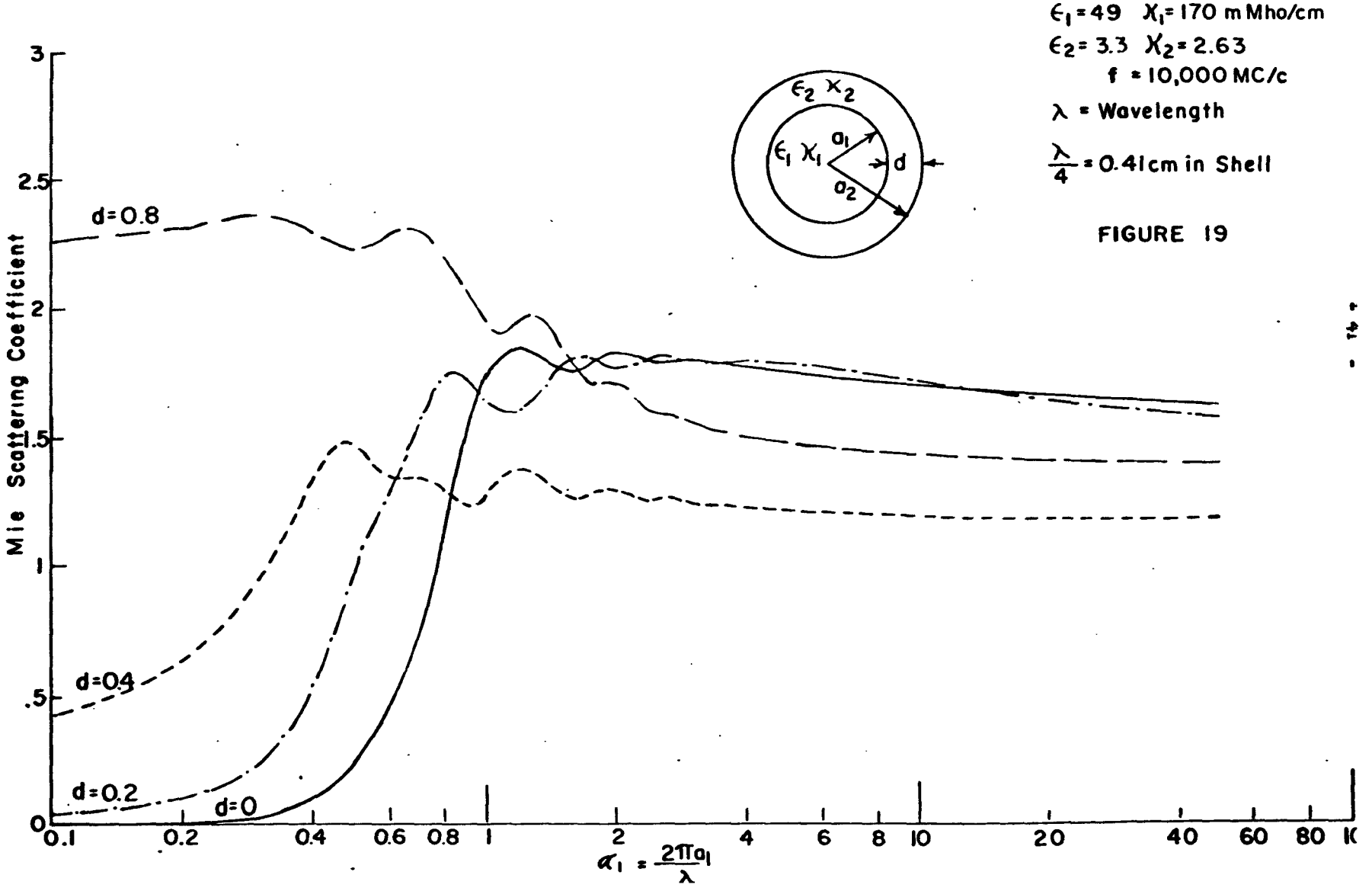
$\epsilon_1 = 49$ $\chi_1 = 170$ m Mho/cm
$\epsilon_2 = 3.3$ $\chi_2 = 2.63$
f = 10,000 MC/c
λ = Wavelength
$\frac{\lambda}{4} = 0.41$cm in Shell
ϵ_2 χ_2
ϵ_1 χ_1
a_1
a_2
d
Mie Scattering Coefficient
d=0.8
d=0.4
d=0.2
d=0
$\alpha_1 = \frac{2\pi a_1}{\lambda}$

FIGURE 19

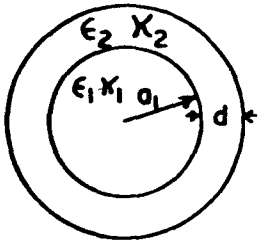

$\epsilon_1 = 60$ $\chi_1 = 10m$ Mho/cm

$\epsilon = 0.8$ $\chi = 7m$ Mho/cm

$f = 400$ MC/s

$d_1 = 2\pi \frac{a_1}{\lambda}$

λ = Wavelength

$\frac{\lambda}{4} = 7cm$ in Shall

FIGURE 20

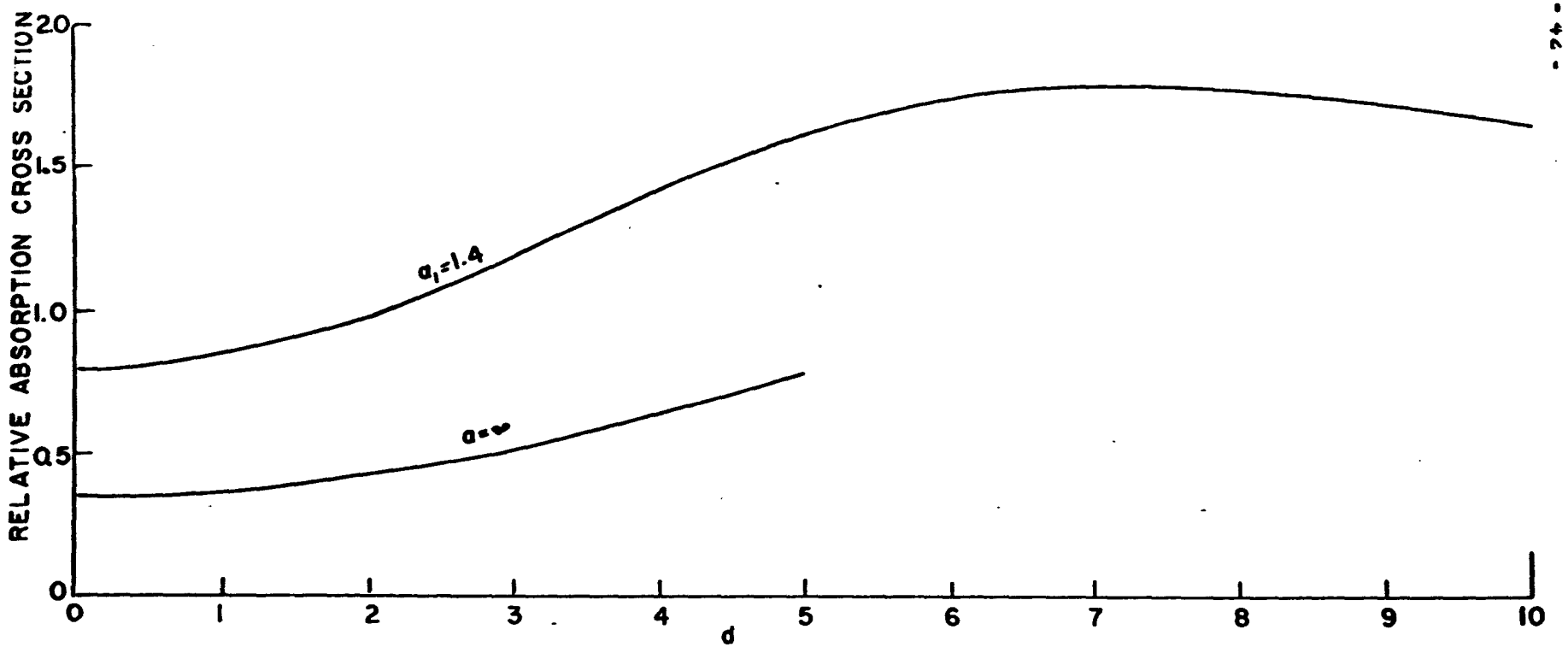

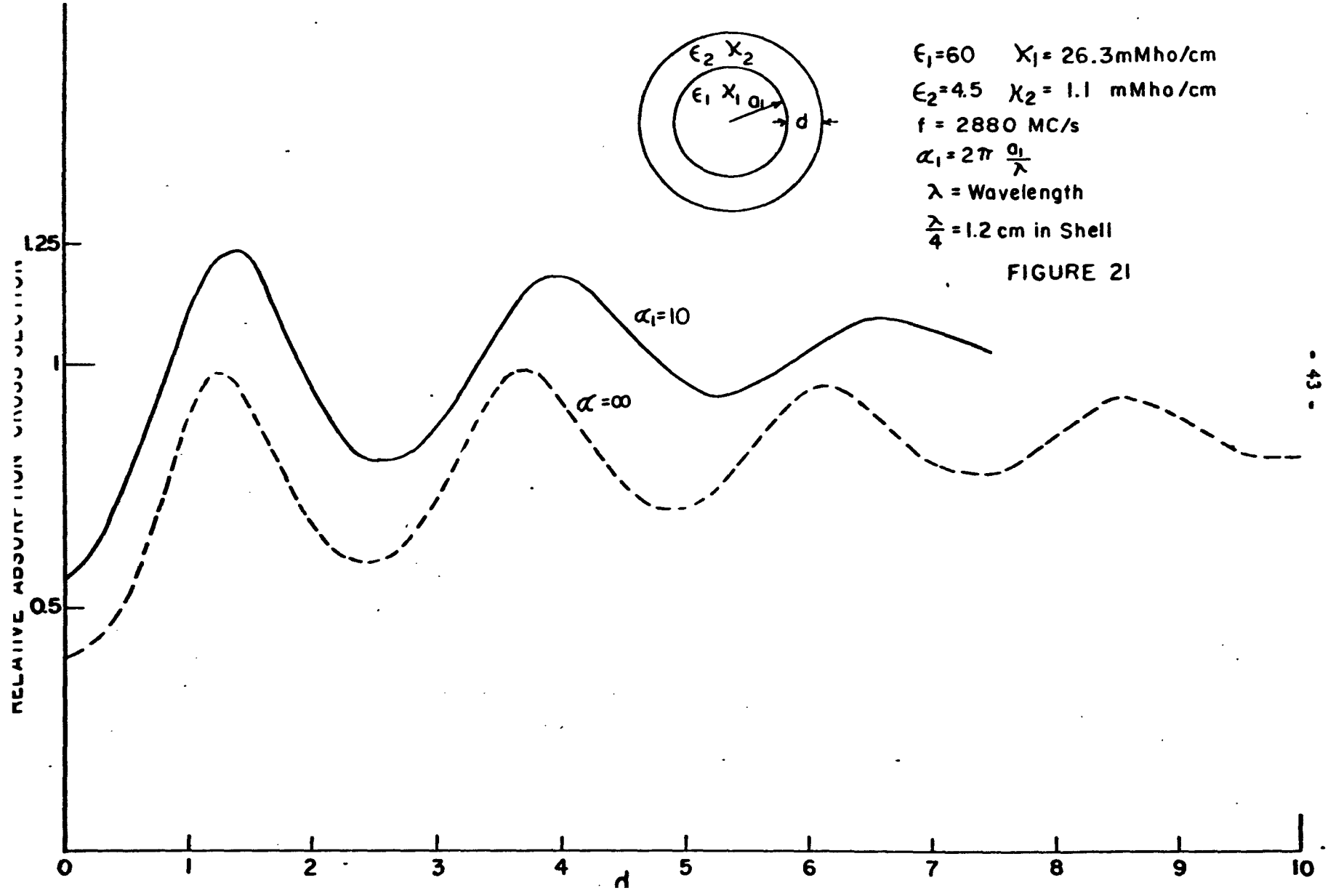
ϵ_2 χ_2
ϵ_1 χ_1 a_1
d
ϵ_1=60 χ_1 = 26.3mMho/cm
ϵ_2=4.5 χ_2 = 1.1 mMho/cm
f = 2880 MC/s
$\alpha_1 = 2\pi \frac{a_1}{\lambda}$
λ = Wavelength
$\frac{\lambda}{4}$ = 1.2 cm in Shell
FIGURE 21
RELATIVE ABSORPTION CROSS SECTION
1.25
1
0.5
α_1=10
α =∞
0
1
2
3
4
5
6
7
8
9
10
d

$\epsilon_1 = 49 \quad \chi_1 = 170$ mMho/cm
$\epsilon = 3.3 \quad \chi = 2.63$ mMho/cm
f = 10000 MC/s
$\alpha_1 = 2\pi \frac{a_1}{\lambda}$
λ = Wavelength
$\frac{\lambda}{4} = 0.41$ cm in Shell

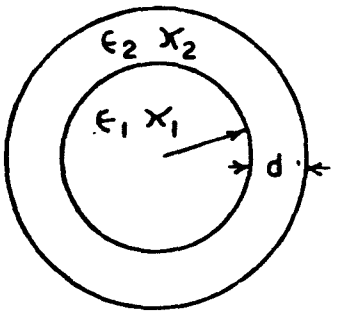

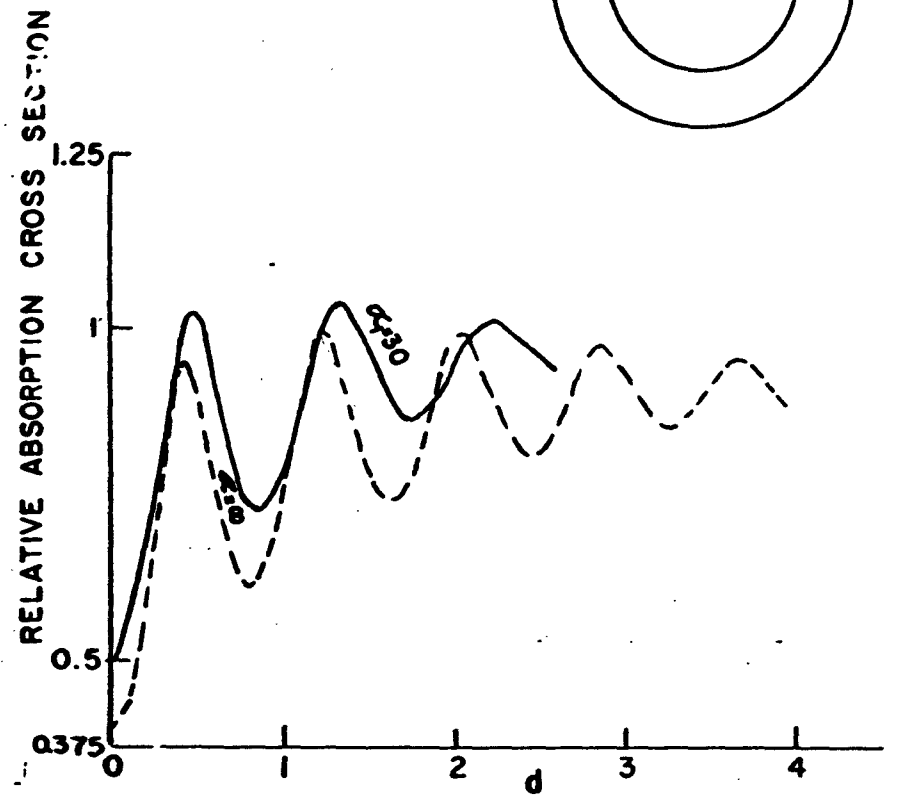

FIGURE 22

III. EXPERIMENTAL STUDIES

1.0 Introduction

Before going into the details of the experimental set-up some statements are necessary with regard to the measurement of relative absorption cross section. The definition of the relative absorption cross section involves several quantities which must be known in order to establish its value:

1. Power density of the incident plane wave field: Power density at the location where the scattering and absorbing obstacle is to be introduced into the field can be determined from the known values of the transmitted power and the gain of the transmitting antenna. Absence of standing waves in the test chamber is a prerequisite for the above determination. Furthermore, the power density of the field should be constant over the shadow cross section of the obstacle.

2. Shadow cross section of the obstacle.

3. Energy absorbed by the obstacle: This quantity can be determined by one of several possible measurements.

   a.) Measurement of field strength inside the obstacle as function of space and determination of the absorbed energy from the volume integral of $E^2\kappa$ where κ is the electrical conductivity of the lossy material filling the obstacle.

   b.) Measurement of temperature rise for a given time of illumination. The volume integral of all temperature

readings divided by the volume itself provides the average temperature rise. Its value, when multiplied with specific weight and heat of the test substance, provides the total energy absorbed.

c.) Measurement of average temperature rise instead of individual temperature rises as in (b). The former is established by vigorous stirring the illuminated test substance immediately after exposure and then measuring its temperature.

Both the (a) and (b) approaches require many readings, particularly when the distribution of E is very variable. This may be expected almost with certainty in view of the limited depth of penetration of the field in comparison with the dimensions of the obstacles of interest. The (b) and (c) approaches share the disadvantage that they require more illuminating power in order to provide sufficient resolution in the temperature readings to be of significance. It was felt that the first disadvantage is more serious than the second. Since approach (c) is furthermore very much simpler than that of (b), it was used in all the experimental work.

2.0 Anechoic Chamber and Antenna

The anechoic chamber used in the experimental study is shown in figure 23. The far wall of the room, facing the horn was covered with 20 gauge sheet copper to protect instruments and the occupants of the adjoining room. Three walls and floor of the room were covered with a

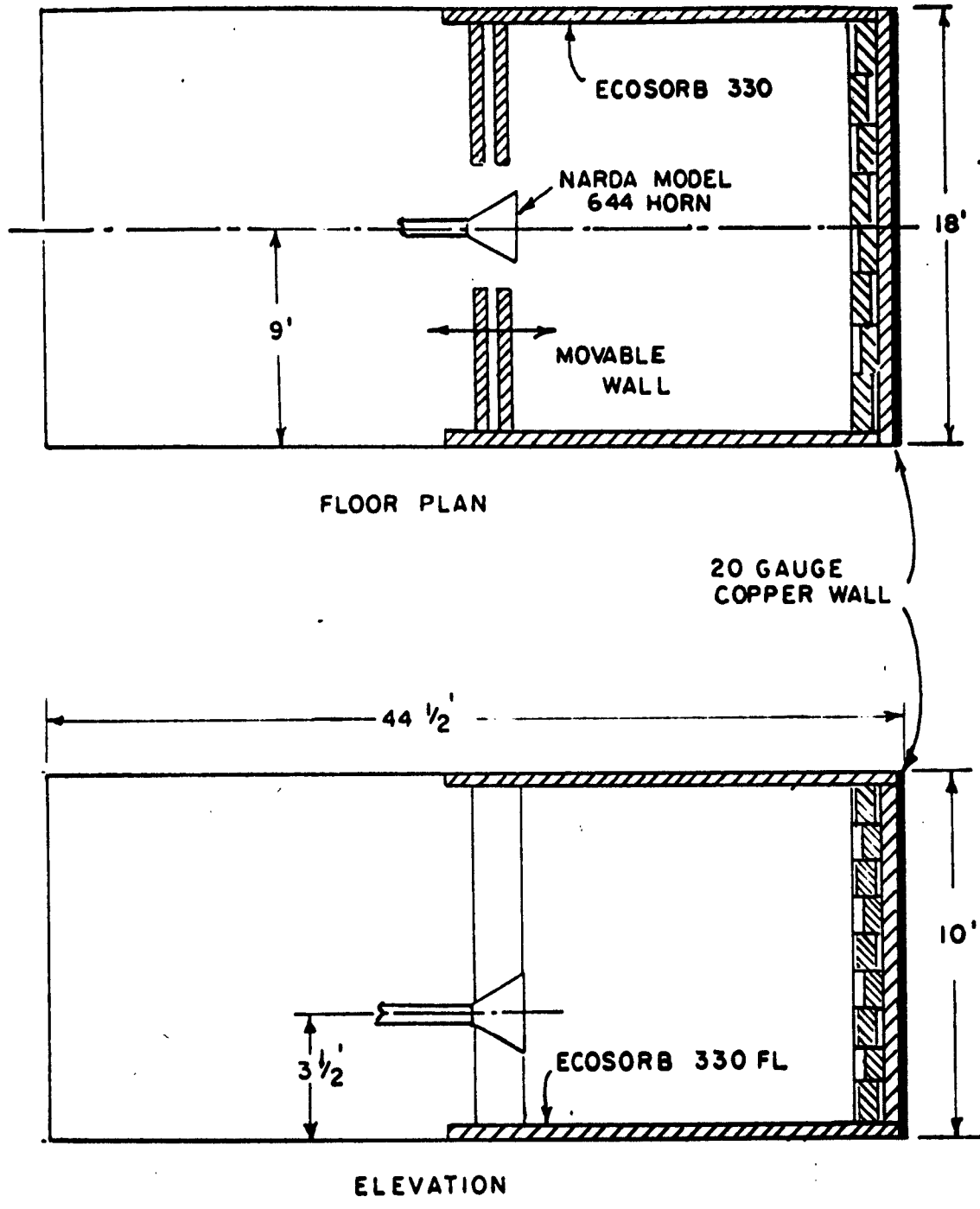

FIGURE 23

ANECHOIC CHAMBER

single layer of Eccosorb 330 microwave absorbing material (the floor was covered with 330 FL so that it could be walked on) whereas the ceiling was covered with a layer of Goodrich microwave absorbing material. The side of the room near the antenna was arranged to have two movable walls of the same material so that dimensional changes were possible. The wall opposite the antenna, the one covered with copper, had a second layer of absorbing material arranged in a stepped or staggered fashion as shown in the figure. This treatment was found necessary in order to reduce reflections in the room and distortion of the transmitting antenna pattern as shown in figures 24, 25, 26 and 27. These relative power patterns were obtained by measuring the electric field strength laterally to the axis of the transmitting antenna using a probe as described later. Each pattern was repeated several times with negligible variation in its shape. Figure 24 shows the variation of the power density in a plane parallel to the antenna aperture at a distance of 12 feet from the aperture when only a single layer of absorbing material was present on all walls. The asymmetry of the pattern about the axis of the antenna indicates the presence of standing waves in the room. Figure 25 is the same as 24 except a second layer of absorbing material was present on the back wall of the room. The change in the patterns indicated that the standing waves were mostly due to the reflection of the field from the back wall. To reduce further the effect of backwall reflections, the second layer of the absorbing material was staggered. The resulting power pattern is shown in figure 26. A smoothed curve passing

FIG. 24

RELATIVE POWER PATTERN

(ONE LAYER OF ABSORBING MATERIAL ON THE BACK WALL)

D = 12 FT.

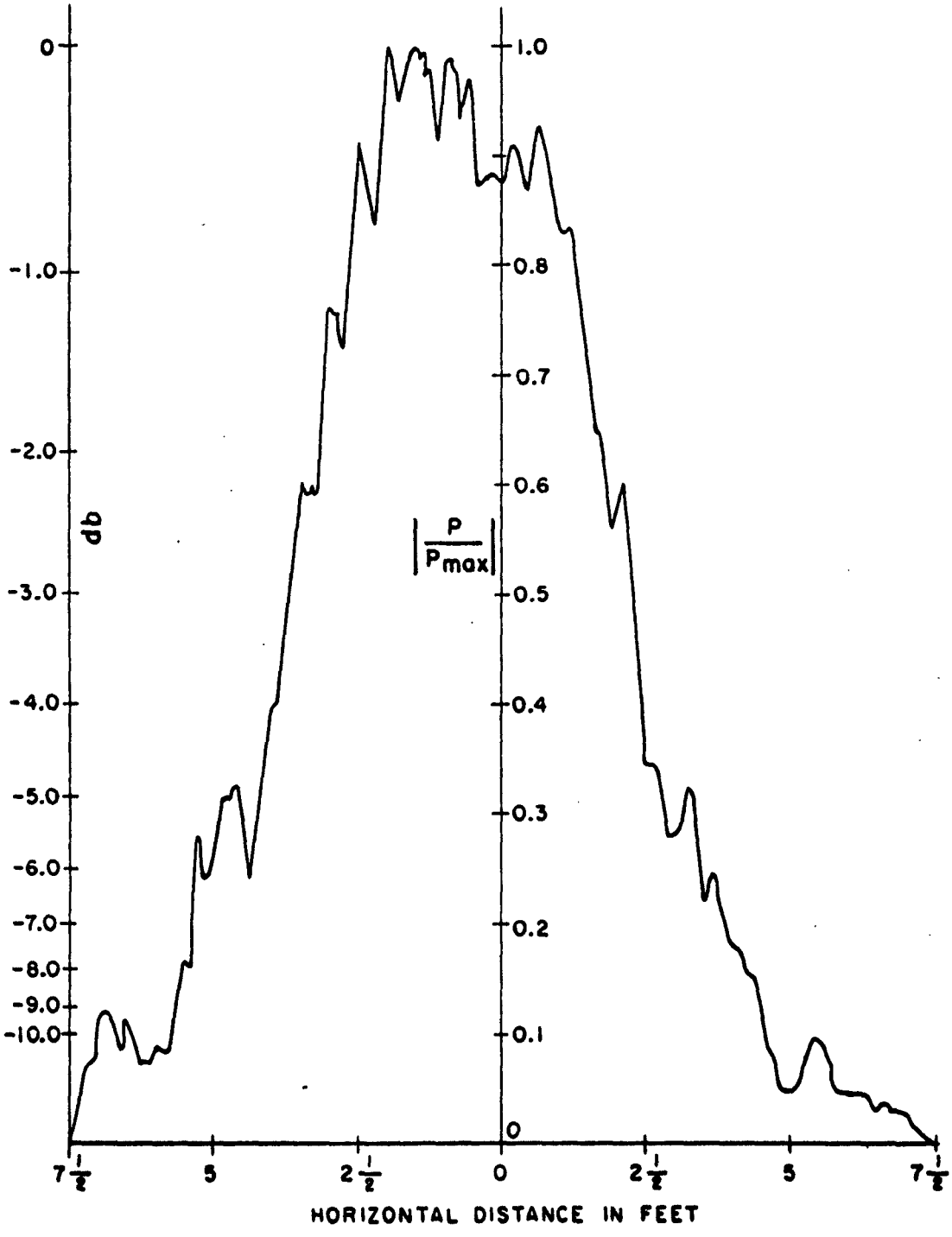

FIG. 25

RELATIVE POWER PATTERN

(TWO LAYERS OF ABSORBING MATERIAL ON THE BACK WALL)

D = 12 FT.

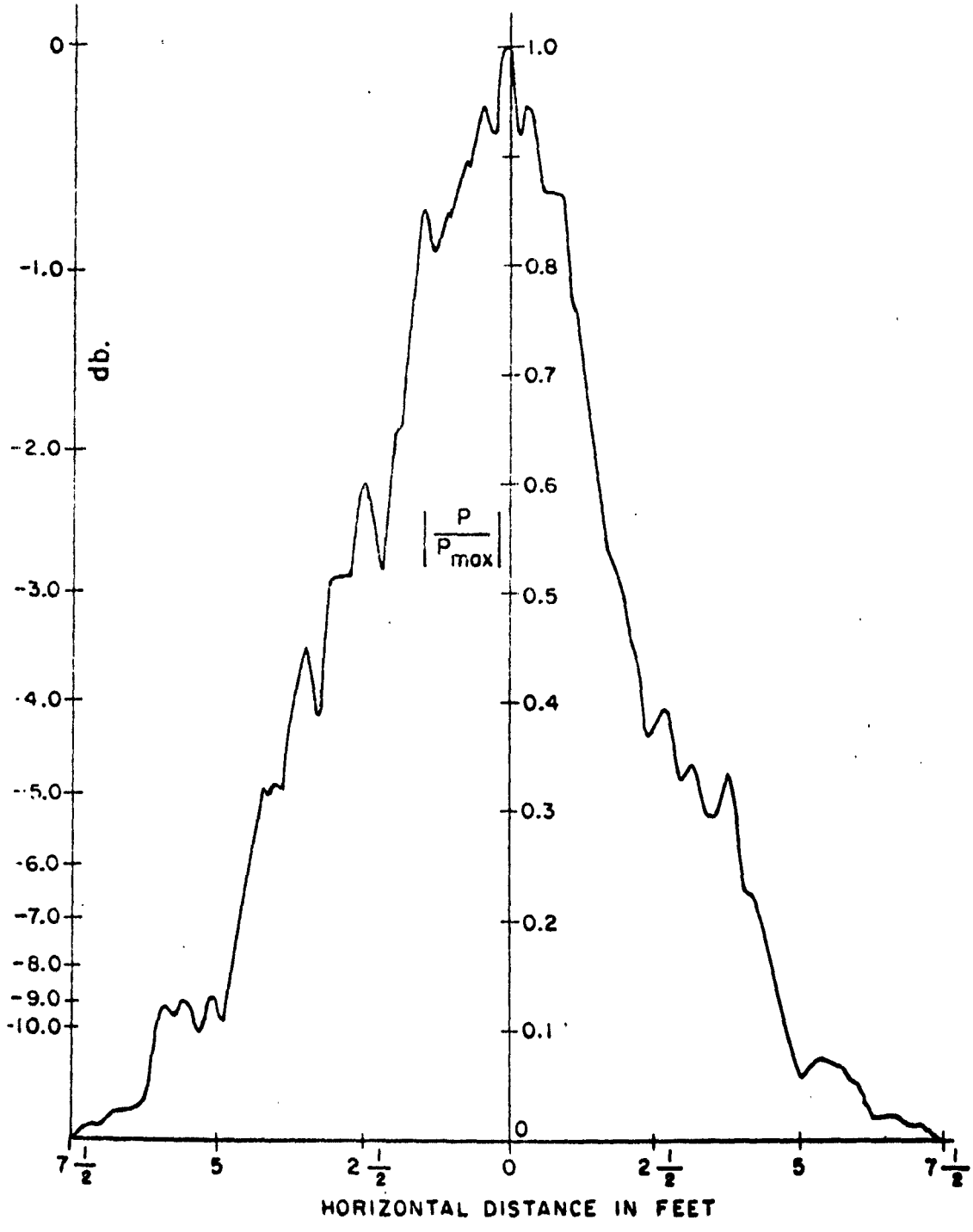

FIG. 26

RELATIVE POWER PATTERN

(TWO LAYERS OF ABSORBING MATERIAL ON THE BACK WALL - STAGGERED SECOND LAYER)

D = 12 FT.

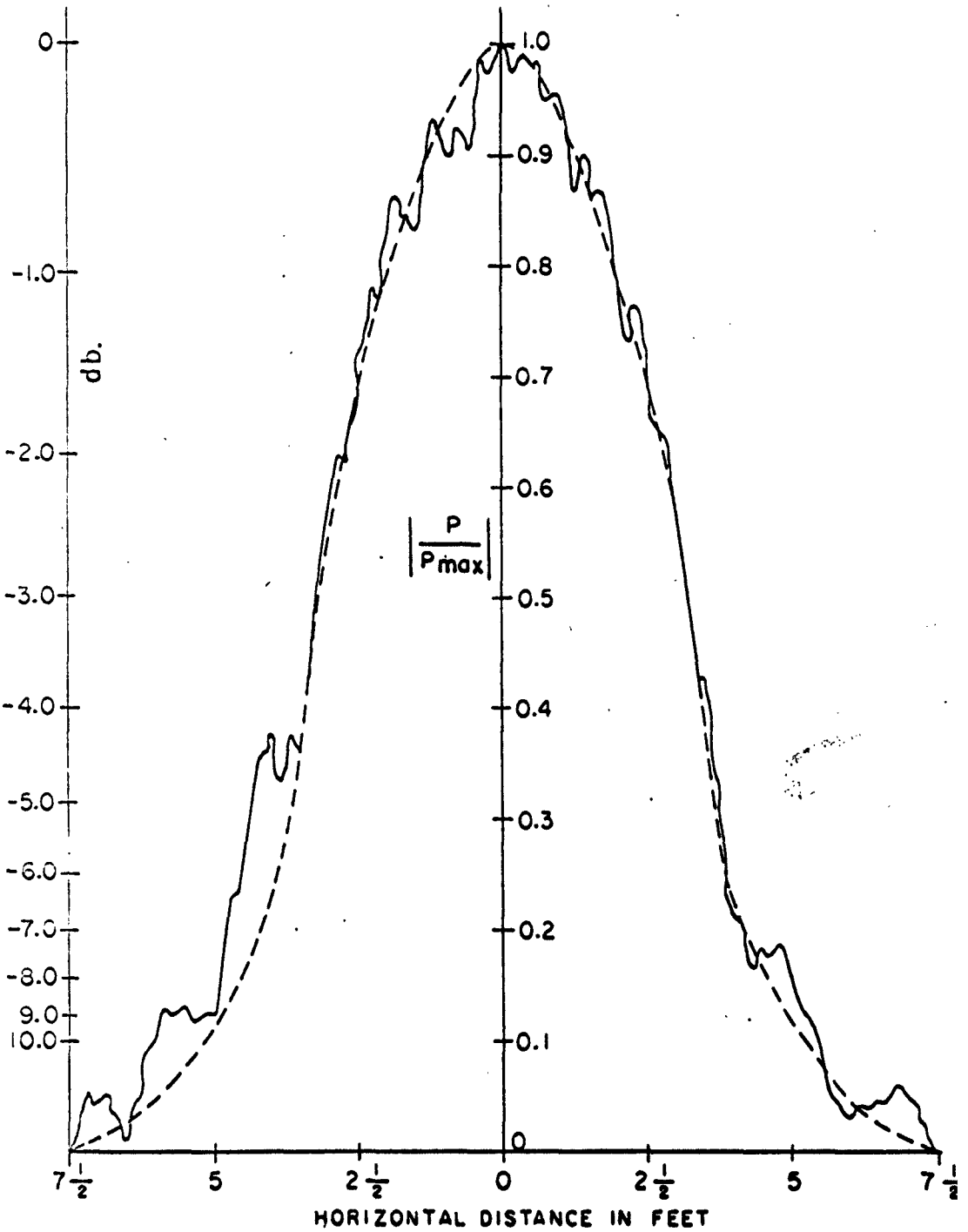

FIG. 27
RELATIVE POWER PATTERN

D = 5 FT.

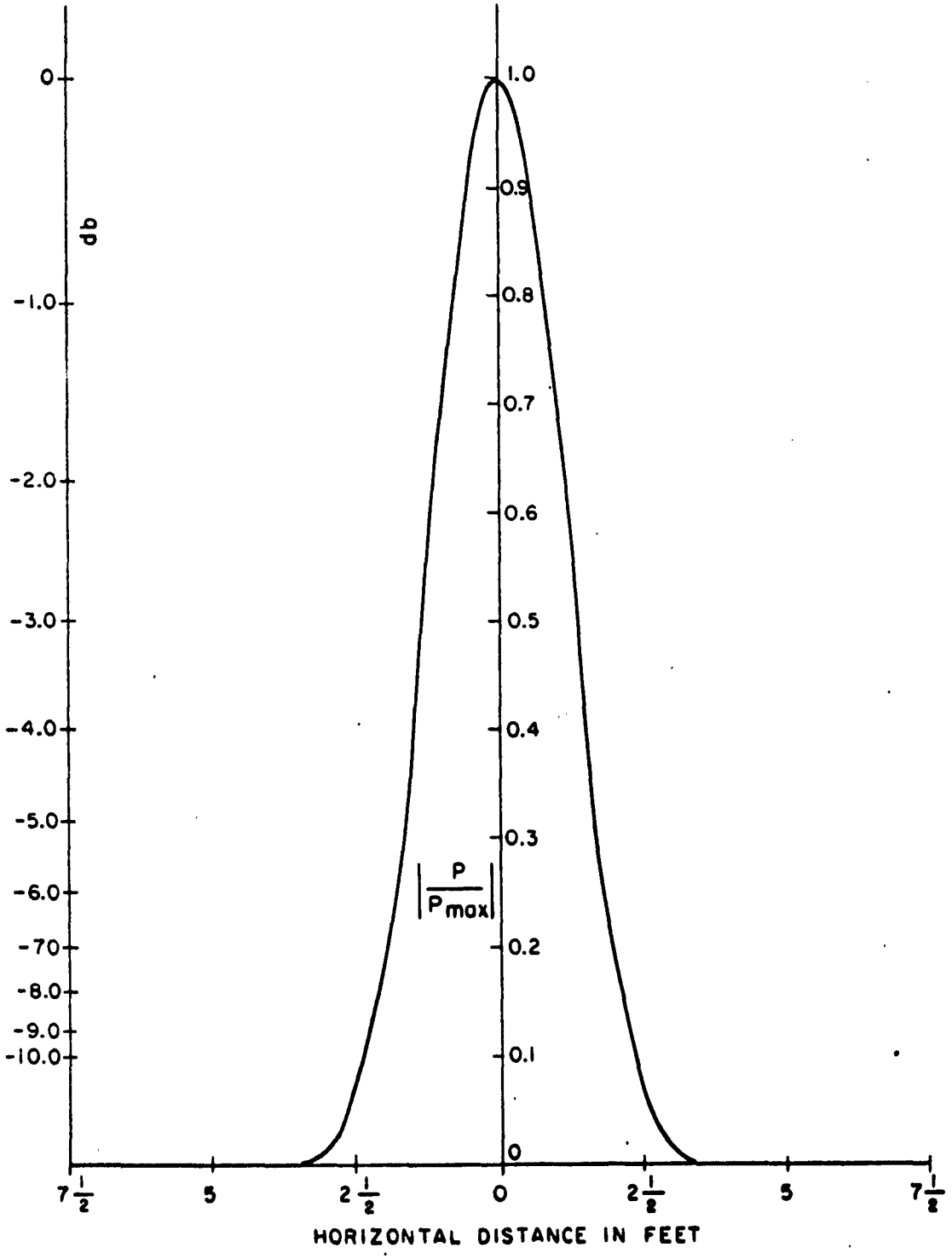

through the half power points of the plot is shown dotted on this figure. The variation of the measured pattern from the smoothed pattern is small. Figure 27 is the same as 26 except it was taken at a distance of five feet from the antenna. The symmetry about the axis of the antenna and the smoothness of the curve indicates the absence of standing waves at this distance.

An exponential horn, Narda Model 644, having a gain of 15 db above an isotropic radiator, was used to illuminate the samples under test. The choice of antenna was made to achieve a tolerable compromise between the necessity of heating the sample well requiring high gain and illuminating it uniformly requiring low gain. The separation boundary between the Fresnel region and the far-zone field for this antenna, defined by the equation (29) on page 60, was at a distance of five feet from the mouth of the horn. Power density contours in a plane parallel to the mouth of the horn at a distance of five feet from the horn are shown in figure 28. The contours are seen to be quite uniform. These contours would help to study the variation of the power density over the geometric cross section of the sample under test. For example, it can be seen from figure 28 that even the largest sphere under test (34.3 cm diameter) the variation of power density over its geometric cross section is less than 15%. All of the above measurements were made using a signal generator to feed the antenna.

A schematic diagram of the set-up for obtaining the relative power patterns is given in figure 29. The microwave signal modulated with a

POWER DENSITY CONTOURS
IN A PLANE PARALLEL TO
THE HORN.

FIGURE 28

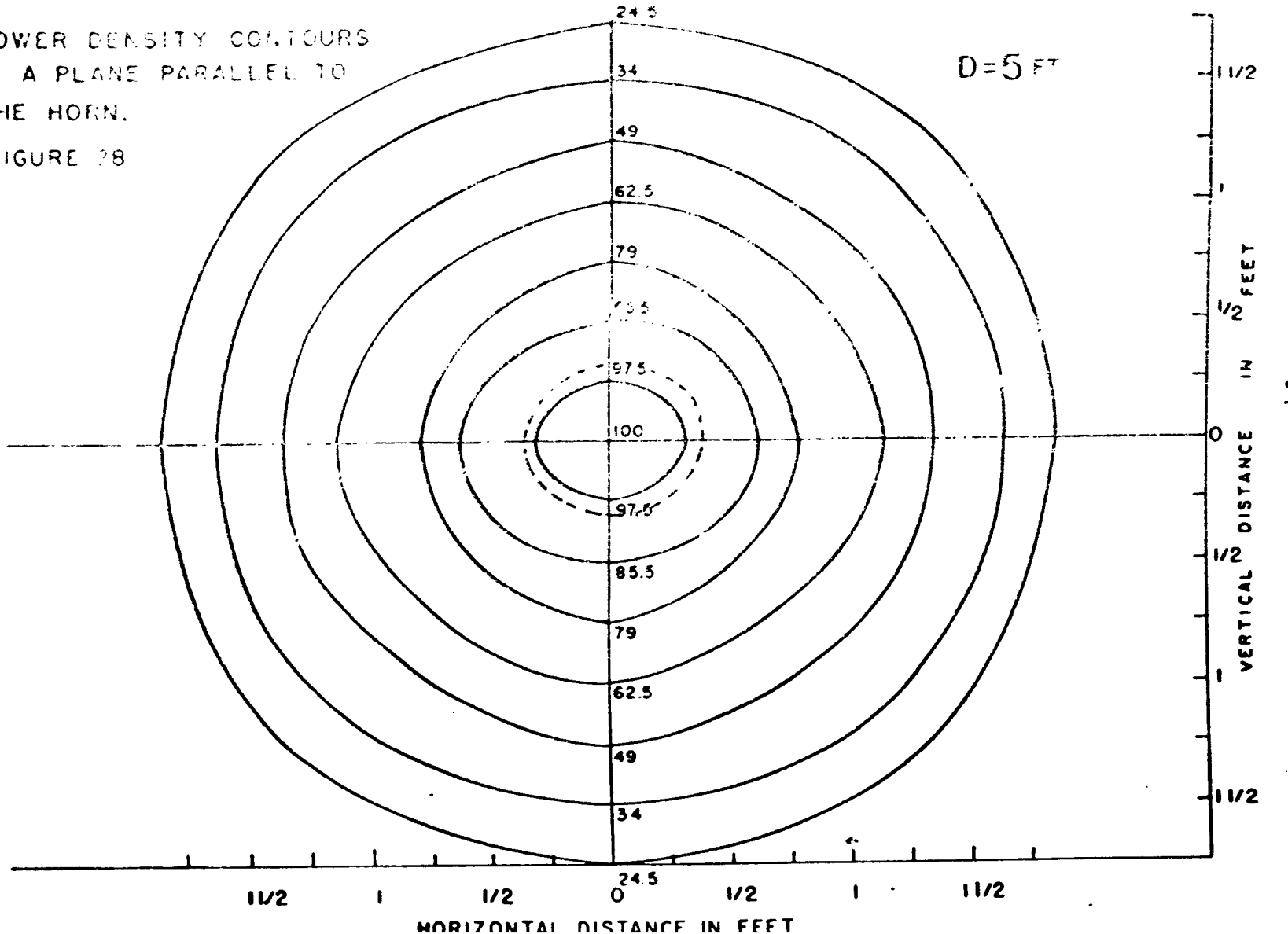

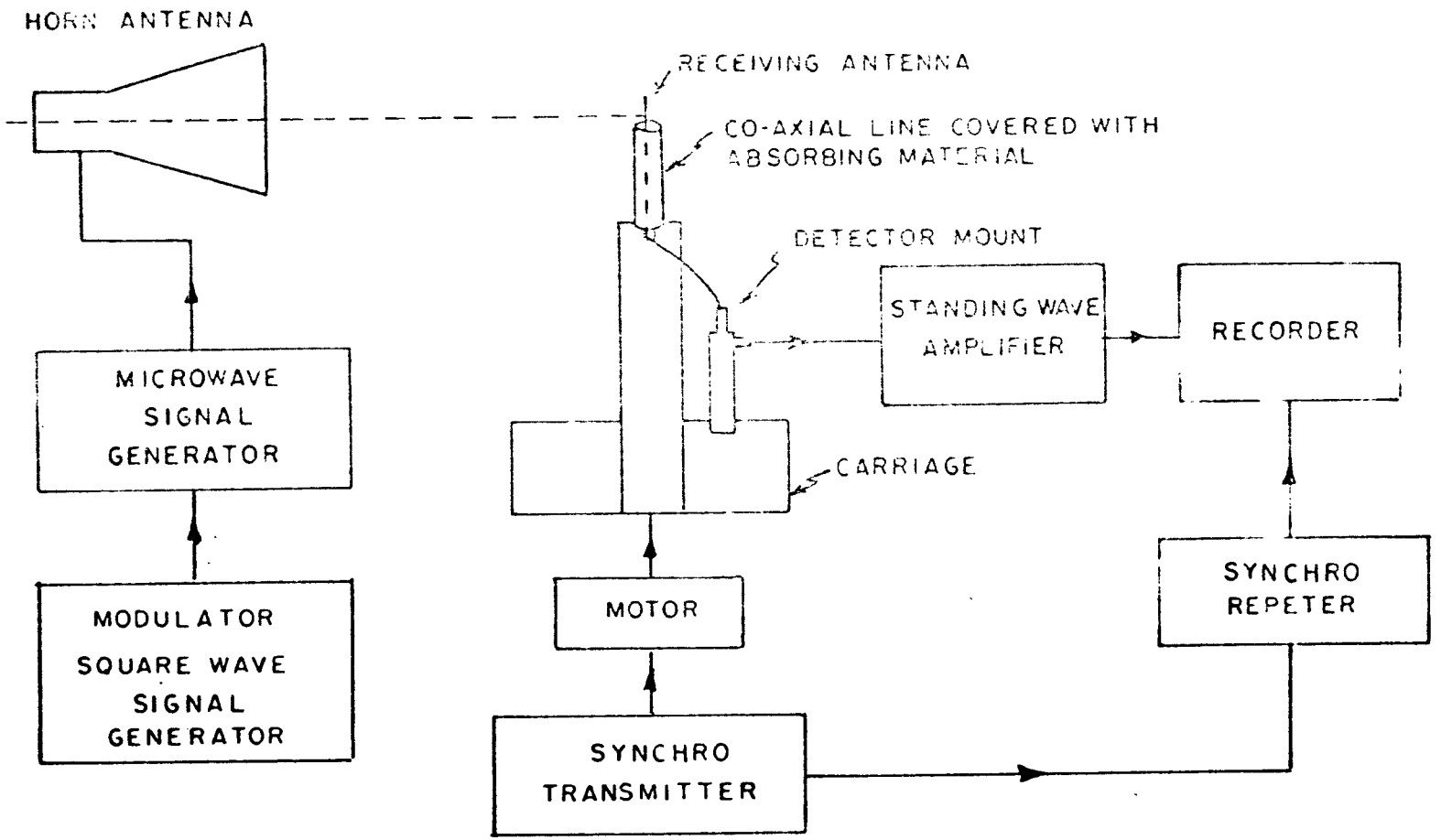

SCHEMATIC DIAGRAM OF THE SET-UP TO OBTAIN RELATIVE POWER PATTERN

FIGURE 29

1000c/s square wave was fed to the horn under test, through a coaxial-to-waveguide adapter. A small vertical probe was used as a receiving antenna to measure the vertically polarized electric field. The length of the probe was about 1 cm. The receiving antenna was mounted on a carriage which could travel on a platform kept on the floor. The carriage was driven by a motor which also drove a synchro-transmitter (Selsyn). The output of the synchro-transmitter was applied to a synchro-repeater (Selsyn) which drove the chart of a recorder. The signal from the receiving antenna was fed to a crystal detector through a co-axial cable. The detector mount was fixed to the carriage. This was done to avoid using a long co-axial cable for the r-f signal, thus reducing the attenuation losses in the cable. The demodulated signal from the detector output was applied to the input of a standing wave amplifier, and the d.c. output of this instrument was used as an input to the recorder. The receiving system was calibrated to obtain a linear power plot by choosing a crystal which had square-law characteristic over the range of the signal amplitudes measured. The movement of the recorder chart was calibrated in terms of the distance traversed by the receiving antenna. Thus by moving the receiving antenna in a plane parallel to the plane of the mouth of the horn, continuous power plots were obtained on the recorder chart.

3.0 Microwave Generator

An experimental model of the APS-20 radar was used as a source of microwave power for the experimental work. The essential

characteristics of this equipment are given below.

Frequency	2880 Mc/s
Wavelength	0.104 meters
Peak power output	1.7×10^6 watts
Average power output	1000 watts
Pulse width	2 microseconds
Repetition rate	300 per second
Output system	RG-48/U "S" band waveguide

For calibration purposes, the output of the radar was connected to a water calorimeter load and to a Hewlett-Packard model 430C power meter and model 477B thermistor mount via a directional coupler as shown in figure 30.

The pulse shape and repetition rate of the radar were monitored via directional coupler B, a crystal detector, and an oscilloscope. The output power (average) was monitored via directional coupler A, attenuators, thermistor mount and power meter. The average power output of the radar was measured by a water calorimeter load using a substitution method. The error of this measurement is < 5%. The voltage standing wave ratio of the load was measured with a slotted section and a standing wave meter and found to be 1.24. The corresponding power reflection coefficient is 0.01 which indicates that 99 percent of the power output of the radar is delivered to the load.

The power output was measured and reference readings were taken on the power meter after allowing about a half hour for equipment warm-up.

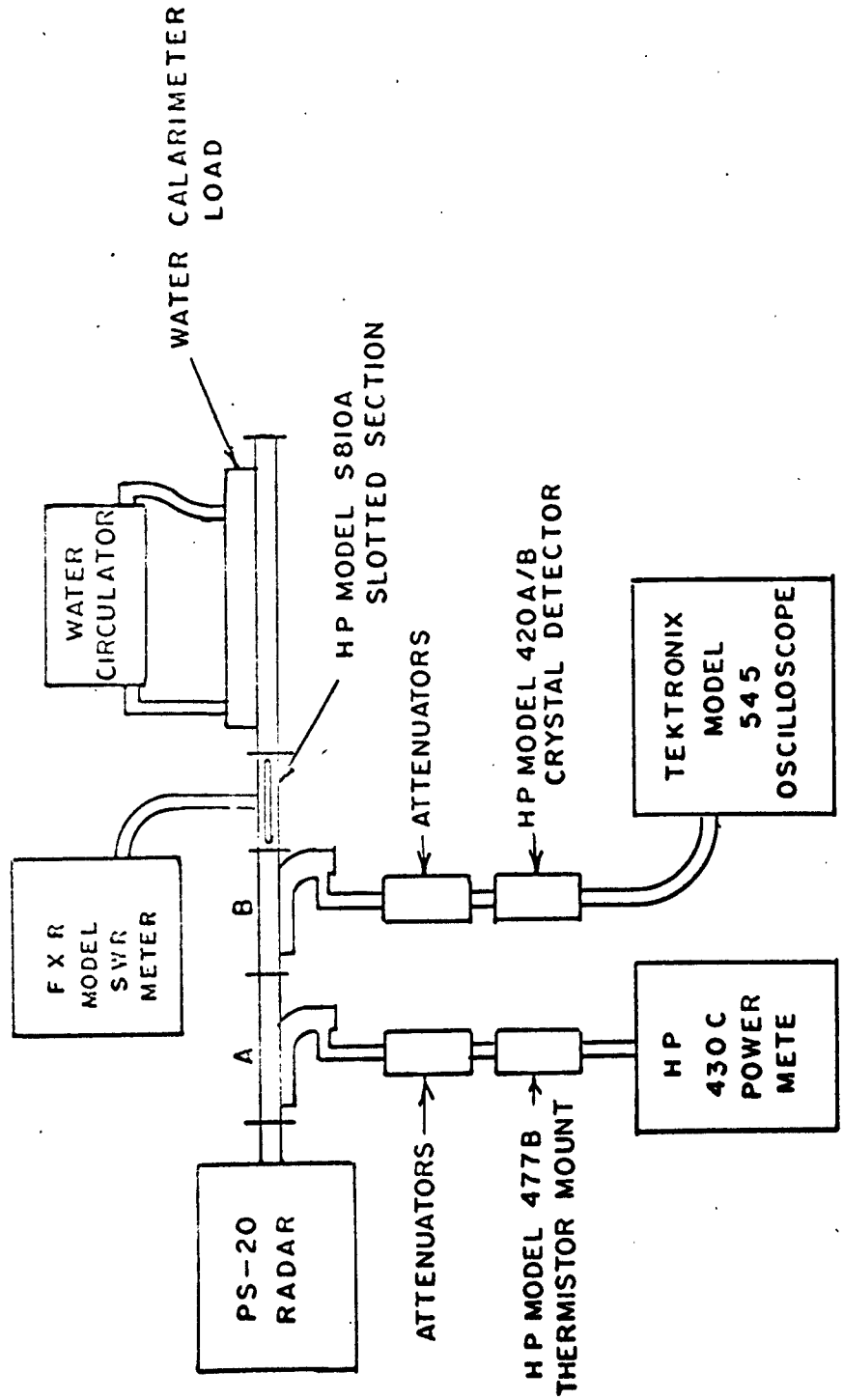

MICROWAVE GENERATOR CALIBRATION

FIGURE 30

After this was completed, the water load was disconnected and the exponential horn antenna was connected to the system. In all measurements, the calibrated reading of the power meter was used as a measure of the power output.

With the horn antenna connected to the radar through two directional couplers used as a reflectometer, the voltage standing wave ratio was 1,188 corresponding to a power reflection coefficient of 0,007, which indicates that almost all of the power delivered to the antenna was radiated.

In the far-field region of the transmitting antenna, the power density at various distances along the axis of the antenna was calculated from the known value of the transmitted power by means of the following formula:[10,17]

$$P_d = \frac{P_t G_t}{4\pi D^2} \qquad (28)$$

where P_d = Power density (watts/square meter) along the axis of the transmitting antenna

P_t = Power (watts) into transmitting antenna

G_t = Power gain (numeric) of the transmitting antenna relative to an isatropic radiator including antenna efficiency.

= 15 db for this antenna

D = distance (meters) from the antenna.

Equation (28) may be used provided the distance D satisfies the

following criterion:

$$D > \frac{2L}{\lambda^2} \tag{29}$$

where L = the largest linear dimension of the transmitting antenna aperture in meters

λ = wavelength in meters.

The power density at various distances along the axis of the transmitting antenna was also measured by means of the probe antenna described earlier on page 53. In this case, the power density was determined by measuring the power available at the terminals of the probe antenna. In free space, the power transfer between two antennae is given by the transmission formula: (10, 17)

$$\frac{P_r}{P_t} = \frac{G_t A_r}{4\pi D^2} \tag{30}$$

where P_r = power (watts) available at receiving antenna terminals

A_r = effective area (square meters) of the receiving antenna

The effective area of a receiving antenna is defined as the ratio of the maximum power available at the terminals of the antenna to the power density of the incident wave. It depends upon the geometry and the electrical losses of the antenna.

The effective area A_r of the probe antenna was first obtained from equation (30) by measuring the power transfer ratio $\frac{P_r}{P_t}$, using a signal generator and a standing wave amplifier. The set up is shown schematically in figure 29. The transmitting and receiving antennas were lined up for maximum received power. The output of the standing wave amplifier was noted when a known power (P_t) was applied to the horn antenna. The crystal detecting system was then connected to the signal generator. The power output of the signal generator was reduced until the output of the standing wave amplifier was the same as before. The power output of the signal generator was equal to P_r. The procedure was repeated for several values of the distance (D) between the transmitting and receiving antennas. In each case, A_r was calculated using equation (30). A_r was found to be independant of D. The radar unit was then connected to the horn antenna and the power density P_d at various distances on the axis of the antenna was calculated from the formula:

$$P_d = \frac{P_r}{A_r} \qquad (31)$$

by measuring the power, P_r, available at the receiving antenna terminals using a power meter.

The calculated (eq. 28) and the measured (eq. 31) values of power density at various distances in the far field on the axis of the horn antenna are shown in table 2. The agreement between these values is sufficiently good so that, for the values of power density needed in the experiments on phantoms, equation (28) alone may be used.

Table 2

Comparison of measured and calculated values of power density at various distances on the axis of the horn.*

Distance from the horn, D, feet	Power density, mw/cm^2	
	Measured	Calculated
5	57	56
6	40	39
7	31	28
8	22	22
9	16	17

* Transmitted power = 510 W

The power densities in the Fresnel region of the antenna were calculated using the methods of reference 6. These values were used in determining the Fresnel region relative absorption cross section (figure 34).

4.0 Thermal Considerations and Phantoms

Hollow, spherical flasks of Pyrex glass of the following sizes were used as phantoms in the preliminary experiments.

Capacity Liters	Radius in Centimeters
0.215	3.71
1.05	6.30
2.05	7.88
5.15	10.74
12.44	14.37
21.15	17.15

The wall thickness of the flasks was less than 1/8 wavelength and is believed to be inconsequential in this work in view of the comparatively low dielectric constant and losses of glass.

The flasks were placed in square boxes made of polystyrene foam ($\epsilon = 1.02$) and air spaces between box and flask loosely packed with polyfoam granules (figure 31). The polyfoam was used as thermal insulation to cut down heat losses due to conduction and convection. It has negligible effect on the microwave properties of the phantoms.

The flasks were filled with the electrolyte mixture of interest and then placed in the anechoic chamber at various distances from the horn antenna along its axis as shown in figure 32.

The relative absorption cross section was calculated by measuring the temperature rise in a known time due to exposure of the phantom to the microwave field.

The heat developed in a homogeneous electrolyte of volume V placed in a uniform plane wave electromagnetic field is:

Photograph of Spherical Phantom
Figure 31

Photograph of Anchoic Chamber
Figure 32

$$H = VhmT \text{ (Calories)} \tag{32}$$

where V = volume of electrolyte (cc)

h = specific heat of the electrolyte (Cal/gram/°C)

m = specific weight of the electrolyte (grams/cc)

T = temperature rise of the electrolyte (°C)

provided that heat losses to the outside can be neglected as shown later.

The power absorbed is then:

$$W_a = \frac{4.18H}{t} \text{ (watts)} \tag{33}$$

where t = exposure time in seconds

The power incident on the geometrical cross section of the phantom is:

$$W_i = AP_d \text{ (watts)} \tag{34}$$

where A = geometric cross section of Phantom (square meters)

P_d = power density of field (watts/square meter)

The relative absorption cross section is then:

$$S = \frac{4.18VhmT}{AP_dt} \text{ (number)} \tag{35}$$

Conduction and convection losses are negligible and equation (32) applicable, if operation does not exceed the "linear portion" of the thermal transient as shown in figure 33. In this typical case a spherical phantom having a volume of 5.15 liters was exposed. It was filled with a saline solution having a low frequency dielectric constant $\epsilon_o = 78$ and a low frequency conductivity $\kappa_o = 9$ millimho/cm. The phantom was exposed to

TEMPERATURE CHARACTERISTIC
OF THE MEASURING SYSTEM.

FIGURE 33

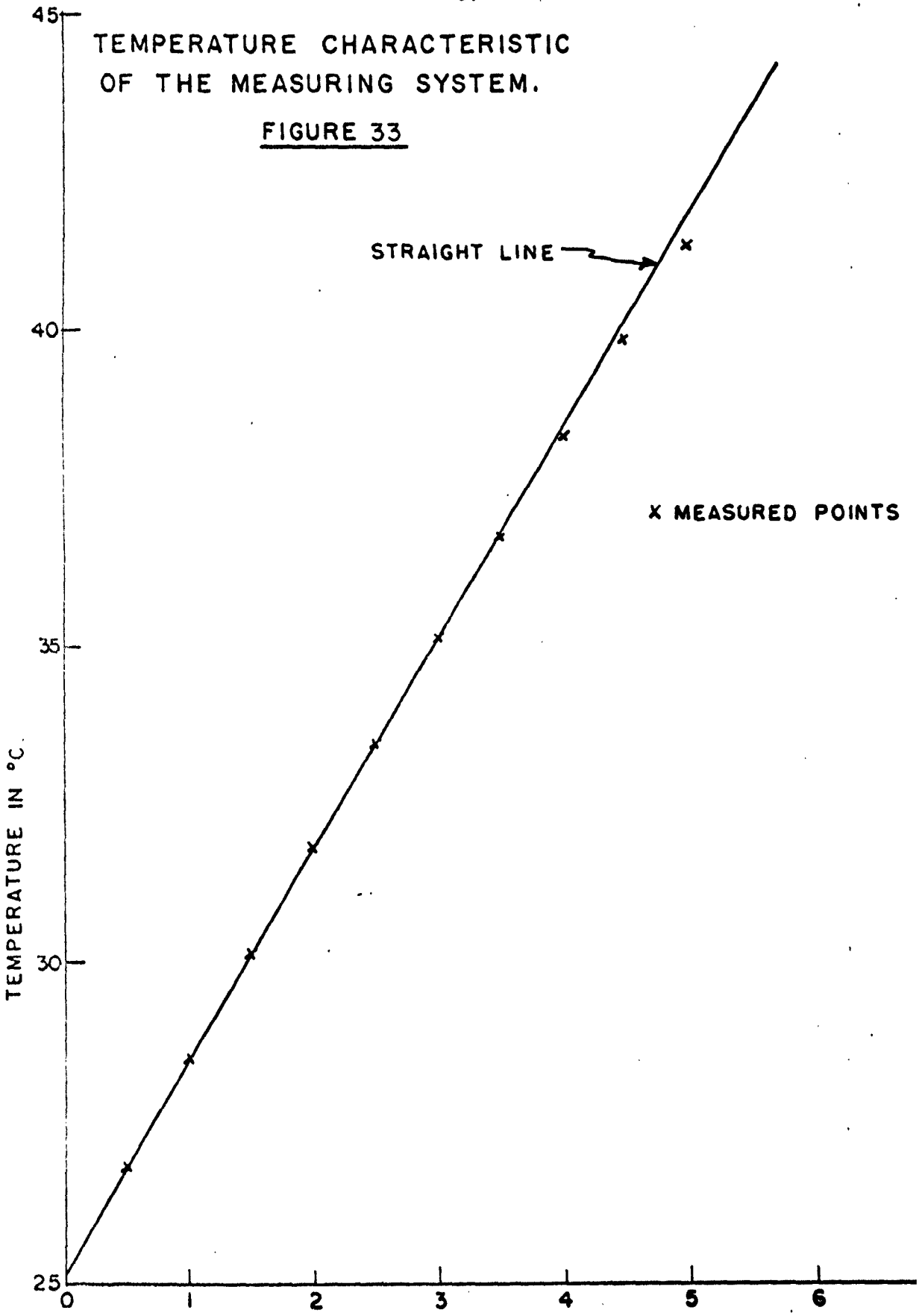

a microwave field of 93 milliwatts per square centimeter, and the average temperature rise of the electrolyte measured as a function of time. The temperature was measured after the solution had been stirred. It can be seen that the temperature rise is a linear function of the time until the difference between the ambient and sample temperature is about 15° C corresponding to an exposure time of about 4 hours.

As discussed earlier, the phantom should be placed in the far field at a sufficient distance from the antenna so that curvature of the wavefront is minimal across the phantom. To establish this distance, the relative absorption cross section was measured as a function of the distance, D, from the mouth of the horn. The separation boundary between the Fresnel and far fields is at a distance of five feet from the horn as given by equation (31). This equation is rather approximate. Hence measurements were made starting from a distance of one foot from the horn. The results are shown in figure 34. The relative absorption cross section increases until D = 3 feet and is a constant value of 0.6 from D = 3 to 12 feet. Beyond 12 feet it deviates from the constant value as shown in the figure. The independence of the relative absorption cross section from D implies that the curvature of the wavefront is minimal across the phantom. Hence it can be assumed that the far field of this horn antenna starts at a distance of 3 feet from the horn rather than at 5 feet. The deviation beyond 12 feet was perhaps due to the presence of residual standing waves in the field near the back wall of the room. Uncertainties due to the rapidly decreasing resolution of the thermal

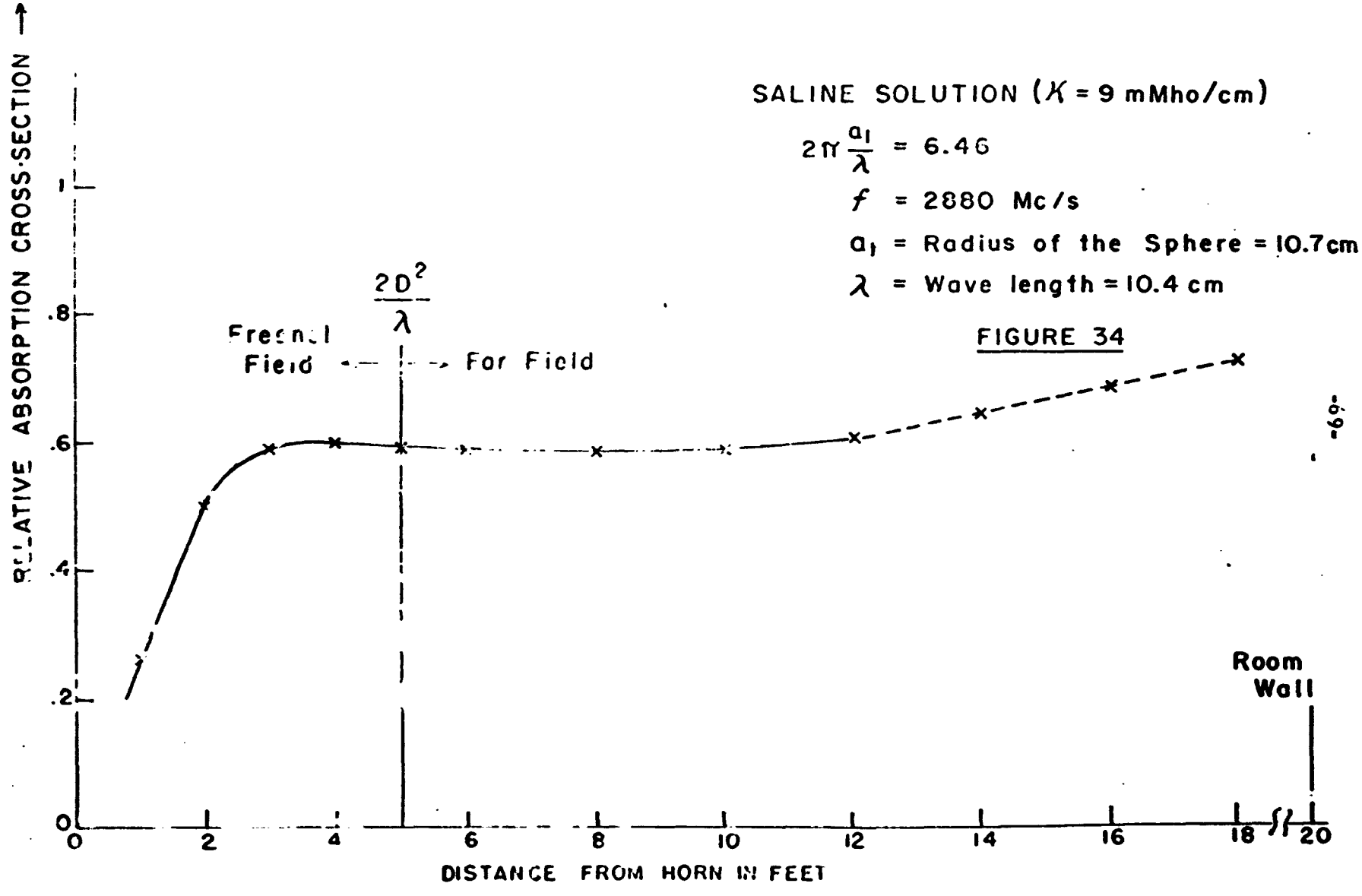
SALINE SOLUTION (K = 9 mMho/cm)
$2\pi \frac{a_1}{\lambda}$ = 6.46
f = 2880 Mc/s
a_1 = Radius of the Sphere = 10.7cm
λ = Wave length = 10.4 cm
$\frac{2D^2}{\lambda}$
Fresnel Field
Far Field
Room Wall
RELATIVE ABSORPTION CROSS-SECTION →
DISTANCE FROM HORN IN FEET
0
.2
.4
.6
.8
1
0
2
4
6
8
10
12
14
16
18
20

FIGURE 34

technique as a consequence of the weakness of the field far from the antenna further complicated this problem at large distances. All subsework was done at distances of 5 and 6 feet from the horn where reasonable temperature rises were obtainable and where standing waves from room reflections were a minimum and Fresnel field effects were essentially negligible.

5.0 Results

5.1 Spherical Phantoms

Solution of KCl-Dioxane-Water mixture was used in the spherical phantoms to simulate the electrical properties of human tissue. The low frequency dielectric constant, ϵ_o, was 60 and the low frequency conductivity, κ_o, 10 millimho/cm, which simulates closely a all soft tissues of high water content. The phantom was placed in the microwave field, and its temperature was measured at intervals of 30 minutes, after stirring the solution thoroughly. The exposure was stopped when the difference between the ambient and phantom temperature was about 15°C. For each phantom, temperature measurements were made twice at a distance of 5 feet from the horn and twice at 6 feet. The relative absorption cross section was calculated for each of these four trials and the average value was found. For example, when a sphere with a radius of 10.74 cm was exposed, the values of relative absorption cross section were found to be 0.63 and 0.64 at five feet and 0.64 and 0.65 at six feet. Table 3 shows the comparison of the experimental and theoretical results for spheres of different sizes. It also includes the

temperature rise per hour in each phantom exposed to a field of 93 milliwatts per square centimeter. Thus, by the good agreement between the experimental and theoretical results, the experimental technique has been proven to be reliable for the study of relative absorption cross sections in general.

Table 3

Relative absorption cross sections of spheres of KCl-dioxane-water

Radius of the sphere a_1, in cm	a_1	T	Relative absorption cross section Freq. = 2880 Mc/s, ϵ = 60, κ = 26.3 mMho/cm	
			Theoretical	Experimental
3.71	2.24	13.70	0.78	0.76
6.30	3.80	≈7.58	0.68	0.71
7.88	4.75	5.76	0.64	0.67
10.74	6.46	4.02	0.60	0.64
14.37	8.67	2.88	0.57	0.63
17.15	10.35	2.32	0.55	0.59

T = Temperature rise in ^{o}C per hour when power density is 93 mw/cm^2

5.2 Doll Phantoms

In order to simulate the shape of mankind and its effect on relative absorption cross section, hollow plastic dolls of the type used by children were adapted as phantoms (figure 35). The individual heights of each doll were 38.1, 50.8 and 87 cm. The complete physical characteristics of the three dolls are given in table 4. Shadowgraphs of the three aspects (front, side and top views) of these doll phantoms are shown in figures 36, 37 and 38. To indicate the variation of power density over the dolls when they were placed at a distance of 5 feet from the horn, contours of constant power density are also shown on the shadowgraphs. For convenience, the small, medium, and large dolls were numbered 1, 2, and 3 respectively.

The dolls were made of polyethylene (dielectric constant $\doteq$ 2, conductivity $\doteq 10^{-11}$ mho/cm). The thickness (2 to 3 mm) of the plastic was very small compared to wavelength (10.4 cm) of the microwave field. Hence it was assumed that the plastic would not affect the results materially. This assumption could be justified from the results obtained on the concentric spheres. As shown in figure 15, for $a_1 > 6$ the increase in the relative absorption cross section was about 15% when the thickness (d) of the concentric shell was increased from 0 to 0.5 cm. In this case, the thickness of the concentric shell was about $\frac{1}{20}$ of the wavelength. In the case of dolls, the thickness of the plastic was about $\frac{1}{50}$ of the wavelength. In addition the plastic

Photograph of Doll Phantom
Figure 35

Doll No.	Height cm	Torso Width cm	Enclosed Volume cc	Plastic Thickness mm	Geometric Cross Section Square Centimeters		
					Front or Back	Side	Top
1 Small	38.1	7.6	1,000	2	349.8	228.4	120.8
2 Medium	50.8	10.8	2,700	2	600.9	390.9	179.5
3 Large	87.0	15.0	10,000	3	1550.6	955.8	435.3

Physical Characteristics of Plastic Dolls

Table 4

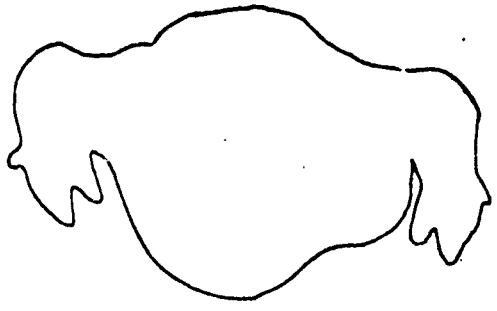

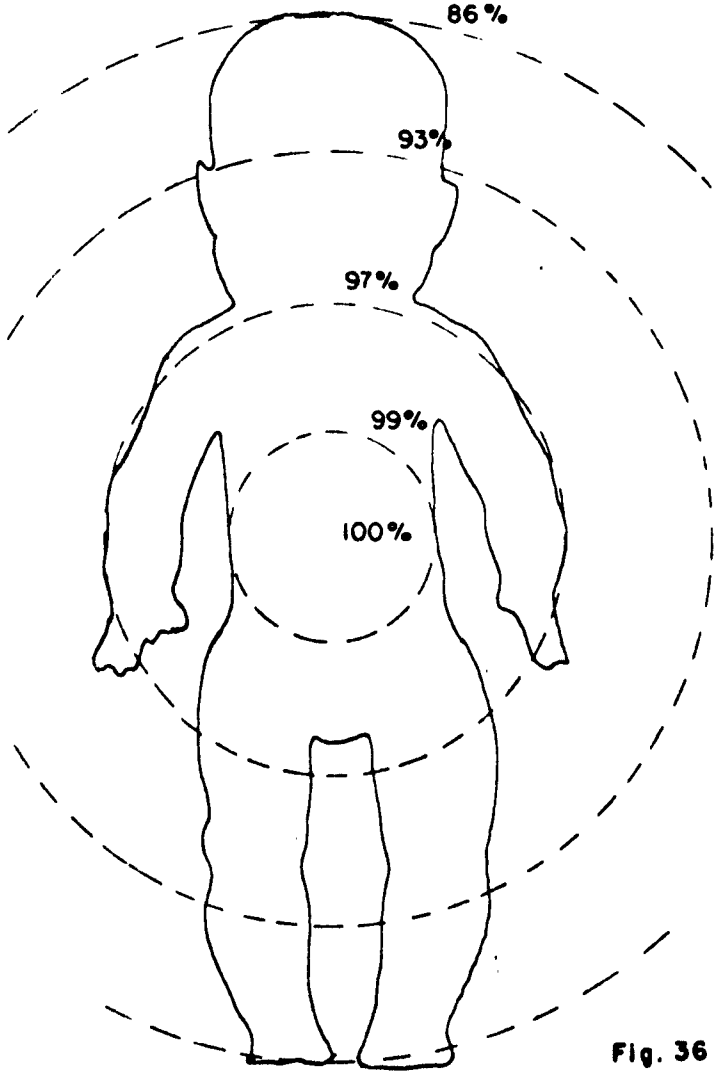

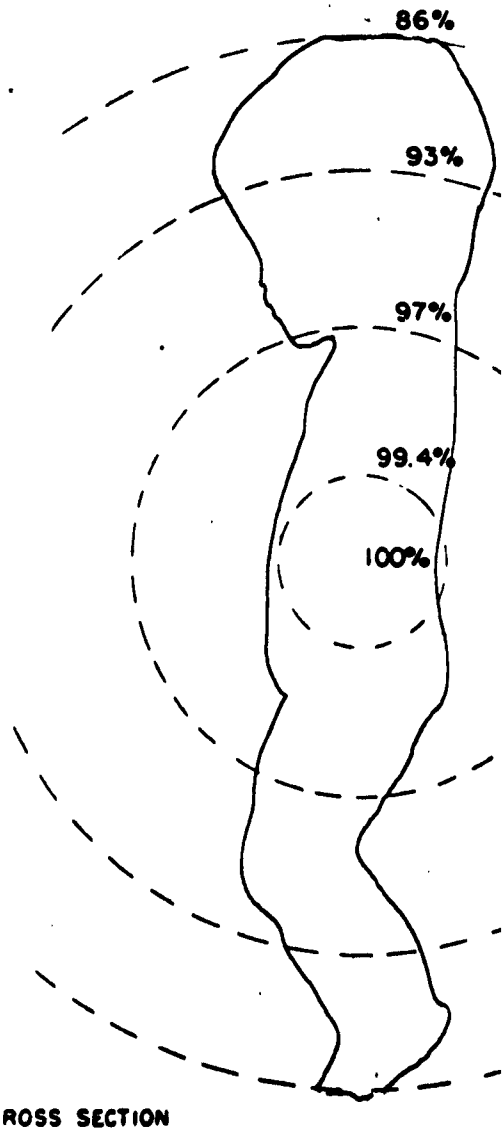

Fig. 36

FRONT, SIDE, AND TOP SHADOW CROSS SECTION
OF SMALL PHANTOM
(DOLL No.1)

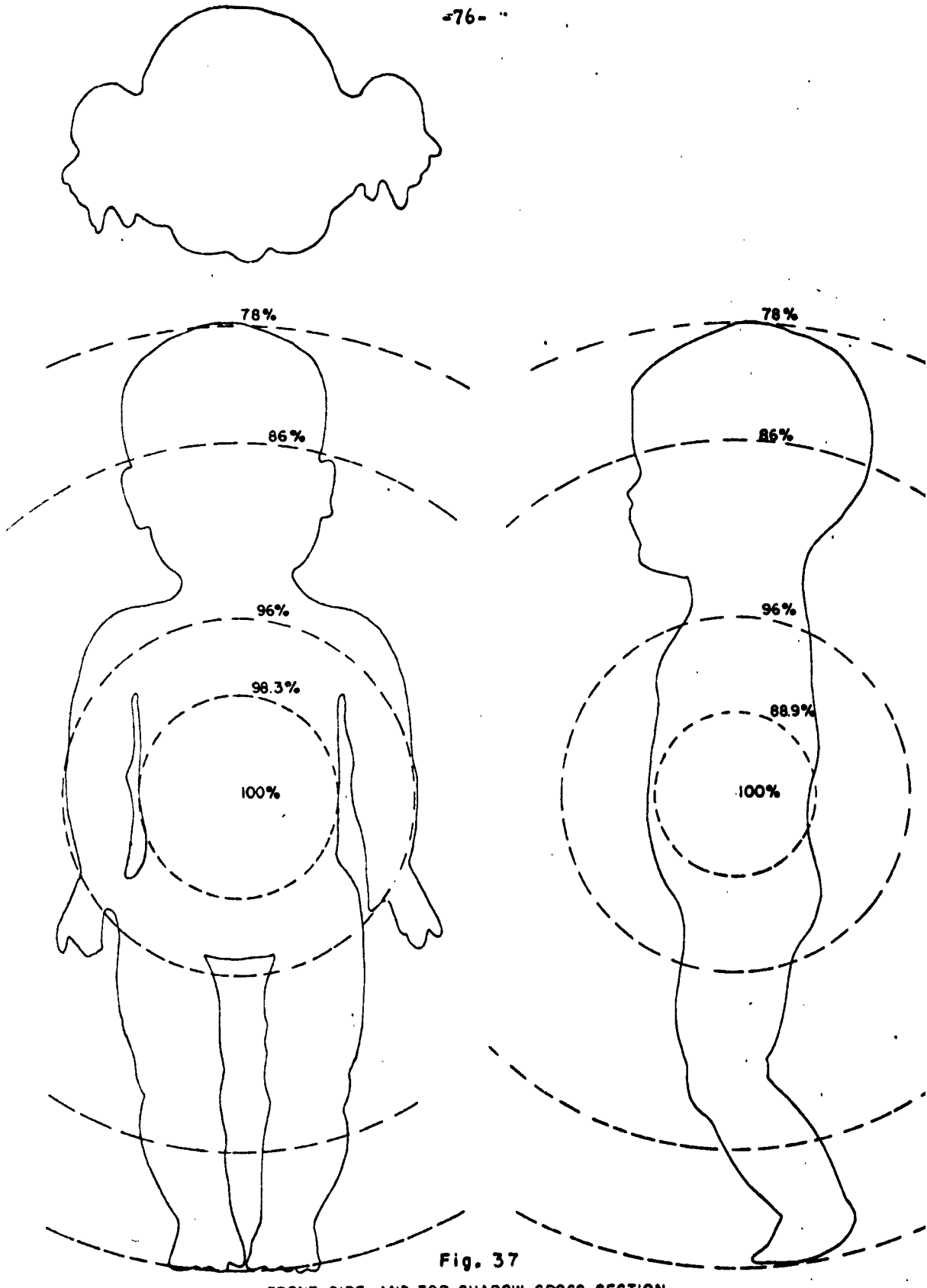

Fig. 37

FRONT, SIDE, AND TOP SHADOW CROSS SECTION
OF MEDIUM SIZED PHANTOM
(DOLL No. 2)

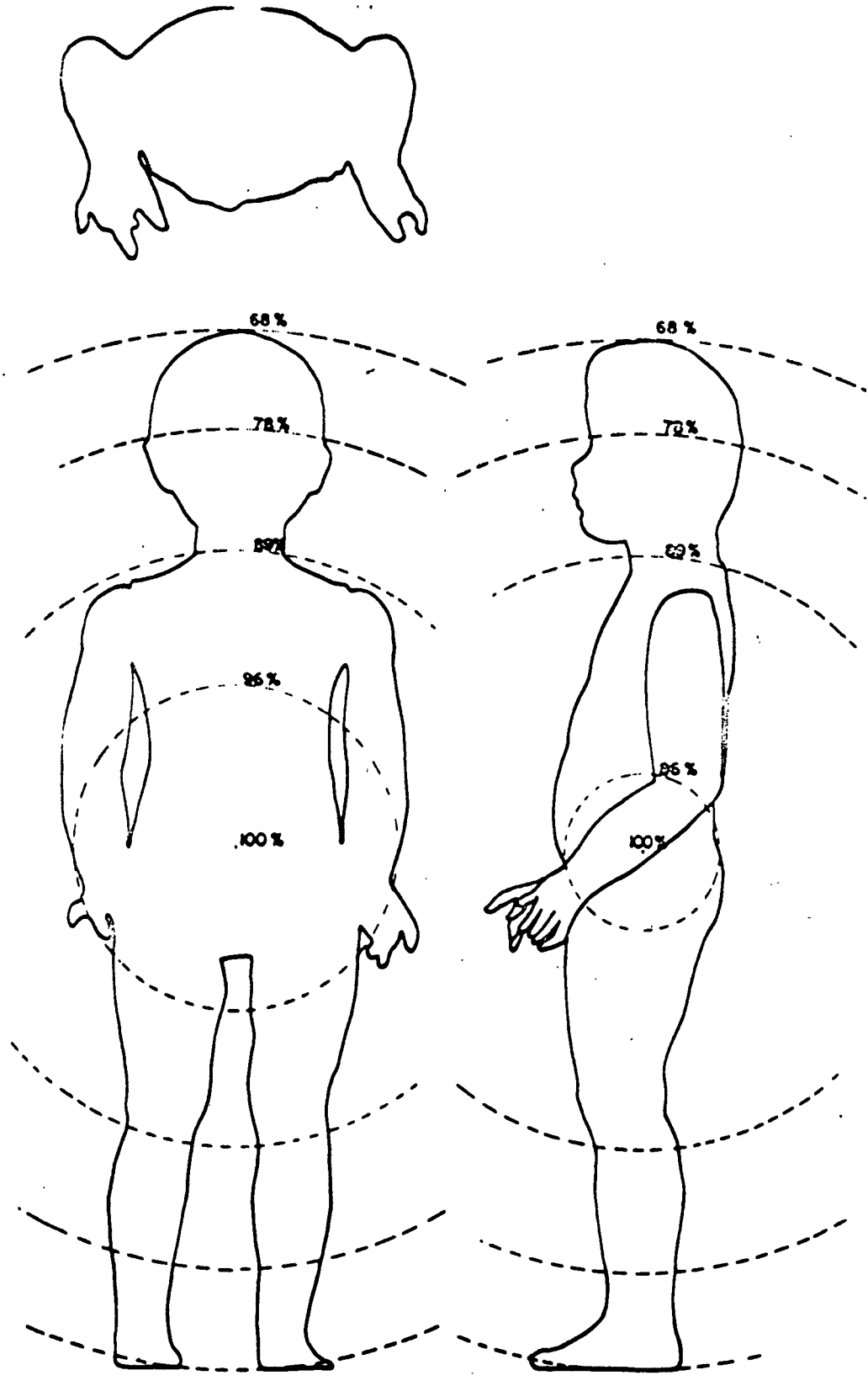

FIG. 38

FRONT, SIDE AND TOP SHADOW CROSS SECTION
OF LARGE PHANTOM
(DOLL No. 3)

had only half of the dielectric constant of the concentric shell and its conductivity was negligible. Hence the plastic would be almost transparent to the incident field. The dolls were filled with saline solution ($\epsilon_o = 78$) rather than KCl-dioxane-water solution ($\epsilon_o = 60$) to avoid decompostion of plastic. The effect of this substitution having a dielectric constant of 78 rather than 60 is to lower the relative absorption cross section but the change would be less than 10% as can be seen from the theoretical calculations on spheres (figure 8). It should be remembered that all the measurements made on dolls are applicable to mankind only if the skin and fat layer are neglected.

The dolls were filled with saline solution having a low frequency conductivity of 10 millimhos/cm. Measurements were made in front, side and top views of dolls for vertical and horizontal polarization of the incident field to investigate the effect of polarization. The incident field is said to be vertically polarized when its electric field vector is parallel to the body and horizontally polarized if the electric field is perpendicular to the body. Table 5 lists the experimental results obtained on dolls 1 and 2 at a frequency of 2880 Mc/s. It can be seen that the polarization of the incident field has less than 5% effect on the relative absorption cross section. However, the relative absorption cross section depends upon the aspect of the phantom exposed, that is, front, side or top. For example, when the small doll was exposed to vertically polarized field, the relative absorption

Part of Doll Subjected to incident plane wave	Doll No. 1 (Small)				Doll No. 2 (Medium)			
	Vertical Polarization		Horizontal Polarization		Vertical Polarization		Horizontal Polarization	
	T	S	T	S	T	S	T	S
Front or Back	10.4	47	10.0	45	8.2	58	7.8	55
Side	8.2	56	8.0	55	4.4	48	4.1	46
Top	6.9	90	---	--	3.9	92	---	--

T = Temperature rise in $^{\circ}C$ per hour when power density is 74 mw/cm^2

S = Relative absorption cross section (percent)

Relative absorption cross sections of dolls (normal size)

Table 5

cross sections were 47, 56 and 90 percent for front, side and top views respectively. The corresponding temperature rises in the phantom were 10.4, 8.2 and 6.9 degrees centigrade per hour when the power density of the field was 74 milliwatts per square centimeter. It can be seen that the relative absorption cross section of the doll for top exposure is nearly twice that for front exposure even though the former produced smaller temperature rise than the latter. This is due to the small shadow cross section in the top view and the fact that the doll actually absorbs energy over its entire surface.

The plastic dolls are believed to be relatively accurate models of babies or children of the same physical size. Hence the results can not be applied to adult man unless the doll phantoms are scaled to the correct height. It was stated earlier on page 20 that, in the case of spheres, the results obtained at a frequency of f_1 can be applied at a frequency of f_2 provided that the complex dielectric constant $(\epsilon - j\frac{\kappa}{\omega\epsilon_v})$ remains constant. The above statement holds good for any shape (Reference 18, section 9.3). It is fortunate that the dielectric constant of most body tissues of high water content is practically frequency independent over the range of 100 to 3000 Mc/s and in addition that small changes in dielectric constant have little effect on relative absorption cross section. Accordingly, if one wishes to scale the measurements made on a doll phantom of height h_1 at a frequency f_1, the results will apply to a man of height h_2 at a frequency

f_2 where:

$$f_2 = \frac{h_1}{h_2} f_1 \tag{36}$$

and provided that the conductivity of the solution used in the phantom has a value κ_1 given by:

$$\kappa_1 = \frac{h_2}{h_1} \kappa_2$$

where κ_2 is the actual conductivity at f_2. This equation is the same as (27) except the radius of the sphere is replaced by the height of the doll.

Table 6 shows the characteristics of the saline solutions used to fill the dolls when they were scaled to a man of 70 inches tall. The scaled measurements were at a frequency (f_1 in eq. 36) of 2880 Mc/s. The conductivity (κ_1) of the saline solution used in each doll was first calculated from eq. (37). Then the low frequency conductivity of the saline solution was calculated from κ_1 using equation 2.

Table 7 shows the results of scaling the three dolls to a man of 70 inches tall. The appropriate scaled frequencies are also shown. It can be seen that an adult man would absorb between 50 and 59 percent of the energy incident on his shadow cross section for front or back and side exposures in the frequency range from 617 to 1409 Mc/s. Top exposure, however, would result in 83 to 97 percent.

Table 6

Characteristics of saline solutions used to fill dolls for scaled measurements

Doll No.	Scaled Frequency Mc/s	Low freq. Conductivity mMho/cm	Low freq. Dielectric Constant	Amount of NaCl in water Grams/1000 cc
1	617	34.0	78	20
2	823	23.5	78	15
3	1409	12.3	78	7

Table 7

Relative absorption cross sections of dolls scaled to a man of height = 70 inches

Part of Doll Subjected to incident plane wave	Relative absorption cross section (percent)		
	Doll No. 1	Doll No. 2	Doll No. 3
Front or Back	57	56	50
Side	55	59	50
Top	92	97	83
Applicable Frequency Mc/s	617	823	1409

Measurements also were made on dismembered dolls to study the relative absorption cross sections of head and body. This was done to study the proximate effects of one on the other. Saline solution with a low frequency conductivity of 10 millimho/cm was used so that the results obtained on the head could be compared with those for spheres of the same size to find the effect of irregular shape of the head. Table 8 shows the results of measurements on dismembered dolls. When the heads and the bodies of dolls were exposed separately, the relative absorption cross section of the head alone was higher than that of the body alone. If the head and the body were placed together but the head was thermally insulated from the body, the relative absorption cross section of the head was again more than that of the body. Finally, the solutions in head and body were mixed after measuring the individual temperatures. The resulting temperature was measured. The corresponding relative absorption cross section was calculated and found to be substantially the same as for the normal doll. It can also be seen from the table that the relative absorption cross sections of detached members of the phantom do not vary appreciably from the values obtained when they are attached together but thermally insulated from one another. The difference is less than 10% and indicates that the body of a person has little effect on the absorption by head and vice versa. Table 9 compares the relative absorption cross sections of the heads of the dolls and spheres

Doll No.	Part of Doll Subjected to incident plane wave	Head and Body measured separately				Head and body together but thermally insulated						Head and Body together (Normal Doll)	
		Head		Body		Head		Body		Resultant			
		T	S	T	S	T	S	T	S	T	S	T	S
1	Front	8.8	61	14.0	53	9.2	64	12.0	45	11.0	49	10.4	47
2	Front	6.6	67	8.7	54	5.9	60	8.8	55	7.9	56	8.2	58

T = Temperature rise in degrees centigrade per hour when power density is 74 mw/cm^2

S = Relative absorption cross section (percent)

Relative absorption cross sections of doll parts.

Table 8

Doll No.	Relative Absorption Cross Section of doll head	Relative absorption cross section of equivalent spheres based on doll heads				Radius of equivalent spheres based on doll heads			
		Volume	Shadow Cross Section	Largest Circum-ference	Smallest Circum-ference	Volume	Shadow Cross Section	Largest Circum-ference	Smallest Circum-ference
1	64%	68%	66%	66%	69%	4.4 cm	5.1 cm	5.1 cm	4.3 cm
2	60%	63%	62%	62%	64%	5.8 cm	6.4 cm	6.6 cm	5.6 cm

Comparison of relative absorption cross sections of heads of the dolls and spheres of same size.

Table 9

of the same size. Since the head has irregular shape, an equivalent sphere can be obtained either based on volume or from the shadow cross section, the largest circumference or smallest circumference of the head. Radii of spheres calculated by the above possibilities are also shown in the table. It can be seen that the difference in relative absorption cross sections of different equivalent spheres is negligible. It can also be seen that the difference in relative absorption cross sections of the head and the equivalent spheres is less than 10% relative for both dolls.

IV. DISCUSSION OF RESULTS

The relative absorption cross section of an irradiated person is a function of body curvature and size, frequency of radiation, skin thickness and thickness of subcutaneous fat as demonstrated in the results obtained on the spheres and the doll phantoms. Schwan and Li [11] calculated the relative absorption cross section of mankind on the assumption that the effect of body curvature and size could be neglected and the trunk of the body could be approximated by a three layer infinite slab made up of skin, subcutaneous fat and muscle tissue. Their results are summarized in Table 10 for frequencies of 150, 400, 900, 3000 and 10000 Mc/s. Thickness of subcutaneous fat is varied between 0 and 3 cm and skin thickness values from 0 to 0.4 cm. These are the ranges of predominant practical interest. Larger values for the thickness of subcutaneous fat may occur occasionally. However, such layers will almost never cover a substantial part of the surface of the human body and will, therefore, be of no concern in a study of the relative absorption cross section of total body irradiation. Furthermore, the general relationships indicated in this study permits one to state how the results can be extended to higher values of subcutaneous fat thickness. Table 11 compares the relative absorption cross sections of concentric sphere and infinite plane slab models at frequencies of 400, 2880 and 10000 Mc/s when the thickness of subcutaneous fat is varied and the skin thickness is taken to be zero. It can be seen that the relative absorption cross

fat thickness cm	skin thickness cm		Relative absorption cross section (percent)			
		150 Mc/s	400 Mc/s	900 Mc/s	3,000 Mc/s	10,000 Mc/s
0	0	26	36	40	42	42
	0.2	26	36	40	45	46
	0.4	27	37	41	49	48
1	0	26	37	48	91	75
	0.2	-	43	68	31	49
	0.4	-	47	71	18	42
2	0	27	42	70	68	97
	0.2	31	54	89	50	41
	0.4	32	60	64	32	45
3	0	28	51	95	77	96
	0.2	-	69	79	43	43
	0.4	-	73	51	25	50

Table 10

Relative absorption cross sections of mankind based on three layer infinite plane slab model for different values of skin and fat thickness at frequencies of 150, 400, 900, 3,000 and 10,000 Mc/s.

Table 11

Comparison of relative absorption cross sections of concentric sphere and infinite plane slab models for different values of fat thickness when the skin thickness is zero.

Frequency	Fat Thickness (d)	Relative absorption cross section (percent)			
		Concentric Spheres			Infinite plane slabs
Mc/s	cm	$a_1 = 6$	$a_1 = 10$	$a_1 = 50$	
400	0	56	51	44	36
	1	61	56	48	37
	2	71	65	54	42
	3	85	77	62	51
2880	0	61	56	48	42
	1	124	110	86	91
	2	109	95	73	68
	3	94	87	75	77
10,000	0	62	57	48	42
	0.2	91	82	63	60
	0.4	128	115	94	95
	0.8	104	89	70	43

section of infinite plane slab is approached by that of an infinite sphere for all the frequencies investigated. In the sequel, the effects of body curvature and size, fat layer and skin layer on the relative absorption cross section of mankind are once more summarized:

a.) The effect of body curvature and size:

The effect of body curvature and size on the relative absorption cross section of mankind is discussed neglecting the effects of the skin and fat layers in order to compare the results obtained on the doll phantoms, the homogeneous spheres and the infinite plane slab.

The relative absorption cross section of mankind is 50 to 59 per cent for front and side exposures in the frequency range of 617 to 1409 Mc/s as demonstrated by the measurements made on doll phantoms (Table 7). Top exposure would result in 83 to 97 percent absorption. The apparently high absorption cross section of the person for top exposure is due to the small geometrical cross section in this aspect and is not as significant from a practical point of view.

It can be seen from figures 2, 3, 4, 8 and 10 that the relative absorption cross section of homogeneous spheres is equal to 50 ± 10 percent for $a_1 > 6$, that is if the radius of the sphere is comparable or greater than the wavelength. This is true regardless of the different combinations of parameters, i.e., frequency, dielectric constant and conductivity, investigated. The near independence of the relative absorption cross section from radius for values of a_1 larger than 6

implies that the curvature does not substantially affect absorption characteristics, at least as long as the radius of the curvature is larger than the wavelength. Thus it appears that structures whose geometrical cross section is larger than $\pi\lambda^2$ have a relative absorption cross section of 50 percent, independent of their shape. This holds provided that no substantial contributions to absorption can result from local structures of rapid curvature, as characterized by a radius much smaller than the wavelength. This statement applies particularly to mankind, since its cross section is almost 10000 cm^2, for wavelength values smaller than 60 cm, i.e., frequencies above 500 Mc/s. Possible high local absorption by structures, such as the nose or ears, should not contribute to the total absorption noticeably in view of the small local volume involved. This does not mean, however, that these parts may not be subjected to high energy absorption while the body, as a whole, is affected negligibly.

Schwan and Li had shown that, if skin and fat layer are neglected, the relative absorption cross section of mankind based on the infinite plane slab model is frequency dependent and varies from 26 to 36 percent when frequency increases from 150 to 400 Mc/s (Table 10. It is almost frequency independent from 600 to 10,000 Mc/s and equal to about 40 percent.

It can be concluded from the above discussion that the relative absorption cross section of mankind is equal to 50 percent if the

effects of skin and fat layer are neglected.

b.) The effect of fat layer:

The effect of a subcutaneous fat layer on the relative absorption cross section is most pronounced at high frequencies as shown in Table 11: At 400 Mc/s, the relative absorption cross section increases monotonously with fat layer thickness. The relative absorption cross section is equal to 100 $\pm$ 10 percent for 2880 Mc/s at d = 1 cm and for 10,000 Mc/s at d = 0.4 cm. It happens at these frequencies that the thickness of fat layer is equal to $\frac{\lambda_f}{4}$ where λ_f is the wavelength in the fat. Here the input impedance at the body surface nearly matches the wave impedance of the air. In other words, the fat layer served as an impedance match between air and muscle. This is possible because the dielectric constant of the fat is approximately equal to the geometric mean of the dielectric constants of air and muscle and the fat is comparatively free of losses. When the thickness of the fat approaches $\frac{\lambda_f}{2}$ (d = 0.8 cm at 10,000 Mc/s), the absorption decreases to a minimum. Hence the relative absorption cross section is affected strongly whenever the thickness of fat layer matches multiples of $\frac{\lambda_f}{4}$. λ_f is about 12 cm at 1000 Mc/s. Consequently, the fat layer has a more pronounced effect on the absorption cross section above 1000 Mc/s than below. The variation of the relative absorption cross section with fat layer thickness is sufficiently similar for both concentric sphere and infinite plane slab models so

that, in general, the difference may be neglected.

In the preceding discussion, the thickness of the skin is taken to be zero. When the skin layer is considered the effect of fatty tissue on the relative absorption cross section would be diminished, especially at higher frequencies where the losses in the skin are high. This is due to the fact that the subcutaneous fat cannot influence the absorbed energy, since almost all the energy is absorbed already in the skin, as indicated by plane slab results.

The effect of skin layer on the relative absorption cross section can be seen from the results obtained in the case of infinite plane slabs (Table 10). Below 400 Mc/s, the relative absorption cross section increases slightly with increasing skin thickness. The increase in the absorption becomes rapidly more pronounced at 900 Mc/s. However, at 3000 Mc/s the relative absorption cross section reduces with increasing skin thickness for all values of fat thickness considered. When the fat and skin thicknesses are 1 cm and 0.4 cm respectively, the relative absorption cross section becomes 18 percent. At 10,000 Mc/s, the relative absorption cross section fluctuates around 50 percent for all values of skin thickness.

The relative absorption cross section of the head of a person is found to be nearly equal to that of a sphere of equivalent circumference. Consequently, it may undergo resonance phenomenon at frequencies below 3000 Mc/s displayed in figure 10 since a_1 becomes less than six and since the circumference of the head of an average person

is about 60 cm. Also, the skin and fat layers have a negligible effect on the relative absorption cross section when the fat thickness is less than 1 cm for frequencies below 3000 Mc/s. For example, at 400 and 2880 Mc/s, a_1 is equal to 0.8 and 5.8 respectively assuming a circumference of 60 cm. The corresponding relative absorption cross sections are 92 and 60 percent (figure 10). Hence the relative absorption cross section of the head of a person may vary between 60 and 100 percent below 3000 Mc/s. However, it is about 50 percent above 3000 Mc/s where a_1 becomes larger than 6.

V. CONCLUSIONS

The relative absorption cross section of mankind exposed to nonionizing microwave radiation has been determined using doll and sphere phantoms whose electrical properties simulated those of a human being. The investigation proceeded in three stages of increasing difficulty: (1) theoretical and experimantal study of homogeneous phantoms, having the electrical properties of muscle tissue; (2) theoretical studies of two-layer phantoms, having the electrical properties of muscle tissue and subcutaneous fat; and (3) extrapolation to three-layer phantoms, having the electrical properties of muscle tissue, subcutaneous fat, and skin (the inclusion of skin being possible only by using the published results of Schwan and Li). The investigation at each stage resulted in certain generalizations which could be used as a guide to the investigations at the succeeding stage. In this way both the theoretical and experimental work necessary was simplified. The final stage involved a synthesis of all the previous work (including that of Schwan and Li) so that the relative absorption cross section of mankind could be predicted with confidence for the total frequency range from 400 to10000 Mc/s.

The Mie scattering coefficient, K_s, was calculated for the cases of homogeneous spheres and concentric spheres. The results of the calculations are included with the cases of homogeneous and two-layer phantoms discussed below.

1. Homogeneous phantoms having the electrical properties of muscle tissue.

As a first approximation for the relative absorption cross section, S, of mankind, measurements were made on doll phantoms of homogeneous electrical properties over the frequency range of 600 Mc/s 1400 Mc/s. S was found to vary from 50-60%, after the dolls had been scaled to the full size of a human being. But to cover the entire frequency range from 100 Mc/s-10,000 Mc/s a very large number of measurements on dolls would have been necessary. Therefore, it was desirable to correlate measurements of S on dolls with the more-easily-obtainable, calculated values of S for spheres. Calculation of S for spheres was facilitated by using Univac I. (Measurement of S for spheres was also done, and the excellent agreement, $\pm$ 5%, with the calculated value served to validate the experimental technique.) The results of these calculation showed that S = 50 $\pm$ 10% for values of the radius comparable to or larger than the wavelength. That is, curvature (or shape) does not substantially affect the absorbing properties for large objects. These conclusions are further supported by the measurements made on dolls. So, sphere calculations were used to predict S in the case of large, homogeneous objects. For man, the condition that he be large compared to the wavelength is approximately equivalent to demanding that the frequency exceed 400 Mc/s (λ = 75 cm). Therefore, the results of the calculations on spheres were considered

valid for mankind if $f > 400$ Mc/s. Thus, to the extent that a human being can be considered to have homogeneous, muscle-tissue-like, electrical properties, his relative absorption cross section will be about 50% for frequencies above 400 Mc/s.

The Mie scattering coefficient was calculated as a function of the radius, a, of the sphere. For $a < \lambda/20$, K_s was found to be independent of the electrical properties and to increase according to the Rayleigh law of scattering. For $\frac{\lambda}{20} < a < \lambda$, K_s was found to oscillate (see figs. 5-7) with an amplitude primarily depending on conductivity and radius. For $a > \lambda$, K_s was nearly a constant (170%).

2. Two-layer phantoms having electrical properties of muscle tissue and subcutaneous fat.

A better model for the determination of the relative absorption cross section of mankind requires that the homogeneous phantom be surrounded by a layer with the electrical properties of fat. In the previous case of homogeneous media, the sphere phantom was shown to give values of S which were very close to those of the doll phantom. In the present case the assumption has been made that a sphere phantom with a concentric shell would give values of S equally close to those of a two-layer doll phantom. The inner sphere was given the electrical properties of muscle and the concentric shell, those of fat. At three different frequencies, 400, 2880 and 10,000 Mc/s, calculations of S, on Univac I, were made, for various values

of concentric shell thickness, d, as a function of the radius of the inner sphere: If the radius of the inner sphere was smaller than the wavelength, the resonance peaks appeared in the case of homogeneous sphere were damped. If the radius of the inner sphere was larger than the wavelength, then the concentric shell sppeared to behave as an impedance-matching transformer between the inner sphere and air. As d increased from zero to $\lambda_f/4$, where λ_f = wavelength in fat, S increased from $\sim$50% to $\sim$100%. At $d = \lambda_f/2$, S had decreased to a relative minimum of $\sim$ 70%. In general, S was either maximum or minimum when d was an odd or even multiple of $\lambda_f/4$, but for all non-zero d, S was always greater than the value for d = 0 (50%). It was assumed that these values for S would be valid for a human being made only of muscle and surrounding fat. Since the usual thickness of subcutaneous fat is less than 3 cm, the first maximum of S could occur only $f \geq$ 1000 Mc/s. Thus, for frequencies between 400 and 1000 Mc/s, S may vary from 50 to 100%; for frequencies above 1000 Mc/s, S may vary from $\sim$ 70 to 100%.

For concentric sphere, the Mie scattering coefficient was calculated for three values of frequency, 400, 2880, and 10,000 Mc/s, and for various values of shell thickness as a function of the radius of the inner sphere, a_1. For $a_1 < \lambda$, K_s was complicated (see figs. 18 and 19). For $a_1 > \lambda$, K_s was found to be independent of a_1 for a given value of d. However, K_s was found to be a sensitive function of d,

behaving similarly but in the opposite sense to S. That is, K_s was either a minimum or a maximum when d was an odd or even multiple of $\lambda/4$.

3. Three-Layer phantoms having the electrical properties of muscle tissue, subcutaneous fat, and skin.

As a final and best approximation for the determination of the relative absorption cross section of mankind, a model of three layers should be considered: muscle, subcutaneous fat, and skin. Not only were experimental methods too difficult, but the theoretical calculations for a sphere with two concentric shells was also too difficult. An alternative method was found which was based on Schwan and Li's published calculations of S for a semi-infinite plane slab model (a semi-infinite medium of muscle tissue separated from air by an infinite plane slab of fatty tissue). It was observed that the dependence of S on the thickness of the infinite plane slab of fatty tissue had the same general behaviour as the dependence of S on the thickness of the concentric shell. On the basis of this observation, it was assumed that the effect of a third layer (representing skin) on the slab model (also calculated by Schwan and Li) would have the same general behaviour as the effect of a second concentric shell on the sphere model. Therefore, Schwan and Li's calculations justify the following conclusions for the effect of adding a second concentric shell, or for adding a layer of skin to the previously discussed model of a human being composed only

of muscle and subcutaneous fat:

The relative absorption cross section may vary from 50 to 100% for frequencies between 400 and 1000 Mc/s; it may vary from 20 to 100% for frequencies between 1000 and 3000 Mc/s; it is about 50% for frequencies between 3000 and 10,000 Mc/s.

Assuming the currently accepted tolerance dosage of 0.01 watt/cm^2 of continuous whole body absorption of microwave energy, then from the above-stated values of relative absorption cross section, the following statements are justified:

1) At frequencies above 3000 Mc/s an incident power density of 0.02 watt/cm^2 can be tolerated.

2) At frequencies below 3000 Mc/s, 0.01 watt/cm^2 should be considered as maximum tolerable level.

APPENDIX I

Theory of Scattering and Absorption of Electromagnetic Radiation by Concentric Spheres

Let us assume that a homogeneous isotropic sphere of radius a_1 and propagation constant k_1 is surrounded by a concentric shell of radius a_2 and propagation constant k_2 and the whole is embedded in an infinite medium of air with propagation constant k_3. The inner sphere, the shell and the surrounding medium are called regions 1, 2, and 3. A uniform plane wave, linearly polarized in the x-direction, is propagated through the medium in the positive z-direction (figure 1).

Assuming that a time dependence of exp (jωt) for the electric and magnetic vectors and further assuming that the permeabilities of the three regions are equal to the permeability of free space (μv) then the propagation constants are

$$K_1 = \sqrt{\omega^2 \mu_v \epsilon_1 \epsilon_v - j\omega \mu_v \kappa_1} \tag{38}$$

$$K_2 = \sqrt{\omega^2 \mu_v \epsilon_2 \epsilon_v - j\omega \mu_v \kappa_2} \tag{39}$$

$$K_3 = \sqrt{\omega^2 \mu_v \epsilon_v} = \frac{2\pi}{\lambda} \tag{40}$$

where ω = angular frequency in radians

λ = wave length in meters

$\mu = 4\pi \times 10^{-7}$ henries/meter (permeability of air)

ϵ_1, ϵ_2 = dielectric constants of regions 1 and 2

κ_1, κ_2 = conductivity in mho/meter of regions 1 and 2

With the above stated conditions, the expressions for the incident plane wave in terms of the vector spherical wave functions have the form given by Stratton[18] (exp(jωt) is assumed rather than exp (-jωt) and the exponential term is omitted, for convenience, in the expressions given here):

$$\bar{E}_i = E_0 \sum_{n=1}^{\infty} (-j)^n \frac{2n+1}{n(n+1)} \left[\bar{m}^{(1)}_{oln} + j\, \bar{n}^{(1)}_{eln} \right] \tag{41}$$

$$\bar{H}_i = -\frac{K_3 E_0}{\omega \mu_v} \sum_{n=1}^{\infty} (-j)^n \frac{2n+1}{n(n+1)} \left[\bar{m}^{(1)}_{eln} - j\, \bar{n}^{(1)}_{oln} \right] \tag{42}$$

where E_0 is the amplitude of the wave and

$$\bar{m}^{(1)}_{\substack{o \\ e} ln} = \pm \frac{1}{\sin\theta} j_n(K_3 R) P_n^1(\cos\theta) \begin{matrix} \cos \\ \sin \end{matrix} \phi\, \bar{i}_2 - j_n(K_3 R) \frac{\partial P_n^1}{\partial \theta} \begin{matrix} \sin \\ \cos \end{matrix} \phi\, \bar{i}_3 \tag{43}$$

$$\begin{aligned} \bar{n}^{(1)}_{\substack{o \\ e} ln} = {} & \frac{n(n+1)}{K_3 R} j_n(K_3 R) P_n^1(\cos\theta) \begin{matrix} \sin \\ \cos \end{matrix} \phi\, \bar{i}_1 \\ & + \frac{1}{K_3 R} \left[K_3 R\, j_n(K_3 R) \right]' \frac{\partial P_n^1}{\partial \theta} \begin{matrix} \sin \\ \cos \end{matrix} \phi\, \bar{i}_2 \\ & \pm \frac{1}{K_3 R \sin\theta} \left[K_3 R\, j_n(K_3 R) \right]' P_n^1(\cos\theta) \begin{matrix} \cos \\ \sin \end{matrix} \phi\, \bar{i}_3 \end{aligned} \tag{44}$$

The primes on the square brackets denote differentiation with respect to the argument k_3R. $\bar{i}_1$, $\bar{i}_2$ and $\bar{i}_3$ are the unit vectors in directions R, θ and φ of a spherical coordinate system with its origin at the center of the sphere.

P_n^1 (cos θ) is the associated Legendre polynomial of the first kind, first order and n^{th} degree.

$j_n(kR)$ is the spherical Bessel function of the first kind which is related to the ordinary Bessel function of the first kind and half-integer order as follows:

$$j_n(KR) = \left(\frac{\pi}{2KR}\right)^{\frac{1}{2}} J_{n+\frac{1}{2}}(KR) \tag{45}$$

The induced secondary field must be constructed in three parts, one applying in each of the three regions. For each of these parts, the expansions are similar to those for the incident wave but with unknown amplitude coefficients. The parts applying outside the shell and inside the sphere will be called the reflected and transmitted fields in accordance with the terminology used for the single sphere problem (reference 18). They will be indicated by subscripts r and t. The formal expansions for these fields are identical to those for the single sphere problem although the amplitude coefficients have different values.

Region 3. $R > a_2$

$$\bar{E}_s = E_0 \sum_{n=1}^{\infty} (-j)^n \frac{2n+1}{n(n+1)} \left[a_n \bar{m}^{(3)}_{o1n} + j b_n \bar{n}^{(3)}_{e1n} \right] \tag{46}$$

$$\bar{H}_s = -\frac{k_3 E_0}{\mu_1 \omega} \sum_{n=1}^{\infty} (-j)^n \frac{2n+1}{n(n+1)} \left[b_n \bar{m}^{(3)}_{e1n} - j a_n \bar{n}^{(3)}_{o1n} \right] \tag{47}$$

The functions $\bar{m}^{(3)}_{e^o_1 n}$ and $\bar{n}^{(3)}_{e^o_1 n}$ are obtained by replacing $j_n(k_3 R)$ by $h^{(2)}_n(k_3 R)$ in equations (43) and (44). $h^{(2)}_n(kR)$ is the spherical Hankel function of the second kind:

$$h^{(2)}_n(KR) = \left(\frac{\pi}{2KR}\right)^{\frac{1}{2}} H^{(2)}_{n+\frac{1}{2}}(KR) \tag{48}$$

These functions are necessary in the solution for the scattered field because this solution must be regular at infinity, that is:

$$\lim_{KR \to \infty} h^{(2)}_n(KR) \longrightarrow 0 \tag{49}$$

Region 1, $R < a_1$

$$\bar{E}_t = E_0 \sum_{n=1}^{\infty} (-j)^n \frac{2n+1}{n(n+1)} \left[a^t_n \bar{m}^{(1)}_{o1n} + j b^t_n \bar{n}^{(1)}_{e1n} \right] \tag{50}$$

$$\bar{H}_t = -\frac{K_1 E_0}{\omega \mu_v}\left[\sum_{n=1}^{\infty}(-j)^n \frac{2n+1}{n(n+1)}\left\{b_n^t \bar{m}_{e1n}^{(1)} - j a_n^t \bar{n}_{o1n}^{(1)}\right\}\right] \tag{51}$$

Since the solution must be finite at the origin, Bessel functions of the first kind are used in equations (50) and (51), that is:

$$\lim_{KR\to 0} j_n(KR) \longrightarrow 0 \tag{52}$$

In addition k_3 is replaced by k_1 in equations (43) and (44).

Region 2. $a_2 > R > a_1$

$$\bar{E}_s = E_0 \sum_{n=1}^{\infty}(-j)^n \frac{2n+1}{n(n+1)}\left[a_n^{ts}\bar{m}_{o1n}^{(1)} + a_n^{rs}\bar{m}_{o1n}^{(3)} + j\left(b_n^{ts}\bar{n}_{e1n}^{(1)} + b_n^{rs}\bar{n}_{e1n}^{(3)}\right)\right] \tag{53}$$

$$\bar{H}_s = -\frac{K_2 E_0}{\omega \mu_v}\left[\sum_{n=1}^{\infty}(-j)^n \frac{2n+1}{n(n+1)}\left\{b_n^{ts}\bar{m}_{e1n}^{(1)} + b_n^{rs}\bar{m}_{e1n}^{(3)} - j\left(a_n^{ts}\bar{n}_{o1n}^{(1)} + a_n^{rs}\bar{n}_{o1n}^{(3)}\right)\right\}\right] \tag{54}$$

In the region of the spherical shell, it is necessary to use Bessel functions of both first and third kinds. The argument of the vector functions $\bar{m}^{(1)}$, $\bar{m}^{(3)}$, $\bar{n}^{(3)}$ is $K_2 R$.

The amplitude coefficients can be evaluated by applying the boundary condition at $R = a_1$,

$$\bar{i}_1 \times \bar{E}_t = \bar{i}_1 \times \bar{E}_s \tag{55}$$

$$i_1 \times H_t = i_1 \times H_s \tag{56}$$

and at $R = a_2$

$$\bar{i}_1 \times \bar{E}_s = \bar{i}_1 \times (\bar{E}_i + \bar{E}_r) \tag{57}$$

$$\bar{i}_1 \times \bar{H}_s = \bar{i}_1 \times (\bar{H}_i + \bar{H}_r) \tag{58}$$

The amplitude coefficients a_n^r and b_n^r, sufficient for our purpose, are given by equations (8) and (9).